Impact of natalizumab therapy on human pathology and an animal model of multiple sclerosis (EAE) with special focus on B cell / plasma cell inflammation

Dissertation

for the award of the degree

"Doctor rerum naturalium" (Dr. rer. nat.)

in the Molecular Medicine Study Program

at the Georg-August University Göttingen

submitted by

Darius Häusler

born in Świdnica (Schweidnitz), Poland

Göttingen 2013

Reviewer / Members of the Thesis Committee

Thesis Committee Member (Reviewer)

Prof. Dr. Wolfgang Brück

Department of Neuropathology

University Medical Center Göttingen, University of Göttingen

Thesis Committee Member (Reviewer)

Prof. Dr. Alexander Flügel

Department of Neuroimmunology

University Medical Center Göttingen, University of Göttingen

Thesis Committee Member

Prof. Dr. Jürgen Wienands

Institute for Cellular and Molecular Immunology

University Medical Center Göttingen, University of Göttingen

Supervisor

Dr. Imke Metz

Department of Neuropathology

University Medical Center Göttingen, University of Göttingen

Date of the oral examination: 18. December 2013

Declaration

I hereby declare that I have written my Ph.D. thesis entitled "Impact on natalizumab therapy on human pathology and an animal model of multiple sclerosis (EAE) with special focus on B cell / plasma cell inflammation" independently and with no other sources and aids than quoted. This thesis has not been submitted elsewhere for any academic degree.

Darius Häusler
Göttingen, October 2013

Abstract

Multiple sclerosis (MS) is considered to be a T cell-mediated demyelinating disease. However, there is increasing evidence for the involvement of B cells and plasma cells in MS pathogenesis: for instance, B cells and plasma cells are present in MS lesions and a subgroup of early active demyelinating lesions is characterized by immunoglobulin and complement depositions. Natalizumab is a humanized monoclonal antibody approved for the treatment of relapsing-remitting MS. It hinders the transmigration of immune cells into the CNS by blocking the interaction between the α4 chain (CD49d) of integrins and their ligands. Although natalizumab is an effective drug with a pronounced reduction of the relapse rate, some patients do not respond to the therapy. Histopathology after natalizumab therapy has not been investigated. Moreover, therapeutic effects of anti-α4 integrin antibody therapy in animals were only investigated in a T cell-dependent but not B cell-dependent mouse model of MS with no detailed characterization of the inflammatory infiltrate.

The first aim of the study was to characterize the lesional pathology with a focus on inflammatory cells in natalizumab-treated patients and to compare the histology with MS patients who had no prior natalizumab therapy as well as to correlate the inflammatory cells after natalizumab treatment with clinical and therapy-related data. The second aim of the study was to investigate therapy effects of a natalizumab analogon (PS/2 antibody) in a B cell-dependent mouse model of MS (OSE) and to compare the findings with human data.

Histological analysis showed that inflammatory infiltrates in CNS lesions of natalizumab treated patients were mainly composed of macrophages, T cells and some B cells and plasma cells. T cell numbers were not significantly reduced as compared to MS patients without natalizumab treatment. However, plasma cell numbers were significantly increased in active demyelinating as well as in inactive demyelinated lesions after natalizumab therapy. Plasma cell numbers tended to be higher and T cells lower when natalizumab was still pharmacologically active as compared to later time points. Higher plasma cell numbers did not correlate with the disease duration or the therapy duration.

Therapy with the natalizumab-analogon PS/2 antibody in OSE mice increased leukocyte numbers in the blood and resulted in a partial internalization of CD49d-antibody complexes in T- and B cells. Treatment improved the clinical outcome and decreased spinal cord demyelination and inflammatory cells of all investigated immune cell subsets if given early in the disease course. However, PS/2 antibody therapy was not effective when given late in the disease course. Moreover, no evidence for a rebound activity was observed after therapy discontinuation. The therapeutic effects of PS/2 antibody injections were independent of the Fc fragment of the antibody, since F(ab')$_2$ injections showed the same beneficial effects as the intact antibody.

In conclusion, although natalizumab is an effective drug for MS it could be shown that therapy with natalizumab does not completely prevent immune cells from entering the CNS. Plasma cell numbers were even increased after natalizumab therapy as compared to controls. Due to the important role also for B cells / plasma cells in MS pathogenesis, these findings could be of therapeutic relevance.

Natalizumab analogon therapy is effective in a B cell-dependent mouse model of MS. PS/2 antibody treatment in the OSE model showed comparable peripheral effects as in MS patients treated with natalizumab. In contrast to human studies, where an increase of plasma cells after natalizumab therapy was observed, all investigated inflammatory cell subsets including T- and B cells, plasma cells and macrophages were decreased after natalizumab analogon therapy. My studies confirm that the therapeutic effect is mediated by antibody binding and leads to a partial antibody-receptor internalization.

Contents

1 Introduction

2 Materials and Methods

3 Results

4 Discussion

List of Figures

1   Introduction

2   Materials and Methods

3   Results

List of Tables

2 Materials and Methods

3 Results

A1   Supplementary Tables

Abbreviations

APC	antigen-presenting cell
BBB	blood-brain barrier
BCR	B cell receptor
CD	cluster of differentiation
CFA	complete Freund's adjuvant
CNP	2',3'-cyclic nucleotide 3'-phosphodiesterase
CNS	central nervous system
CSF	cerebrospinal fluid
EA	early active
EAE	experimental autoimmune encephalomyelitis
EBV	Epstein-Barr-Virus
ERM	early remyelination
FCS	fetal calf serum
FDA	food and drug administration
FSC	forward scatter
HBECs	human brain-derived endothelial cells
IA	inactive
ICAM	intracellular adhesion molecule
IFN-ß	Interferon beta
IL	interleukin
IPA	isopropyl alcohol
KLH	keyhole limpet hemocyanin
LA	late active
LAL	limulus amebocyte lysate
LFA-1	lymphocyte function-associated antigen-1
LPAM-1	lymphocyte peyer patch adhesion molecule-1
LRM	late remyelination
MAdCAM-1	mucosal addressin cellular adhesion molecule-1
MAG	myelin-associated glycoprotein
MFI	median fluorescence intensity
MMP	metalloproteinases
MOG	myelin oligodendrocyte glycoprotein
MS	multiple sclerosis
MWCO	molecular weight cut off
OCB	oligoclonal bands
OSE	optico-spinal-encephalomyelitis
pa	parenchymal
PBMCs	peripheral blood mononuclear cells
PCR	polymerase chain reaction
PFA	paraformaldehyde

PLP	proteolipid protein
PML	progressive multifocal leukoencephalopathy
PNAd	peripheral node adressin
PP	primary-progressive
PR	progressive-relapsing
PSGL-1	P-selectin glycoprotein ligand-1
pv	perivascular
RR	relapsing-remitting
SDS-PAGE	sodium dodecyl sulphate-polyacrylamide gel electrophoresis
SP	secondary-progressive
SSC	side scatter
TCR	T cell receptor
TGF-ß	transforming growth factor beta
TNF	tumor necrosis factor
VCAM-1	vascular cell adhesion molecule-1
VLA-4	very late antigen-4
WBCs	white blood cells

1 Introduction

1.1 Multiple sclerosis

1.1.1 History and epidemiology

Multiple sclerosis (MS), also known as *encephalomyelitis disseminata*, is an inflammatory demyelinating disease of the central nervous system (CNS). The first description of MS dates back to the 14th century (Kumar et al., 2011; Herndon, 2003). The first illustration of MS lesions in medical literature was published by Robert Carswell in 1838, and more extensive descriptions were depicted by Jean Cruveillier in the publication *Anatomie pathologique du corps human* (1829-1842) (Herndon, 2003; Murray, 2009). However, Jean Martin Charcot was the first who made a correlation between the clinical features of MS and the pathological changes in 1868 (Fig. 1) (Kumar et al., 2011; Herndon, 2003).

Fig. 1.1: Jean-Martin Charcot (1825-1893) (adapted from Kumar et al., 2011).

In Northern Europe the general population prevalence ranges between 60-200/100.000. The disease is mainly diagnosed in patients between the ages 20 and 40, whereas it is twice as common in female as in male. The exact cause of MS is still unknown; however, it is considered to be an autoimmune-mediated disease triggered by environmental, genetic or infectious factors or a combination of these (Korn, 2008; Marrie, 2004; Barcellos et al., 2003; Willer et al., 2003; Serafini et al., 2007; Handel et al., 2010). Especially, smoking, vitamin D deficiency, EBV infection and hormonal imbalance are discussed as possible determining factors for susceptibility to MS. (Sospedra and Martin, 2005).

1.1.2 Clinical course

Different clinical courses can be distinguished. A successful therapy strategy of MS is dependent on the clinical phenotype, with the four main subtypes of the disease characterized as follows (Lublin and Reingold, 1996):

The *relapsing-remitting* subtype is the most frequent form of MS and is diagnosed in approximately 85 percent of MS patients. It is characterized by disease relapses with full or partial recovery and no disease progression in periods between relapses (Fig. 2 A).

Patients with a relapsing-remitting disease course usually convert to a *secondary progressive* subtype marked by a steady progression of disability without clear phases of remission (Fig. 2 B). The possibility of entering the secondary progressive phase increases with longer ongoing disease duration (Scalfari et al., 2013).

The characteristics of a *primary progressive* subtype are a steady progression of disability from disease onset with no distinct relapses (Fig. 2 C).

The rare *progressive relapsing* disease course is characterized by progressive disability from disease onset with or without full recovery and steady worsening of symptoms in periods between disease relapses (Fig. 2 D).

Fig. 1.2: MS patients show four different clinical courses (modified from Lublin et al., 1996).

(A) relapsing-remitting disease course,

(B) secondary-progressive disease course,

(C) primary-progressive disease course,

(D) progressive-relapsing disease course.
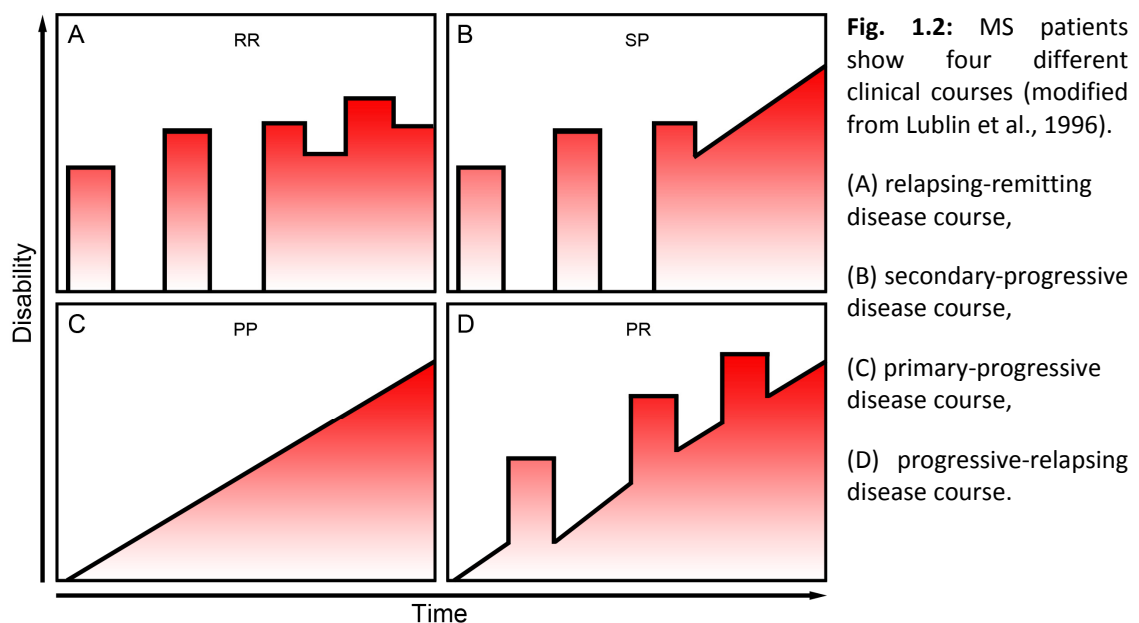
1.1.3 Neuropathology

The pathological hallmarks of MS lesions include CNS infiltration by inflammatory cells (Fig. 3 A), white matter demyelination (Fig. 3 B), reactive gliosis (Fig. 3 D) as well as relative axonal preservation (Fig. 3 C) (Kuhlmann et al., 2002; Kuhlmann et al., 2008). MS lesions can also occur in the gray matter, both in the cortex and the deep gray matter (Kutzelnigg et al., 2005). The normal-appearing white matter (NAWM) may also be affected by diffuse axonal injury with profound microglia activation, reactive gliosis and T cell infiltration.

In early MS lesions, inflammatory cell infiltrates are mainly composed of massive infiltration by macrophages containing myelin debris within the cytoplasm as a product of myelin destruction (Fig. 3 E). Furthermore, lesions are also characterized by perivascular and parenchymal T cells including $CD4^+$ and $CD8^+$ cells (Fig. 3 F, G), but also by few B cells and plasma cells (Kuhlmann et al., 2002; Kuhlmann et al., 2008) (Fig. 3 H). Only in early active demyelinating lesions with minor myelin proteins incorporated in macrophages, immunopathological patterns of demyelination can be determined (Brück et al., 1995). Four fundamentally different patterns of demyelination were defined based on the extent of oligodendrocyte preservation, geography and extension of plaques, myelin protein loss and immunoglobulin and complement deposition (Lucchinetti et al., 2000).

MS pattern I is characterized by a sharp border to the normal-appearing white matter. The active demyelination is associated with T cell- and macrophage-dominant inflammation. The myelin loss when staining for the different myelin components PLP, MOG, MAG, MBP and CNP is even.

MS pattern II shows features similar to pattern I. However, it is distinguished by the deposition of immunoglobulins and complement C9neo antigen at sites of active myelin destruction along myelin sheaths as well as within macrophages. Thus, a role for the humoral immune response in myelin destruction has been postulated.
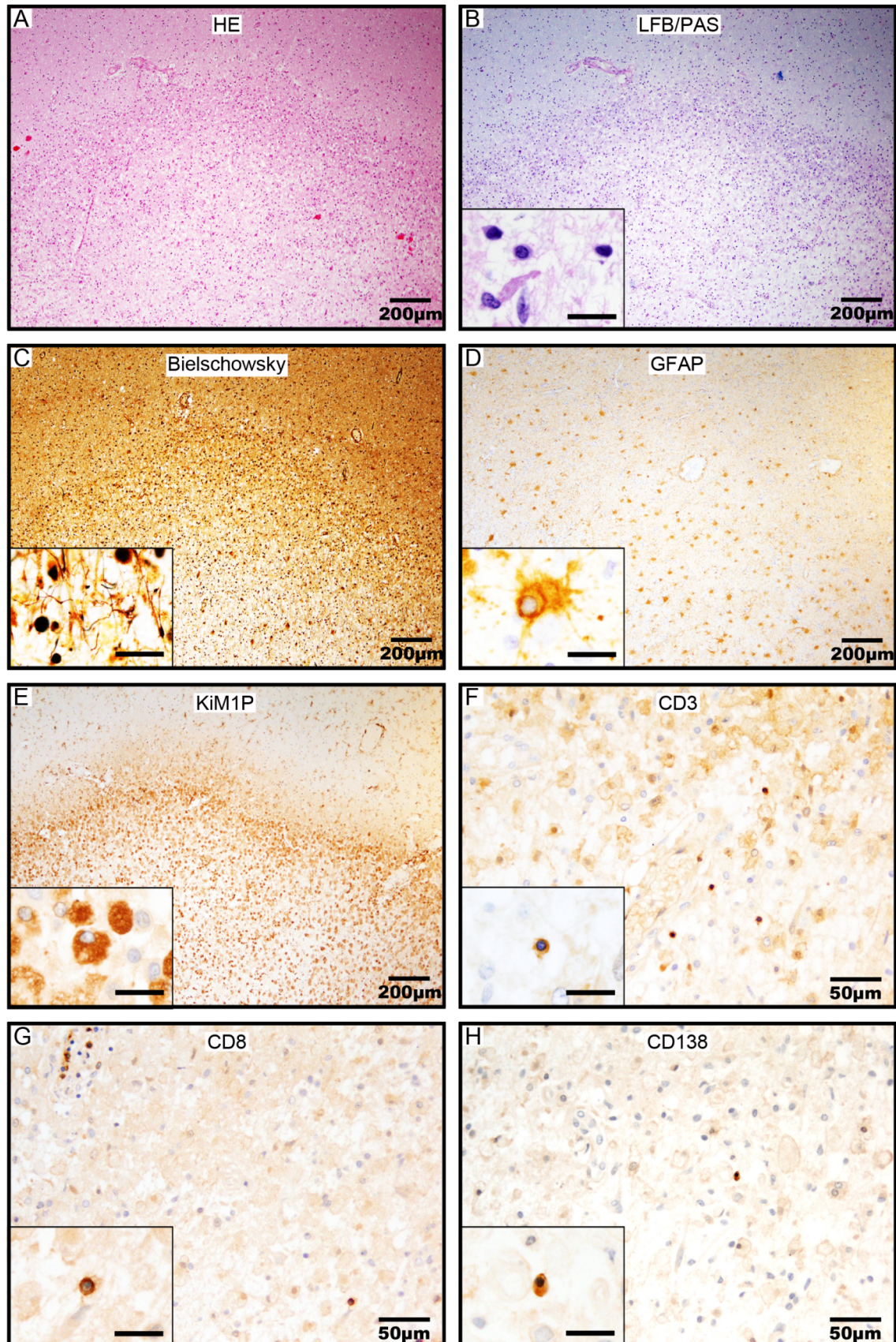
Fig. 1.3: Histological characteristics of a typical early MS brain lesion including inflammation (A), white matter demyelination (B), relative axonal preservation (C) and reactive gliosis (D). Inflammatory infiltrates are mainly composed of macrophages (E), T cells (F, G) as well as B cells and plasma cells (H). Scale bar in inset = 20 μm.

The characteristics of pattern III are also an inflammatory cell infiltrate composed of T cells and macrophages as well as the absence of immunoglobulin and complement deposition as described for pattern I. However, the lesions are characterized by a diffuse border. A prominent feature of this pattern is preferential loss of the myelin protein MAG compared to other myelin proteins such as MOG as well as a pronounced apoptotic oligodendrocyte cell death.

MS pattern IV has been observed only in a few cases with primary progressive MS (Kornek et al., 2003; Brück, 2005) and is thus of minor clinical relevance. Inflammatory cell infiltrates are also dominated by T cells and macrophages. Furthermore, immunoglobulin and complement deposition are absent in this pattern. The hallmark of pattern IV lesions is non-apoptotic degeneration of oligodendrocytes in a small rim of periplaque white matter adjacent to a sharp lesion border.

1.1.4 Pathogenesis

MS is assumed to be an autoimmune inflammatory disease. Although the factors which trigger this process are still unknown, researchers are attempting to explore the development of the disease in experimental autoimmune encephalomyelitis (EAE), an animal model of MS. On the basis of immunological findings in EAE as well as the observations in MS patients, possible immunological pathways in the MS disease process have been suggested.

In the past, MS was considered to be primarily a T cell-mediated disease (Sospedra and Martin, 2005; Chitnis, 2007). According to this theory, autoreactive T helper 1 (Th1) cells are activated in the periphery, and in their activated state they are able to adhere to the blood brain barrier (BBB) and transmigrate into the CNS. After local re-activation, T cells proliferate and secrete pro-inflammatory cytokines as well as chemokines. As a result, microglia, macrophages and astrocytes are activated, the BBB is disrupted and other immune cells, including monocytes, T cells and B cells, are recruited from the peripheral blood into the CNS which leads to demyelination, axonal loss and subsequent neurological disability. Recently, Th17 cells as well as CD8^{+} T cells

have been discussed as possibly contributing to the pathogenesis of MS (Saxena et al., 2011).

According to this theory of MS pathogenesis, B cells and plasma cells were considered to play a secondary T cell-dependent role. However, several lines of evidence indicate also an important role for B cells and plasma cells in MS, e.g. an expansion of B cells and plasma cells is found in the cerebrospinal fluid (CSF). Moreover, oligoclonal immunoglobulins (oligoclonal bands) are found in more than 90 percent of MS patients in the CSF and are even a helpful diagnostic tool (Owens et al., 1998; Qin et al., 1998; Baranzini et al., 1999; Colombo et al., 2000; Monson et al., 2005; Obermeier et al., 2008; Owens et al., 2009). Furthermore, B cell accumulations in close proximity to T cells, plasma cells and follicular dendritic cells are observed in meninges of MS patients. Here also the chemokines CXCL13, CCL21 and peripheral node adressin (PNAd) were found, assuming a formation of germinal-center-like structures which may maintain a humoral autoimmunity, resulting in increased disability (Prineas, 1979; Serafini et al., 2004; Magliozzi et al., 2007; Howell et al., 2011). In addition the depletion of B cells in the blood of MS patients by treatment with rituximab showed beneficial effects on the disease (Stüve et al., 2005; Cross et al., 2006; Chan et al., 2007; Petereit et al., 2008; Hauser et al., 2008; del Pilar Martin et al., 2009). Furthermore, plasmapheresis in MS patients is assumed to deplete antibodies from the immune system and thus result in clinical improvement (Keegan et al., 2005). Moreover, the presence of B cells and plasma cells in the CNS parenchyma of MS patients as well as the immunoglobulin and complement depositions in a subgroup of early active lesions support a key role for B cells as well as plasma cells in MS pathogenesis (Ozawa et al., 1994; Kuhlmann et al., 2002; Vercellino et al., 2009; Frischer et al., 2009; Lucchinetti et al., 2000).

1.1.5 MS therapy

1.1.5.1 Treatment concepts

Treatment of MS can be generally grouped into immunosuppressive and immunomodulatory therapies (Stüve, 2009 a). The mode of action of immunosuppressive agents is the deletion of leukocytes in the periphery. This results in reduced disease severity, but also in impaired immune surveillance. The beneficial impact can also be supported by further effects such as a decrease in pro-inflammatory cytokine secretion, induction of apoptosis in dendritic cells as well as inhibition of monocyte and lymphocyte migration as shown after mitoxantrone therapy (Vollmer et al., 2010). The most widely used immunomodulatory agents are interferon-beta (IFN-β) and glatiramer acetate. Immunomodulatory drugs have diverse functions modulating the immune system, e.g. IFN-β reduces matrix metalloproteinase activity as well as inhibits T cell activation and proliferation. Furthermore, both a reduction in pro-inflammatory cytokine production as well as an increase in apoptosis in autoreactive T cells have been described (Dhib-Jalbut and Marks, 2010). Glatiramer acetate is a synthetic random basic copolymer composed of glutamic acid, lysine, tyrosine and alanine. In a mouse model of MS, an increase in anti-inflammatory type II monocytes was observed, characterized by enhanced secretion of interleukin-10 (IL-10) and transforming growth factor-β (TGF-β) as well as decreased production of interleukin-12 (IL-12) and tumor necrosis factor (TNF) (Weber et al., 2007). Furthermore, it is believed that glatiramer acetate causes a shift in T cells from a pro-inflammatory Th1 state to a Th2 anti-inflammatory phenotype (Schrempf and Ziemssen, 2007).

A better understanding of the immunological processes behind MS has promoted the development of new agents with specific targets involved in the MS pathology. One concept of these new agents is to prevent migration of inflammatory cell infiltrates into the CNS. The movement of ions, molecules and cells between the blood and the CNS is regulated by the BBB. It is a physical barrier formed by microvascular endothelial cells which are connected by tight junctions and surrounded by pericytes, basement membranes and astrocytes (Takeshita and Ransohoff, 2012) (Fig. 4). The

perivascular space, the area between the endothelial cells and astrocytes, is limited by their basement membrane. The astrocytes form with their endfeet the glia limitans, which represents the outer site of the BBB. Microglial and neuronal processes can also contribute to the glia limitans (Takeshita and Ransohoff, 2012).
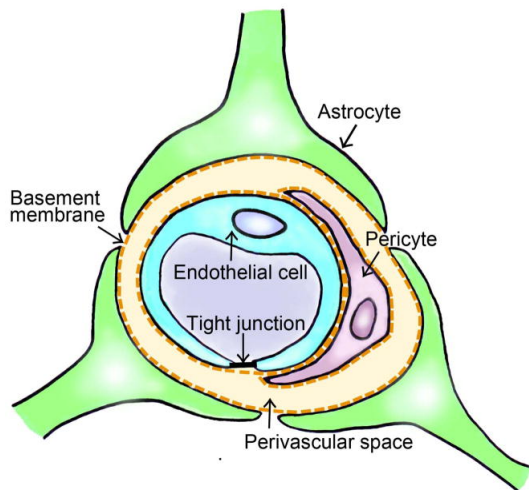
Fig. 1.4: Cellular components of the BBB (adapted from Takeshita and Ransohoff et al., 2012).

The recruitment of circulating immune cells through the BBB into the CNS is mediated by several steps (Fig. 5). This multistep procedure comprises cell rolling and capture to the endothelium surface, activation of adhesion molecules, arrest, crawling and transmigration to the perivascular space as well as passing of the glia limitans into the brain parenchyma.

Rolling / capture (Fig. 5 I)

The transmigration process begins with an initial transient contact of the circulating immune cell with the endothelial cell. This process is mediated by adhesion molecules of the selectin family, mainly by P-selectin and its respective glycosylated ligand P-selectin glycoprotein ligand-1 (PSGL-1). In the past it was assumed that the rolling step is also supported by α-4 integrins such as VLA-4 (CD49d/CD29) and its ligand vascular cell adhesion molecule-1 (VCAM-1). However, growing evidence indicates no essential role for these integrins at least for T cells during the rolling / capture process (Coisne et al., 2009, Bauer et al., 2009). Due to the low binding affinity of selectins and their

ligands, the immune cell rolls along the vascular wall with greatly reduced velocity (Engelhardt and Ransohoff, 2012; Takeshita and Ransohoff, 2012).

Activation (Fig. 5 II)

It is assumed that during the rolling process the immune cell can bind chemokines presented on the endothelial surface. The interaction of these chemokines with G protein-coupled receptors on the immune cell surface results in a G protein-mediated intracellular signal (inside-out signal), which increases the affinity and avidity of integrins such as VLA-4 (CD49d/CD29) and lymphocyte function-associated antigen-1 (LFA-1) by both conformational changes and clustering (Engelhardt and Ransohoff, 2012; Takeshita and Ransohoff, 2012).

Arrest (Fig. 5 III)

The immune cell arrest can only take place when integrin activation has occurred. During this process activated integrins such as VLA-4 and LFA-1 bind to their respective ligands VCAM-1 and intracellular adhesion molecule-1 (ICAM-1). This results in cytoplasmic signaling cascades in both immune cells and endothelial cells (Engelhardt and Ransohoff, 2012; Takeshita and Ransohoff 2012).

Crawling (Fig. 5 IV)

The arrest of the immune cell by integrin-ligand binding leads to a crawling process of the immune cell on the endothelium surface. During this process, which is predominantly regulated by LFA-1 and its ligands ICAM-1 and ICAM-2, the immune cell probes the endothelium in search of optimal sites for transmigration (Engelhardt and Ransohoff, 2012; Steiner et al., 2010).

Transmigration (Fig. 5 V)

Up to now the transmigration process is not yet fully understood, and two distinct migration pathways are being discussed. One possible migration route for immune cells could be through the tight junctions of the endothelium. Another potential route is proposed by a large pore or vacuole in the endothelial cell. After crossing the endothelium, high amounts of CXCL12, produced by endothelial cells and astrocytes, are required to retain the immune cell in the perivascular space. Furthermore, active

matrix metalloproteinases MMP-2 and MMP-9 are necessary to cleave the extracellular matrix receptor β-dystroglycan from the astrocyte end-feet to enable the access of the immune cell across the glia limitans into the CNS parenchyma (Engelhardt and Ransohoff, 2012; Takeshita and Ransohoff, 2012).

Apart from the migration route through the BBB, immune cells can also enter into the CNS by migration via the choroid plexus into the cerebrospinal fluid (CSF) as well as through the blood-leptomeningeal barrier in meningeal microvessels on the surface of the brain and spinal cord (Engelhardt and Ransohoff, 2012).
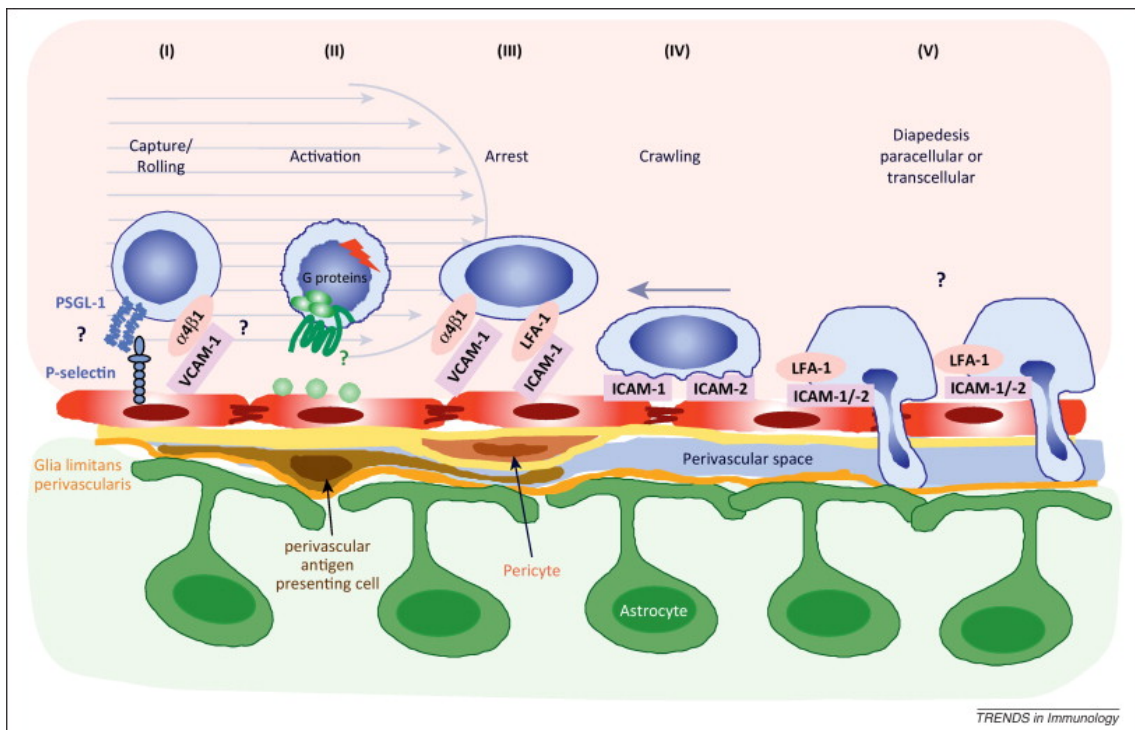
Fig. 1.5: Molecular mechanisms involved in leukocyte recruitment into the CNS (adapted from Engelhardt and Ransohoff et al., 2012). Not fully understood pathways are indicated by interrogation marks.

1.1.5.2 Natalizumab therapy

Natalizumab (*Tysabri®*) is one of the new drugs which prevent the migration of inflammatory cells into the CNS. It is a humanized IgG4κ monoclonal antibody and received food and drug administration (FDA) approval in 2004 for the treatment of

relapsing-remitting MS based on the AFFIRM and SENTINEL phase 3 clinical trials (Rudick et al., 2006; Polman et al., 2006). MS patients are treated intravenously with a dosage of 300 mg every four weeks. Natalizumab selectively binds to the α4-integrin (CD49d) component of adhesion molecules such as VLA-4 and lymphocyte peyer patch adhesion molecule-1 (LPAM-1), which are expressed on all leukocytes except neutrophils (Stüve at al., 2006 a), thereby preventing the interaction with the ligand VCAM-1 and mucosal addressin cellular adhesion molecule-1 (MAdCAM-1), respectively. While the interaction between LPAM-1 and MAdCAM-1 is mainly required for homing of lymphocytes into the intestine (Holzmann et al., 1989, Hamann et al., 1994) and not into the CNS (Engelhardt et al., 1998; Jain et al., 2010; Haanstra et al., 2013), blocking of the α-4 chain of VLA-4 is believed to inhibit cell migration into the CNS as shown *in vitro* by a BBB migration model consisting of human immune cells and human brain-derived endothelial cells (HBEC) (Alter et al., 2003) and *in vivo* by intravital two-photon imaging of T cells on leptomeningeal vessels in a Lewis rat model of EAE (Bartholomäus et al., 2009). Blood analysis before and after natalizumab infusion revealed different α-4 integrin expression patterns on mononuclear cells (Niino et al., 2006). Before natalizumab injection higher expression levels of α-4 integrin were observed on monocytes (> 2-fold) and B cells (> 1.5-fold) as compared to T cells. Among the T cell population CD8^{+} T cells showed more than twice as many α-4 integrins on the cell surface as CD4^{+} T cells. Furthermore, the α-4 integrin levels were also higher in memory T cells and B cells as compared to naïve cells. The administration of natalizumab led to a significant decrease in free binding sites of the α-4 integrin receptor, whereby T cells and B cells showed a more pronounced reduction as compared to monocytes (Wipfler et al., 2011). The lymphocyte number in the blood also increased 1.5-fold after natalizumab therapy (Krumbholz et al., 2008). Investigation of blood cells before and after natalizumab infusion across a fibronectin layer, which is a surrogate for the endothelium, showed decreased migration of peripheral blood mononuclear cells (PBMCs) after the infusion (Niino et al., 2006). Analysis of the CSF after natalizumab therapy supported the beneficial therapeutic effect by showing decreased WBC numbers such as T cells, B cells and plasma cells (Stüve et al., 2006 a; Stüve et al., 2006 b). Data showing histopathological changes of the CNS parenchyma after natalizumab therapy are very limited. Only one histological

study has been published analyzing a single patient with confounding pathology, as the patient had developed progressive multifocal leukoencephalopathy (PML) due to natalizumab therapy (del Pilar Martin et al., 2008).

1.2 Animal models of MS

The investigation of immunological pathways of MS in humans is very restricted. Animal models are therefore essential to understand the complex pathology of MS. Several animal models of MS have been established to examine different aspects of the disease.

1.2.1 Toxin-induced demyelinating models

Several models of experimental demyelination are based on the use of toxins. For instance, injections of agents such as ethidium bromide or lysolecithin into defined areas of the CNS cause focal demyelinating lesions (Blakemore and Franklin, 2008). Cuprizone is a copper-chelating agent discovered and described in the early 1950s that also belongs to toxin-based demyelinating agents (Messori et al., 2007). The demyelinating process is induced by feeding of cuprizone and results in an almost completely demyelinated corpus callosum 5-6 weeks after onset of cuprizone feeding. This demyelinating process is neither associated with a BBB disruption nor a contribution of T cells is observed (Bakker and Ludwin, 1987; Kondo et al., 1987; McMahon et al., 2001). Normal diet without cuprizone leads to spontaneous remyelination during subsequent weeks (Kipp et al., 2009). Thus, the cuprizone-induced demyelinating model is suitable for example to study de- and remyelination as well as oligodendrocyte recruitment.

1.2.2 Experimental autoimmune encephalomyelitis (EAE) model

The experimental autoimmune encephalomyelitis (EAE) model is used to investigate immune cell-mediated demyelination of the CNS. EAE was first described in 1933 (Rivers et al., 1933) and became the most frequently used animal model of MS.

EAE can be generated by *active immunization*. It has been induced in different rodents and mammals and may have a variable pathology and clinical course depending on the species and the protein used for immunization (Gold et al., 2006). In general, animals are actively immunized by injecting proteins that are part of the myelin sheath such as MBP, PLP, and MOG (Kipp et al., 2009). In mice, MOG peptide with the amino acids position 35 to 55 (MOG_{35-55}) emulsified in complete Freund's adjuvant (CFA) is a common approach for active immunization (Mendel et al., 1995; Stromnes and Goverman, 2006 a). The injected peptide is presented by professional antigen-presenting cells (APC) such as dendritic cells and macrophages to $CD4^+$ T cells in the periphery. After activation the myelin-specific $CD4^+$ T cells are able to cross the BBB. Local reactivation takes place, $CD4^+$ T cells proliferate and secrete pro-inflammatory cytokines as well as chemokines. As a result microglia, macrophages and astrocytes are activated, BBB is disrupted and other T cells and macrophages are recruited from the peripheral blood into the CNS, leading to demyelination and axonal loss.

A further possibility to induce EAE is by *adoptive transfer*, e.g. pathogenic, myelin-specific $CD4^+$ T cells generated in donor animals by active immunization and then transferred into recipient mice (Stromnes and Goverman, 2006 b).

Classical EAE by active immunization or adoptive transfer is mainly driven by $CD4^+$ T cells (Schreiner et al., 2009; Constantinescu et al., 2011). Growing evidence of the important role for B cells and plasma cells in MS pathogenesis promoted the development of EAE models with stronger contribution of these cells to the disease. The opticospinal EAE (OSE) mouse model is a double *transgenic*, spontaneous EAE model. Here the demyelination is mediated by both T cells and B cells (Bettelli et al., 2006; Krishnamoorthy et al., 2006). The OSE mouse model is generated by the interbreeding of the two single transgenic mouse strains 2D2 (Bettelli et al., 2003) and Th (Litzenburger et al., 1998). In the 2D2 mouse most $CD4^+$ T cells express a transgenic TCR, recognizing MOG peptide in the amino acid position 35 to 55.

The Th mouse is generated with knock-in technology by inserting the recombinant heavy chain of a demyelinating MOG specific antibody in the IgJ region. 20-30% of B cells and plasma cells express B cell receptors (BCR) that recognize MOG protein and produce MOG-specific antibodies, respectively (Ransohoff, 2006). After crossing the two single transgenic strains, about 50% of mice spontaneously develop a severe EAE with infiltrated and demyelinated areas in the spinal cord as well as the optic nerve by 6 ± 2 weeks of age (Bettelli et al., 2006; Krishnamoorthy et al., 2006). Cellular infiltrates are mainly composed of CD11b$^+$ cells, CD4$^+$ cells, CD8$^+$ and B220$^+$ cells (Bettelli et al., 2006; Krishnamoorthy et al., 2006).

1.2.3 Natalizumab analogon treatment in EAE models

In the past, several clones of the antibody directed against α-4 integrin were used as natalizumab analogon in the animal model of MS. The first in vivo study with a natalizumab analogon was published in 1992 (Yednock et al., 1992). EAE was induced in rats by passive transfer of myelin-specific T cells. Two days after the EAE induction, a single intraperitoneal injection of a monoclonal antibody clone HP2/1 directed against α-4 integrin resulted in a complete prevention of clinical signs in 75% of treated animals. In those rats that developed disease, disease onset was delayed and clinical severity was reduced as compared to untreated animals. Several additional studies confirmed these results in the mouse model of EAE induced by passive transfer (Baron at al., 1993; Brocke et al., 1999; Kanwar et al., 2000) or active immunization (Theien et al., 2001) when the anti α-4 integrin antibody clone PS/2 was administered immediately after the onset of disease. Treatment during priming or remission phases showed a mild effect on the clinical course or even resulted in increased numbers of relapses and augmentation of Th1 responses (Theien et al., 2001; Tsunoda et al., 2007). However, until today no study was performed in B cell-dependent EAE models. Also, a detailed description of the inflammatory infiltrate after treatment with the natalizumab analogon was not provided.

1.3 Aims of the study

MS is one of the most common diseases of the CNS in the northern hemisphere, and usually leads to significant disability. Although the exact cause of MS is still unknown, it is considered to be an autoimmune disease mainly mediated by T cells but also B cells and plasma cells. Natalizumab is a humanized monoclonal antibody directed against the α4-integrin of the adhesion molecule VLA-4 and has been approved for the treatment of MS. It is thought to hinder the transmigration of inflammatory cells into the CNS. Although natalizumab is an effective treatment with a relapse reduction of 80 % even in patients with insufficient response to other disease modifying therapies as well as in patients with high disease activity, some patients do not respond at all to natalizumab treatment (Phillips et al., 2006; Krumbholz et al., 2007; Hellwig et al., 2008; Leussink et al., 2008; Killestein et al., 2009). The histopathological changes after natalizumab treatment are still unknown. Moreover, whether natalizumab is effective in B cell-dependent models of MS has not yet been analyzed. A detailed characterization of the inflammatory cell infiltrate is still lacking.

In the first part of my thesis I investigated human tissue from patients treated with natalizumab. The aims of this part are:

A1.   to characterize the MS pathology with a focus on inflammatory cells in natalizumab-treated patients and to compare the histology with MS patients who had no prior natalizumab therapy;

A2.   to correlate the inflammatory cells after natalizumab treatment with clinical and therapy-related data.

In the second part of my thesis the results of natalizumab therapy in humans are reviewed in a B cell-dependent EAE model of MS (OSE) after treatment with a natalizumab analogon. The goals of the second part are:

B1.   to examine treatment effects on peripheral blood cells;

B2. to investigate the histological changes within the CNS after different treatment paradigms including

a) short-term therapy

b) long-term therapy

c) therapy in the late phase of the disease

d) discontinuation of the therapy;

B3. to study the mode of action of the natalizumab analogon.

2 Materials and Methods

For additional information on buffers, chemicals, reagents, equipment and manufacturers see appendix A2, A3 and A4.

2.1 Patients

In the first part of my study I investigated formalin fixed and paraffin embedded tissue from MS patients that had received natalizumab treatment. All patients fulfilled the neuropathological diagnostic criteria of inflammatory demyelinating disease consistent with MS.

Natalizumab treated MS patients

A collection of 12 biopsies and 3 autopsies of MS patients treated with natalizumab was investigated using immunohistochemistry (Tab. 2.1). PML, a known severe side effect of natalizumab treatment, was excluded in all patients by immunohistochemistry and / or *in situ* hybridization for JC-Virus. Natalizumab therapy occurred for different periods of time ranging from 1 infusion to 78 infusions. Patient #5 received an oral anti α-4 integrin inhibitor (firategrast) instead of natalizumab injections. Furthermore, patient #3 and patient #10 had a plasmapheresis between the last natalizumab infusion and biopsy.

Controls (MS patients with no prior natalizumab therapy)

Control patients were matched according to disease duration. 11 biopsy (Tab. 2.2) and 10 autopsy controls (Tab. 2.3) were investigated.

Tab. 2.1: Clinical characteristics of MS patients treated with natalizumab.

	Patient #	Age	Sex	Histology	Medication - Natalizumab						Disease course	Disease duration [years]
					Nat. onset	Nat. end	# of infusions	Therapy duration [months]	Date of Bx/death	Days after last infusion and Bx/death		
Biopsy	Pat. #1	35	♀	EAII	01.12.06	01.12.06	1	1	17.01.07	47	RR	2
	Pat. #2	23	♂	IA	01.08.06	20.11.07	16	16	12.12.07	22	SP	4
	Pat. #3**	31	♀	EAI	01.11.06	01.11.08	20	24	09.03.09	128	RR	10
	Pat. #4	33	♀	IA	01.08.06	01.01.07	6	5	23.01.12	1848	RR	9
	Pat. #5	37	♀	EAII/LA	01.12.08*		0	5.5	15.05.09	165	RR	10
	Pat. #6	34	♀	EAIII/LA	08.07.10	04.08.10	2	2	14.09.10	41	RR	8
	Pat. #7	49	♀	LA	01.01.07	07.06.10	43	42	09.05.11	336	SP	19
	Pat. #8	46	♂	EAI/LA	07.05.10	14.06.11	14	14	16.12.11	185	RR	15
	Pat. #9	36	♂	LA	01.09.07	04.04.11	46	43	13.06.12	436	RR	12
	Pat. #10**	40	♀	EAIII/LA	01.09.08	01.06.11	38	33	07.02.13	617	SP	16
	Pat. #11	35	♀	LA	n/a	n/a	10	9	n/a	n/a	RR	n/a
	Pat. #12	46	♀	EAII/LA	01.07.06	01.12.12	84	78	12.04.13	101	SP	18
Autopsy	Pat. #13	39	♀	EAII/IA	08.11.07	01.05.08	6	6	11.11.08	194	RR	8
	Pat. #14	43	♀	EAII/LA/IA	01.04.08	01.08.08	5	5	15.02.09	198	RR	20
	Pat. #15	62	♂	IA	20.01.07	11.03.11	51	51	31.03.11	20	SP	13

EA = early active, I II III = immunopattern number, LA = late active, IA = inactive, RR = relapsing-remitting, SP = secondary progressive.

* = one oral administration, ** = plasmapheresis between natalizumab end and biopsy, n/a = data are not available.

Tab. 2.2: Clinical characteristics of MS biopsy controls.

	Ctrl. #	Age	Sex	Histology	Disease course	Disease duration [years]
Biopsy	Ctrl. #1	44	♀	IA	RR	14
	Ctrl. #2	30	♀	EAII	RR	7
	Ctrl. #3	14	♂	EAI	RR	6
	Ctrl. #4	32	♀	EAII	SP	7
	Ctrl. #5	24	♀	EAIII	SP	5
	Ctrl. #6	29	♀	IA	SP	6
	Ctrl. #7	37	♀	IA/ERM	RR	10
	Ctrl. #8	28	♀	IA/ERM	RR	5
	Ctrl. #9	45	♀	EAII	SP	11
	Ctrl #10	36	♀	EAIII	RR	9
	Ctrl #11	52	♂	EAII/LA	SP	10

EA = early active, I II III = immunopattern number, LA = late active, IA = inactive,

ERM = early remyelination, RR = relapsing-remitting, SP = secondary progressive.

Tab. 2.3: Clinical characteristics of MS autopsy controls.

	Ctrl. #	Age	Sex	Histology	Disease course	Disease duration [years]
Autopsy	Ctrl. #1	36	♀	IA/LRM	PP	5
	Ctrl. #2	47	♂	IA/LRM	CP	18
	Ctrl. #3	71	♀	IA/LRM	PP	13
	Ctrl. #4	42	♂	IA/LRM	PP	6
	Ctrl. #5	47	♂	IA	n/a	12
	Ctrl. #6	28	♂	IA/LRM	PP	3
	Ctrl. #7	41	♂	IA	n/a	6
	Ctrl. #8	61	♀	IA/LRM	SP	18
	Ctrl. #9	54	♂	IA/LRM	SP	23
	Ctrl #10	56	♀	IA	CP	9

IA = inactive, LRM = late remyelination, PP = primary progressive, CP = chronic

progressive, SP = secondary progressive, n/a = data are not available

2.2 Histochemical stainings

Tissue preparation before staining procedures:

Before starting with the histological staining procedure it is necessary to remove the paraffin from the tissue sections by melting it off in an oven at 60°C for at least 1 hour followed by xylol incubation as well as to perform a rehydration by graded isopropyl alcohol series as follows:

4 x 10 min xylol -> 5 min 100% isopropyl alcohol (IPA) / xylol (1:1) -> 2 x 3 min 100% IPA

-> 3 min 90% IPA -> 3 min 70% IPA -> 3 min 50% IPA -> dH_2O

Tissue preservation after staining procedures:

For the preservation stained tissue sections were dehydrated, mounted in DePex medium and coverslipped. The dehydration was done as follows:

dH_2O -> 3 min 50% IPA -> 3 min 70% IPA -> 3 min 90% IPA -> 2 x 3 min 100% IPA -> 5 min 100% IPA / xylol (1:1) -> xylol

2.2.1 Hematoxylin-Eosin (HE) staining

HE staining is useful to obtain a general overview of the tissue. Hematoxylin is binding to basic nucleoproteins and results in blue coloured cell nuclei. In contrast, eosin stains acidophilic and basic extra- and intracellular proteins, therefore the parenchyma appears red. The procedure was performed as follows:

■ deparaffinization and rehydration (see 2.2)

■ rinse 3 x with dH_2O

■ incubate in Mayer's hemalaun solution for 6 min

■ rinse with dH_2O

■ differentiation by short dip into 1% HCl-alcohol (1% HCl-alcohol in 90% isopropyl alcohol)

■ blueing of the tissue by rinsing under tap water for 10 min

■ incubate in 1% eosin solution for 2-3 min (1% eosin in 70% isopropyl alcohol + 10 drops glacial acetic acid)

■ shortly rinse with dH_2O

■ dehydrate and mount in DePex medium

2.2.2 Luxol Fast Blue/Periodic Acid Schiff (LFB/PAS) staining

Myelin was visualized by LFB/PAS staining. LFB stains myelin deep blue by binding to lipoproteins, whereas PAS colors grey matter and demyelinated parenchyma pink. The procedure was performed as follows:

<u>LFB staining</u>

■ deparaffinization and rehydration till the 90% IPA step (see 2.2)

■ incubate in LFB solution over night at 60°C

■ wash with 90% IPA

■ differentiation by short dip into 0.05% lithium carbonate solution followed by a short dip into 70% IPA and a rinsing step with dH_2O

<u>PAS staining</u>

■ incubate in 1% periodic acid for 5 min

■ rinse under flowing tap water for 5 min

■ wash shortly with dH_2O

■ incubate in Schiff's solution for 20 min

■ rinse under flowing tap water for 5 min

■ incubate in Meyer's hemalun solution for 2 min

■ wash shortly with dH_2O

■ differentiation by short dip into 1% HCl-alcohol (1% HCl-alcohol in 90% isopropyl alcohol)

■ blueing of the tissue by rinsing under tap water for 10 min

■ dehydrate and mount in DePex medium

2.2.3 Bielschowsky silver staining

Bielschowsky silver staining was performed to determine axonal density. The axons appear black / dark brown and the surrounding tissue yellow / brightly brown.

■ deparaffinization and rehydration (see 2.2)

■ rinse 3 x with dH_2O

■ incubate in 20% silver nitrate solution (in dH_2O) for 20 min under exhaust hood

■ rinse with ddH_2O

■ add dropwise 32% ammonium hydroxide (in dH_2O) to used silver nitrate solution until the formed precipitate cleared while stirring

■ incubate in cleared silver nitrate/ammonium hydroxide solution for 15 min in the dark

■ transfer slides to ddH_2O containing few drops of ammonium hydroxide

■ add 10 drops of developer solution to used silver nitrate/ammonium hydroxide solution and incubate the slides until nerve fibers appear black and the parenchyma brown

■ rinse with dH_2O

■ incubate in 2% sodium thiosulfate solution (in dH_2O) for 2 min and rinse with dH_2O

■ dehydrate and mount in DePex medium

2.3 Immunohistochemical stainings

Immunohistochemical stainings allow specific detection of cell marker proteins by antibodies. Signal visualization was done with the aid of the avidin biotin method. That is, tissue was incubated with an antigen of interest specific primary antibody followed by a further incubation with a biotin conjugated secondary antibody, which was directed against the primary antibody. More information on antibodies used for human tissue see Tab. 2.4, mouse tissue see Tab. 2.6 and secondary antibodies see Tab. 2.5. After the binding of avidin coupled peroxidase (POX) to the biotin and the oxidation of DAB (or AEC for anti-C9Neo antibody) in the presence of H_2O_2 by POX, a visual signal was obtained. The binding efficacy of some antibodies might be impaired due to the fixation of the tissue. In this case antigen retrieval was done with heat, acid

or protease treatments. The immunohistochemical stainings were performed as follows:

■ deparaffinization and rehydration (see 2.2)

■ rinse 3 x with dH$_2$O

■ Antigen retrieval

Antigen retrieval: Citric acid- or Tris-EDTA buffer:

Slides were placed in polystyrene cuvettes, filled with 1mM citric acid buffer (pH 6) or 1mM Tris-EDTA buffer (pH 9) and boiled 5 times in a microwave at 800W for 3 min. After each boiling step the cuvettes were alternately filled with buffer or dH$_2$O. Finally the cuvettes were cooled down for 30 min at RT and rinsed three times with dH$_2$O.

Antigen retrieval: Proteinase solution:

Slides were incubated in 37°C warm proteinase solution for 10 min followed by two rinse steps with dH$_2$O.

■ wash with PBS

■ blockage of endogenous peroxidase to reduce unspecific signals by incubation with 3% H$_2$O$_2$ (in PBS) for 20 min at 4°C

■ rinse 3 x with PBS

■ pre-incubation with 10% FCS (in PBS) for 20 min at RT in a humidified chamber to prevent unspecific antibody binding

■ incubate with primary antibody (diluted in 10% FCS/PBS) over night at 4°C in a humidified chamber (for the detection of mouse plasma cells a biotin conjugated anti mouse IgG was used as a primary antibody without an incubation with a secondary antibody)

■ rinse 3 x with PBS

■ incubate with biotin conjugated secondary antibody (diluted in 10% FCS/PBS) for 1 h at RT in a humidified chamber

■ rinse 3 x with PBS

■ incubate with 0.1% streptavidin conjugated peroxidase (POX) (diluted in 10% FCS/PBS) for 1 h at RT in a humidified chamber

■ rinse 3 x with PBS

■ signal development with DAB solution (or with AEC solution for anti C9Neo antibody)

■ rinse 3 x with PBS

■ DAB signal amplification for the detection of human and mouse CD3 positive cells by incubation with 2% copper sulphate in 0.9% sodium chloride for 10 min

■ wash with dH_2O

■ counterstaining of nuclei with Meyer's hemalaun solution for 30 sec followed by a short dip (1 sec) in dH_2O

■ wash shortly with dH_2O

■ differentiation by short dip into 1% HCl-alcohol (1% HCl-alcohol in 90% isopropyl alcohol)

■ blueing of the tissue by rinsing under tap water for 10 min

■ dehydrate and mount in DePex medium

Tab. 2.4: Antibodies used for formalin fixed and paraffin embedded human tissue.

Antigen	Marker for	Species	Clone	Dilution	Antigen retrieval	Manufacturer
C9Neo	Complement	Rabbit	polyclonal	1:1500	Steamer Citrate	University Cardiff, UK
CD3	T cells	Rat	CD3-12	1:50	MW Citrate	AbD Serotec
CD8	Cytotoxic T cells	Mouse	C8/144B	1:50	MW Citrate	Dako
CD20	B cells	Mouse	L26	1:100	-	Dako
CD138	Plasma cells	Mouse	MI15	1:50	MW EDTA	Dako
CNP	Myelin protein	Mouse	SMI-91	1:200	MW Citrate	Covance
JC-Virus	JC Virus	Mouse	Pab 2003	1:10	Steamer Citrate	uncommercial
KiM1P	Macrophages and Microglia	Mouse	KiM1P	1:5000	MW Citrate	University Kiel, Germany
MAG	Myelin protein	Rabbit	polyclonal	1:1000	MW Citrate	uncommercial
MBP	Myelin protein	Rabbit	polyclonal	1:2000	-	Dako
MOG	Myelin protein	Rat		1:1000	MW Citrate	uncommercial
PLP	Myelin protein	Mouse	PLPC1	1:500	MW Citrate	AbD Serotec

Tab. 2.5: Secondary antibodies conjugated with biotin for immunohistochemistry.

Antigen	Species	Dilution	Manufacturer
Mouse IgG	Sheep	1:200	Amersham
Rabbit IgG	Goat	1:500	Dianova
Rat IgG	Rabbit	1:200	Dako

Tab. 2.6: Antibodies used for formalin fixed and paraffin embedded mouse tissue.

Antigen	Marker for	Species	Clone	Dilution	Antigen retrieval	Manufacturer
B220	B cells	Rat	RA3-6B2	1:200	MW Citrate	BD
CD3	T cells	Rat	CD3-12	1:50	MW Citrate + 1% Triton X	Serotec
CNP	Myelin protein	Mouse	SMI-91R	1:200	MW Citrate	Covance
IgG	Plasma cells	Sheep		1:200	Protease	Amersham
Mac-3	Macrophages / Macroglia	Rat	M3/84	1:200	MW Citrate	BD
MBP	Myelin protein	Rabbit	polyclonal	1:200	none	Dako

BD = Becton Dickinson Biosciences.

2.4 Determination of lesion activity in human CNS tissue

Myelin sheaths are composed of major myelin proteins such as MBP and PLP as well as minor myelin proteins such as CNPase, MAG and MOG. The lesional demyelinating activity of multiple sclerosis lesions can be classified according to myelin proteins incorporated by macrophages (Brück et al., 1995). During the "early active" demyelination process (an early stage in lesion formation) major as well as minor myelin protein degradation products can be detected in the cytoplasm of macrophages (Fig. 2.1 A). In later disease stages termed as "late active" lesions, the minor myelin proteins are already completely degraded and only major myelin proteins can be found in the cytoplasm of macrophages (Fig. 2.1 B). By contrast, "inactive" MS lesions are characterized by lower macrophage numbers, increased microglia activation and neither minor nor major myelin proteins present within macrophages (Fig. 2.1 C).

C
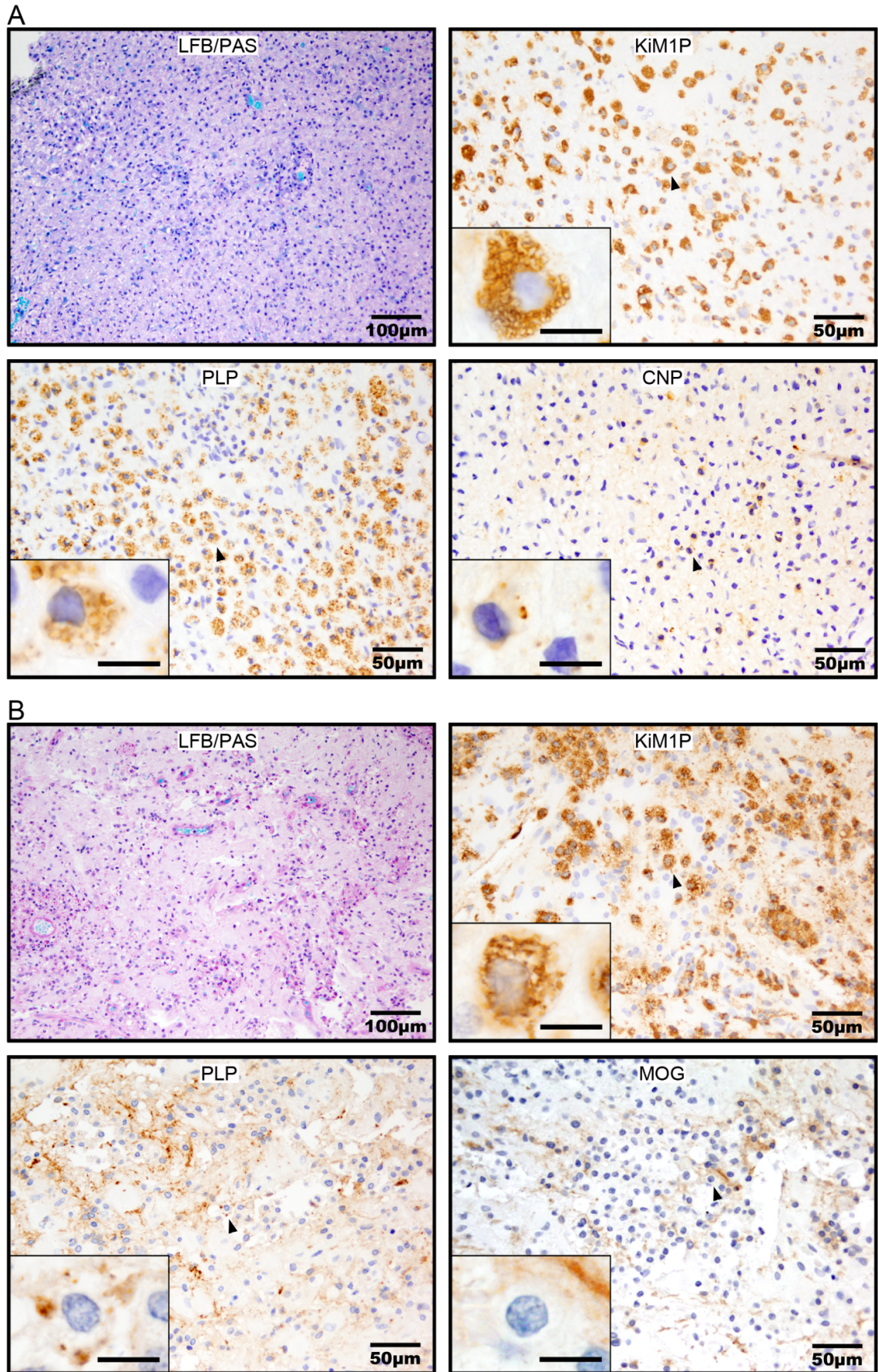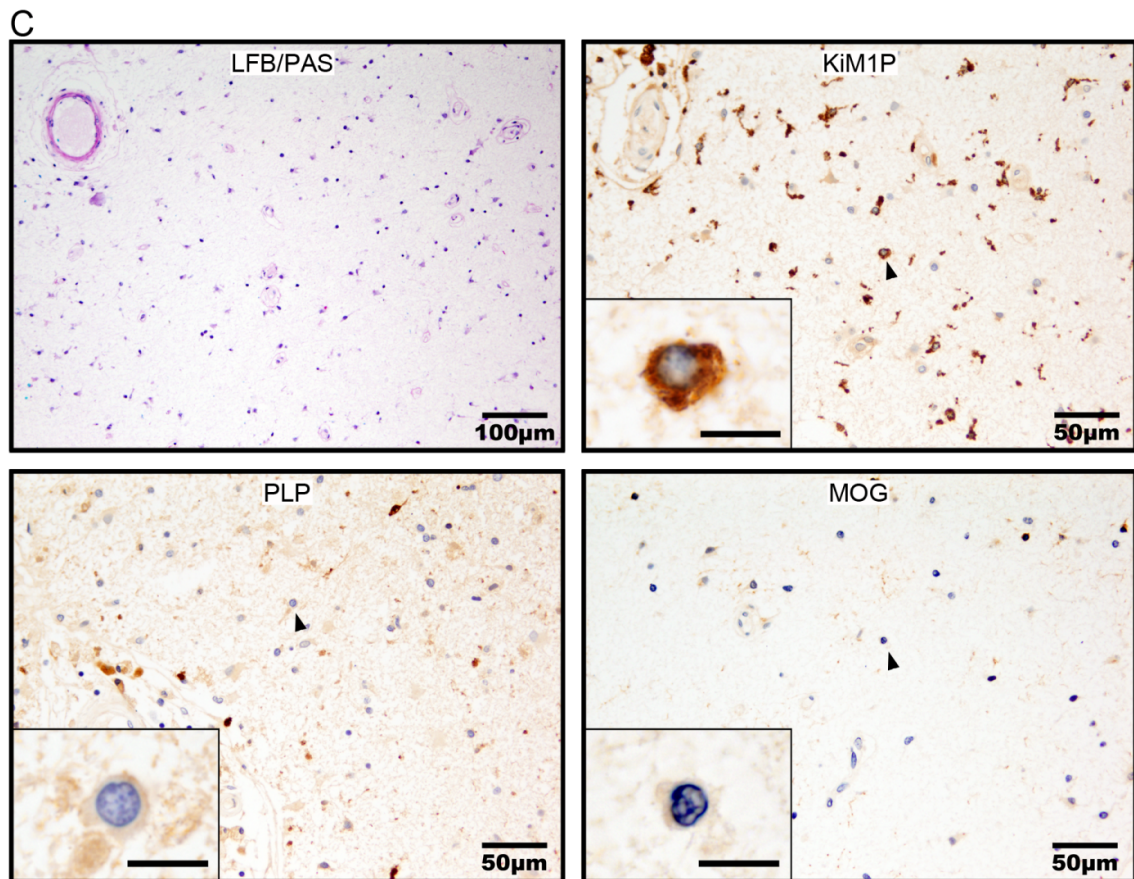
Fig. 2.1: Classification of demyelinating activity. (A) Early active lesion. (B) Late active lesion. (C) Inactive lesion. Scale bar in inset = 10 μm.

2.5 Morphometry in humans

Number of T cells, plasma cells and macrophages / microglia cells stained with the corresponding antibodies was determined in at least 10 standardized microscopic fields defined by an ocular morphometric grid at a 400x magnification and shown as cells/mm².

2.6 Animals

In the second part of my study the results of natalizumab therapy in humans were reviewed in a B cell-dependent EAE model of MS (OSE) after treatment with a natalizumab analogon (PS/2 antibody).

Th mice (Litzenburger et al., 1998) and 2D2 mice (Bettelli et al., 2003) were kindly provided by Prof. Dr. Flügel, Institute for Multiple Sclerosis Research (IMSF) Göttingen Germany and housed under specific pathogen-free (SPF) conditions. The double transgenic OSE mice (Th x 2D2) (Bettelli et al., 2006; Krishnamoorthy et al., 2006) were bred in the central animal facility of the University Medicine Göttingen. Experiments with double transgenic mice were performed under conventional conditions. The mice had access to food and water ad libitum and a 12h/12h light/dark cycle.

2.7 Genotyping

Tissue for the genotyping of the double transgenic mice was obtained during the earmarking procedure or with a tail biopsy. After DNA extraction transgenes were amplified with specific primers and separated by agarose gel electrophoresis. Genotyping was done with a GoTaq PCR kit from Promega and is described in detail below.

<u>DNA extraction:</u>

■ digestion of tissue in 500 µl DNA lysis buffer (activated with 0.1 mg proteinase K) for at least 4 h at 55°C while shaking

■ centrifuge for 2 min at 835g

■ collect supernatant, add 500 µl isopropanol and vortex for 15 sec

■ incubate for 15 min at RT for DNA precipitation

■ centrifuge for 30 min at 2320g

■ discard supernatant and wash pellet with 1 ml cold EtOH

■ centrifuge for 30 min at 2320g

■ discard supernatant and dry pellet

■ add 200 µl DEPC H$_2$O and elute overnight at 55°C

Genotyping PCR Protocol 2D2 (per sample):

9.5 µl   ddH$_2$O

4.0 µl   5x buffer

0.4 µl   dNTPs (10 mM of 2.5 mM each)

0.5 µl   Primer 1 (Va3.2-2D2-M: CCC GGG CAA GGC TCA GCC ATG CTC CTG)

0.5 µl   Primer 2 (Ja18-2D2-M: GCG GCC GCA ATT CCC AGA GAC ATC CCT CC)

(synthesized by Microsynth)

5.0 µl   DNA

0.1 µl   Taq-polymerase (5 U/µl)

Genotyping PCR Protocol Th (per sample):

8.5 µl   ddH$_2$O

4.0 µl   5x buffer

0.4 µl   dNTPs (10 mM of 2.5 mM each)

0.5 µl   Primer 1 IgG WT (mIgH-sense #1: ATT GGT CCC TGA CTC AAG AGA TG)

0.5 µl   Primer 2 IgG WT (mIgH-AS #2: TGG TGC TCC GCT AGT CA AA)

0.5 µl   Primer 1 Th (8.18C5-sense #1: TGA GGA CTC TGC CGT CTA TTA CTG T)

0.5 µl   Primer 2 Th (8.18C5-AS #2: GGA GAC TGT GAG AGT GGT GCC T)

(synthesized by Microsynth)

5.0 µl   DNA

0.1 µl   Taq-Polymerase (5 U/µl)

PCR conditions (T3 Biocycler):

■ Initial denaturation: 94°C, 2 min

■ Denaturation: 94°C, 30 sec

■ Annealing: 2D2: 58°C, 1 min

        Th: 61°C, 1 min

■ Extension: 72°C, 1 min

■ 35 cycles (denaturation till extension)

■ Final Extension: 72°C, 5 min

■ End   4°C, ∞

Agarose gel electrophoresis:

The gel contained 1.8% agarose in TBE buffer and 0.005% ethidium bromide. The electrophoresis was performed in Sub-Cell GT Agarose Gel Electrophoresis System filled with TBE buffer at 120V for 30 min. The visualization and documentation of the PCR products occurred by UV light in a gel-documentation device.

2.8 Clinical evaluation of EAE

Four weeks after birth the OSE mice were weighted and scored for disease severity every other day. After appearance of the first clinical symptoms the mice were monitored every day. EAE scoring system is shown in table 2.7.

Tab. 2.7: Scoring system for clinical symptoms in mice.

Score	Clinical symptoms
0	no clinical symptoms
0.5	tail paresis
1.0	tail paralysis
1.5	slight hind limb paresis
2.0	distinct hind limb paresis, waddling gait, lowered pelvis
2.5	severe hind limb paresis, no ground contact at least with one sole
3.0	hind limb paralysis
3.5	slight fore limb paresis
4.0	severe fore limb paresis
4.5	tetraparalysis, moribund
5.0	death

2.9 Antibody treatment of OSE mice

A monoclonal antibody directed against the murine α-4 integrin with the clone name PS/2 as well as an isotype control antibody rat IgG2bκ directed against the antigen keyhole limpet hemocyanin (KLH) protein were obtained from Bio X Cell (West Lebanon, USA). The endotoxin level for both antibodies was < 2 EU/mg (LAL). Treatments of mice occurred intraperitoneally either with 75 µg of PS/2 antibody in 100 µl sterile PBS or with 100 µl PBS every other day. Two days after the last injection mice were sacrificed. To investigate short-term as well as long-term treatment effects, mice were treated either twice or fifteen times with 75 µg PS/2 antibody or with PBS starting from disease onset (clinical score ≥ 1.0) (Fig. 2.2 A, B). To examine therapy effects in the chronic disease stages mice were treated nine times either with 75 µg PS/2 antibody or with PBS, starting 13 days post disease onset (Fig. 2.2 C). To address the question whether the cessation of the PS/2 antibody therapy leads to a return of disease activity, similar to as before the medication or to a more severe disease activity as compared to before the therapy (rebound), mice were treated fifteen times either with 75 µg of the PS/2 antibody or with PBS starting from disease onset (clinical score ≥ 1.0). After the fifteenth injection, mice were observed for another 15 days before sacrifice (Fig. 2.2 D). In addition, treatment effects were also investigated after long-term treatment with a reduced PS/2 dosage (5 µg) and after short-term treatment with PS/2 F(ab')$_2$ fragments or isotype control F(ab')$_2$ fragments.

The different therapeutic regimens are illustrated below:

A

B

C

D
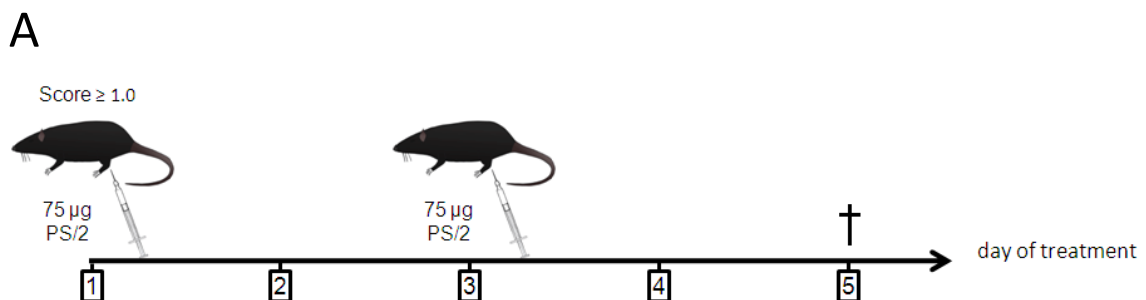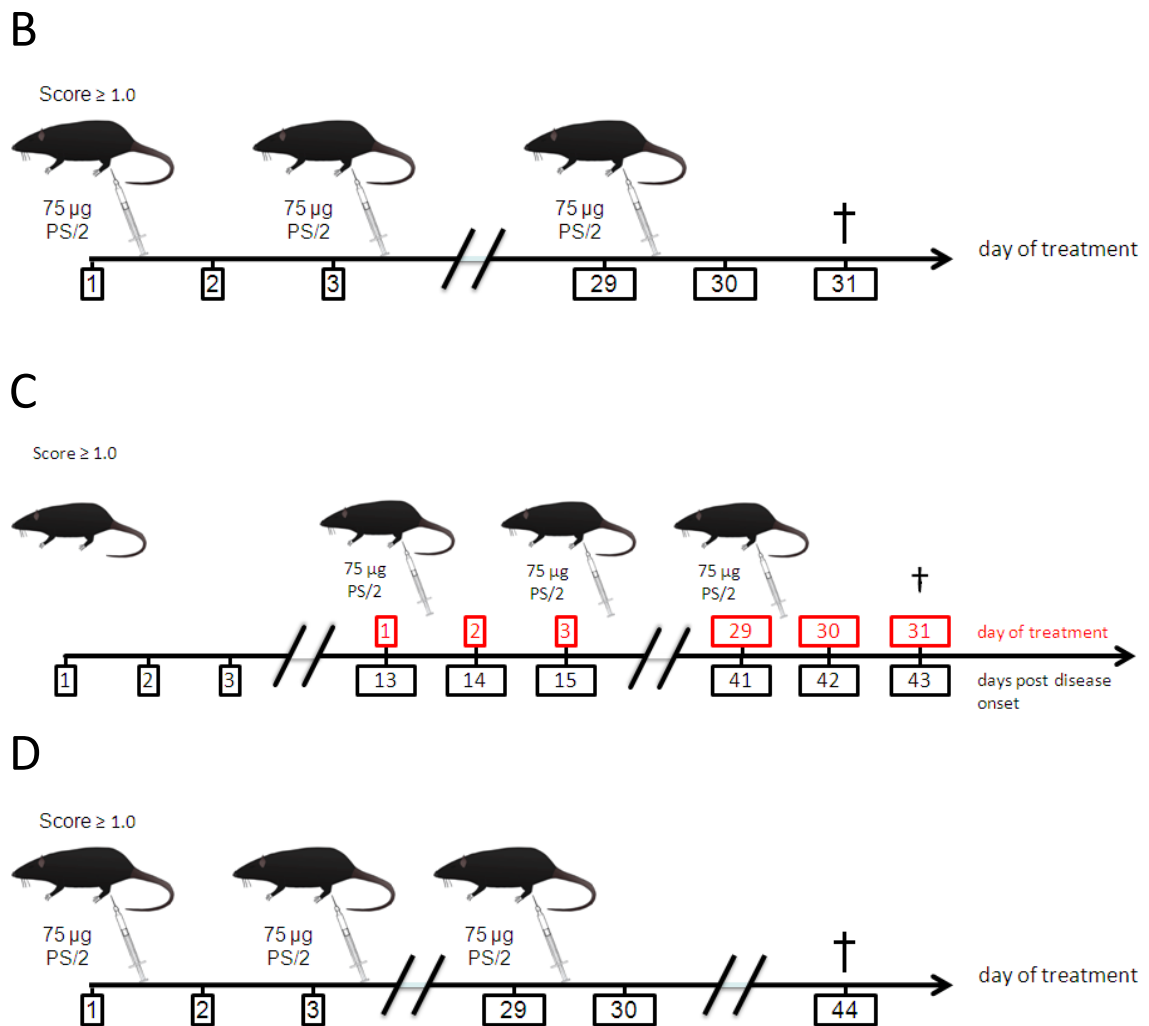
Fig. 2.2: Experimental design.

2.10 Tissue preparation

Mice were deeply anesthetized by an overdose i.p. injection of a ketamine/xylazine mixture. After loss of consciousness the progress of the anesthesia was checked by a pain stimulus as well as the eyelid reflex. The thorax was then opened and a transcardial perfusion was performed through the left cardial ventricle with PBS until all blood was washed out. Subsequently the perfusion occurred with 4% paraformaldehyde to fix the tissue. Head, spine, spleen and liver were extracted and postfixed in 4% PFA over night at 4°C. To make the preparation of the optic nerve easier, the optic nerves were cut off at the eyeball before postfixation. On next day the

brain, including the optic nerves and the spinal cord were taken from the head and spine, respectively. The brain was cut in 2 mm thick coronal slices with the aid of a brain-slice-matrix and the spinal cord with a razor blade into 3 mm long pieces. Then the tissue was washed in water, dehydrated and incubated in paraffin over night. On the following day tissue was embedded in paraffin blocks with Shandon Histocentre 2. 0.5 µm thin sections were cut with a microtome and coated onto glass slides. The sample slides were dried in oven at 37°C over night and stored at RT until further staining procedure (see 2.2 and 2.3).

2.11 Morphometry in mice

Number of T cells, B cells, plasma cells and macrophages was quantified in at least 8 spinal cord cross sections or in 4 optic nerve cross sections at a 400x magnification using an ocular counting grid and shown as cells/mm². For the determination of B cell aggregates in spinal cord meninges more than 20 accumulated B cells were considered as a B cell aggregate. For the determination of white matter demyelination, myelinated as well as demyelinated white matter areas were measured in at least 8 spinal cord cross sections after LFB/PAS staining using Cell^A software. The percentage of demyelinated white matter was calculated relative to the whole white matter area.

2.12 Flow cytometry

The acquisition of samples occurred with the FACS instruments FACSCalibur and FACSCanto II. The evaluation of data was performed using FlowJo software.

2.12.1 Blood collection

Few blood drops were collected from mice by *vein facialis* puncture (Golde et al., 2005) in a tube containing 300 µl blood collection buffer. For WBC number determination a small volume of blood suspension was incubated with RBC lysis buffer

for few minutes followed by WBC quantification with a Neubauer counting chamber. WBC numbers were then calculated as follows:

$$\frac{WBCs}{\mu l} = \frac{cNo * df(1) * df(2)}{sNo * 0.1}$$

cNo   = counted cell number

df(1)   = dilution factor of blood by blood collection buffer

df(2)   = dilution factor of blood-collection buffer by RBC lysis buffer

sNo   = number of investigated squares

*0.*1   = square volume (µl)

2.12.2 Antigen detection on cell surface

For the detection of antigens on the cell surface, blood (in blood collection buffer) containing 60 000 WBCs was pipetted into FACS tubes and the staining procedure continued as follows:

■ wash with FACS buffer by centrifugation at 300 x g for 8 min at 4°C

■ blocking of Fc receptors by resuspension of the cell pellet in 100 µl FACS buffer containing an anti-CD16/32 antibody (Tab. 2.8); antibody incubation for 10 min at 4°C in the dark

(antibody dilution according to the recommendation on the data sheet)

■ wash with FACS buffer by centrifugation at 300 x g for 8 min at 4°C

■ staining of cell surface antigens by resuspension of the cell pellet in 100 µl FACS buffer containing fluorochrome-labelled antibodies (Tab. 2.8, Tab. 2.9); antibody incubation for 20 min at 4°C in the dark

(antibody dilution according to the recommendation on the data sheet)

■ wash twice with FACS buffer by centrifugation at 300 x g for 8 min at 4°C

■ RBC lysis by pipetting of 1000 µl 1x BD lysis buffer to the cell pellet while votexing; after incubation for 3 min at RT the lysis reaction is stopped by addition of 3 ml FACS buffer

The lysis buffer contains also 1.5% paraformaldeyde. Therefore during the lysis procedure cells are also simultaneously fixed.

■ wash with FACS buffer by centrifugation at 300 x g for 8 min at 4°C

■ resuspension of the cell pellet in FACS buffer and short-term storage at 4°C in the dark until FACS analysis

2.12.3 Detection of intracellularly located PS/2 antibody

The detection of intracellularly located (internalized) PS/2 antibody was done with a secondary antibody (anti-rat IgG2b) specific for the PS/2 antibody. In order to prevent binding of the secondary antibody to bound PS/2 antibody to receptors on the cell surface, surface PS/2 antibody was blocked by incubation with a non-fluorophore-conjugated secondary antibody according to the staining protocol 2.12.2. After the last washing step cells were suspended in 100 µl BD cytofix/cytoperm solution and incubated for 30 min at 4°C in the dark. During this step cells are simultaneously fixed and permeabilized. After two washing steps with BD perm/wash buffer at 300 x g for 8 min at 4°C, cells were incubated with fluorophore-conjugated secondary antibody diluted in 100 µl BD perm/wash buffer according to the recommended concentration for 30 min at 4°C. Afterwards cells were washed twice with BD perm/wash buffer at 300 x g for 8 min at 4°C, resuspended in FACS buffer and FACS analysis performed within a narrow time frame. During the intracellular staining the secondary antibody may also unspecifically bind to other intracellular located immunoglobulins. Therefore the measured MFIs were always corrected by the MFIs before PS/2 injection.

Tab. 2.8: Antigen specific FACS antibodies.

Antigen	Species	Isotype	Clone	Fluorochrome	Manufacturer
Anti Rat IgG2b	Mouse	IgG1, κ	MRG2b-85	-	BL
Anti Rat IgG2b	Mouse	IgG1, κ	MRG2b-85	FITC	BL
B220/CD45R	Rat	IgG2a, κ	RA3-6B2	APC	BD
CD3e	Armenian Hamster	IgG1, κ	145-2C11	PE	BL
CD4	Rat	IgG2a, κ	RM4-5	PerCP	BL
CD8a	Rat	IgG2a, κ	53-6.7	APC	BL
CD11b	Rat	IgG2b, κ	M1/70	PE-Cy5	BL
CD16/32	Rat	IgG2a, λ	93	-	BL
CD45	Rat	IgG2b, κ	30-F11	PE	BD
CD45.2	Mouse	IgG2a, κ	104	FITC	eB
CD45.2	Mouse	IgG2a, κ	104	PE	eB
CD49d	Rat	IgG2a, κ	9C10	PE	BL
CD49d	Rat	IgG2b, κ	PS/2	FITC	BL
GR-1	Rat	IgG2b, κ	RB6-8C5	PE	BD
NK 1.1	Mouse	IgG2a, κ	PK136	APC	BL
Syndecan-1	Rat	IgG2a, κ	281-2	PE	BD

Conjugated fluorochromes: FITC = fluorescein isothiocyanate, APC = allophycocyanin,
PE = phycoerythrin, PerCP = peridinin chlorophyll protein, PE-Cy5 = phycoerythrin-cyanine 5.
BL = BioLegend, BD = Becton Dickinson Biosciences, eB = eBioscience

Tab. 2.9: Isotype control FACS antibodies.

Species	Isotype	Clone	Fluorochrome	Manufacturer
Mouse	IgG1, κ	MOPC-31C	FITC	BD
Rat	IgG2a, κ	R35-95	PE	BD
Rat	IgG2b, κ	A95-1	FITC	BD

Conjugated fluorochromes: FITC = fluorescein isothiocyanate, PE = phycoerythrin.
BD = Becton Dickinson Biosciences.

2.12.4 Gating on cell populations

The investigation of T cells (CD3$^+$, CD4$^+$, CD8$^+$), B cells (B220$^+$), plasma cells (Syndecan-1$^+$) and NK cells (NK1.1$^+$) occurred while gating on the lymphocyte population in SSC/FSC (Fig 2.3 A). By contrast, the determination of granulocytes and monocytes was performed while gating on more granular cells and larger cells in SSC/FSC, respectively (Fig. 2.3 B, Fig 2.3 C). In the monocyte gate cells were considered as monocytes with high expression levels for CD11b and moderate to no expression for Gr-1 (Fig 2.3 C), whereas cells in the granulocyte gate with high expression levels for Gr-1 and high to moderate expression levels for CD11b were termed as granulocytes (Fig 2.3 B).
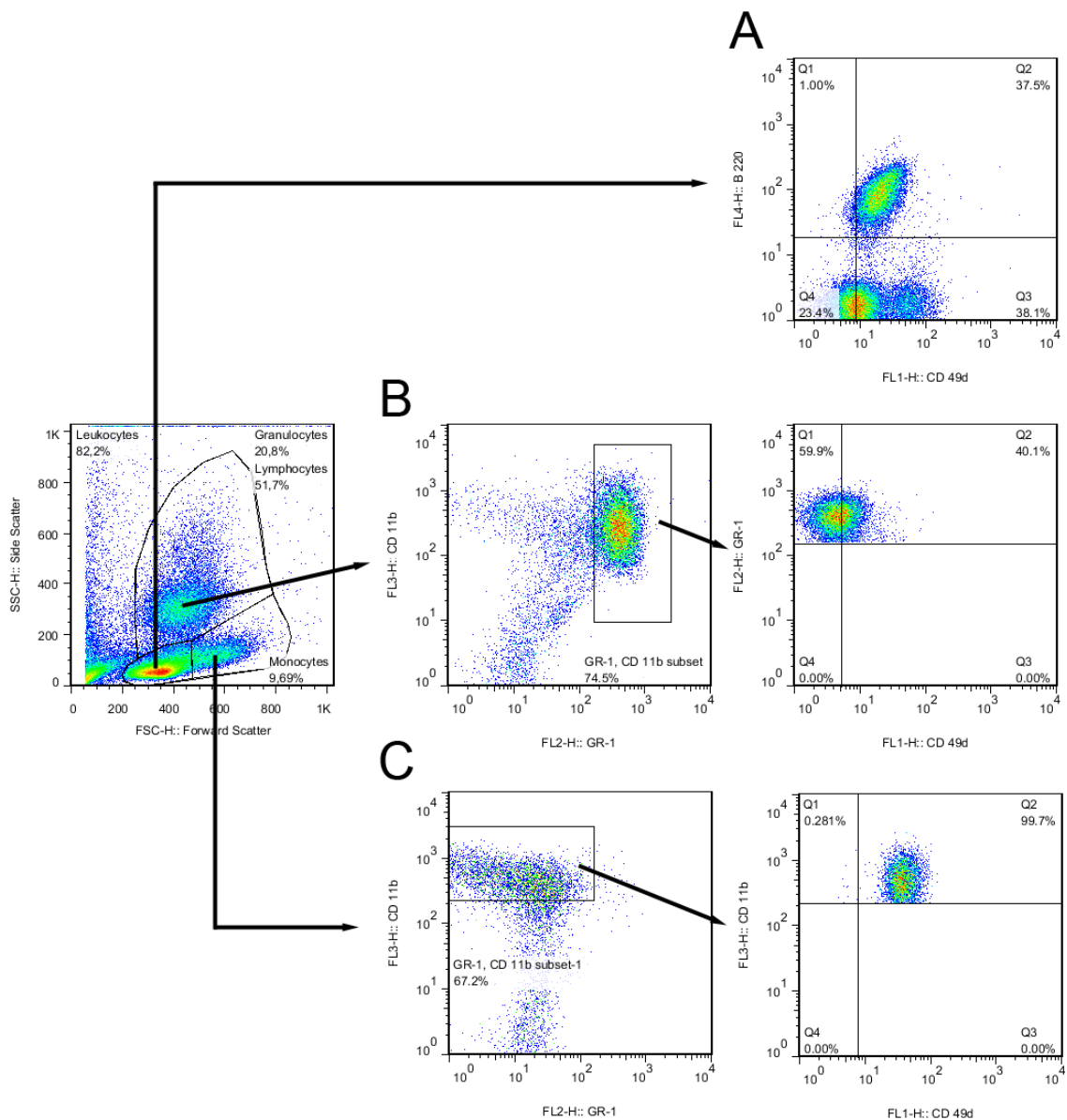
Fig. 2.3: Gating example. (A) B cells, (B) granulocytes, (C) monocytes.

2.13 Generation of F(ab')$_2$ fragments

For the isotype of the PS/2 antibody were described several effector functions (Hughes-Jones et al., 1983; Woof et al., 1986; Haagen et al., 1995). To address the question whether PS/2 therapy without the Fc regions has the same effects as therapy with intact PS/2 antibody, PS/2 F(ab')$_2$ fragments were generated.

2.13.1 Antibody fragmentation

The generation of F(ab')$_2$ fragments occurred by digestion of the PS/2 antibody and isotype control with immobilized pepsin (Fig 2.4). Afterwards the digest was purified by centrifugation and size exclusion steps to get rid of immobilized pepsin as well as Fab and Fc fragments. In a pilot study, incubation of antibody with pepsin in a ratio of 10:1 for 24 hours provided the best yield of F(ab')$_2$ fragments and no remaining intact antibody as determined by sodium dodecyl sulfate polyacrylamide gel electrophoresis (SDS-PAGE) (see 2.13.2). Therefore this ratio was chosen for the following fragmentation experiment. Before fragmentation, antibody was concentrated to 10 mg/ml as well as buffer exchange to digestion buffer was performed to ensure best conditions for the pepsin by centrifugation with vivaspin column containing a membrane with 50kDa molecular weight cut off (MWCO). Antibody concentration was determined by NanoDrop ND-1000 spectrophotometer at 280nm. Immobilized pepsin was washed with digestion buffer by centrifugation at 1000 x g for 5 min. After pepsin resuspension with digestion buffer antibody in a concentration of 10 mg/ml was added in a ratio 10:1 (substrate to enzyme) and incubated at 37°C while shaking for 24 hours. Afterwards the digest was separated from the immobilized pepsin by centrifugation at 1000 x g for 5 min. For maximum fragment recovery immobilized pepsin was washed with washing buffer and the supernate added to the digest. The fragmentation result was then validated by SDS-PAGE. The purification as well as buffer exchange to PBS occurred by centrifugation with vivaspin column containing 30kDa MWCO.
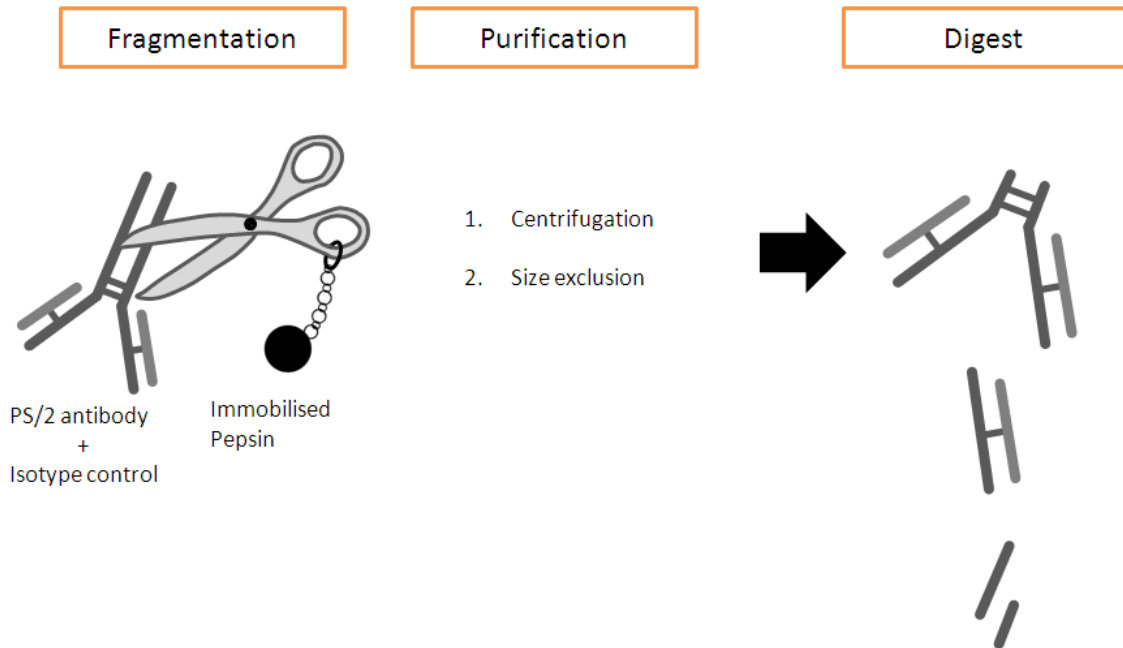
Fig. 2.4: Generation of F(ab')$_2$ fragments.

2.13.2 SDS-PAGE

Fragmented antibodies were analysed by SDS-PAGE under non-reducing and reducing conditions using 6% or 12.5% resolving gels with 4% stacking gels containing loading pockets. Components and proportions for the gels are summerized in Tab 2.10. After pipetting of tetramethylethylenediamine (TEMED) and ammonium persulfat (APS) to the components the resolving gels and stacking gels solidified for 60 min and 20 min, respectively. Afterwards fragmented antibodies were diluted in 4x sample buffer for non-reducing conditions or with 4x sample buffer containing 5% ß-mercaptoethanol for reducing conditions. Non-reduced samples were heated to 70°C and reduced samples to 95°C for 5 min. Samples were loaded onto the gel together with a Precision Plus Protein^{TM} standard marker. Electrophoresis was performed in 1x SDS-PAGE running buffer containing 0.1% SDS. Samples were run in case of one gel by 30mA and in case of two gels by 60mA for 1 hour with the *Mini PROTEAN® 3 Electrophoresis Cell System*. The gels were then rinsed with warm ddH$_2$O and the fragments visualized by incubation with warm coomassie solution while shaking for 15 min. Afterwards the gels were rinsed with warm ddH$_2$O until the fragment bands were clear distinguishable. Gel documentation occurred with a digital camera.

Tab. 2.10: Component proportion in resolving and stacking gel.

	Resolving gel			Stacking gel
	6%	12.5%		4%
Acrylamide/ bis-acrylamide	20%	41.7%	Acrylamide/ bis-acrylamide	16.6%
1.5M Tris/HCl pH 8.9	25%		0.5M Tris/HCl pH 6.8	25%
10% SDS	1%		10% SDS	1%
TEMED	0.05%		TEMED	0.2%
10% APS	0.5%		10% APS	0.5%
add ddH$_2$O to 100%			add ddH$_2$O to 100%	

2.14 Statistical analysis

Graph visualization and statistical analysis was performed using GraphPad Prism 5.o1. Significance between two groups was examined by the Mann-Whitney U test. Significant difference before and after treatment was verified by the Wilcoxon matched pairs test. If more than two groups were compared the one-way analysis of variance (ANOVA) Kruskal-Wallis test was used followed by Dunn's test for multiple comparisons. Investigation of the relationship between two variables occurred with the Spearman r test. Clinical score data, percental reduction of free CD49d binding sites and percental epitope overlap between α-CD49d antibodies are presented as mean ± SEM. Flow cytometry data are shown as mean ± SEM of the median fluorescence intensities (MFIs). All other data are given as median. A value of $p \leq 0.05$ was considered significant and is shown by one asterisk. Significance ≤ 0.01 and ≤ 0.001 is indicated by two asterisks and three asterisks respectively.

3 Results

3.1 Part one: Impact of natalizumab treatment on inflammatory cell infiltrates in CNS tissue of MS patients

<u>Clinical characteristics</u>

12 biopsies and 3 autopsies of natalizumab-treated MS patients with a disease duration between 2 (patient #1) and 20 years (patient #14) (Tab. 2.1) were investigated. 10 of the patients showed relapsing-remitting and 5 patients a secondary progressive disease course. The mean age during biopsy and autopsy was 37 and 48 years, respectively, and the majority of patients were women. The natalizumab medication was very heterogeneous in regard to the number of natalizumab infusions, varying between 1 (patient #1) and 84 infusions (patient #12). In addition one patient (patient #5) received an oral anti α-4 integrin inhibitor (firategrast) instead of natalizumab injection. Furthermore, the interval between the last natalizumab infusion and biopsy / death also varied between 20 days (patient #15) and more than 5 years (patient #4).

<u>General histopathology</u>

Biopsies and autopsies showed typical MS characteristics including white matter demyelination, inflammation, axonal damage and reactive gliosis.

3.1.1 Histology shows increased plasma cell numbers after natalizumab treatment in MS patients

To study the effect on inflammatory cell infiltrates in the CNS after natalizumab therapy, brain biopsies and autopsies were stained immunohistochemically for different cell subsets. The number of T cells (CD3), plasma cells (CD138) and macrophages (KiM1P) was quantified in the lesion and compared to a disease-matched control group. Active demyelinating and inactive demyelinated lesions were evaluated separately as the inflammatory infiltrate varies depending on the disease stage.

Furthermore, autopsies, which most often represent late disease stages, show lower inflammatory cell infiltrates as compared to biopsies. The evaluation of lesions in biopsies and autopsies therefore also was performed separately.

T cells were present in inflammatory demyelinating lesions of natalizumab-treated patients. Quantification of T cell infiltrates in active demyelinating biopsy lesions did not show a significant decrease in T cell numbers compared to controls (natalizumab median: 53 cells/mm², control median: 82 cells/mm²). Also, macrophages were not significantly reduced in natalizumab-treated patients compared to controls (natalizumab median: 1376 cells/mm², control median: 1766 cells/mm²). By contrast, plasma cells numbers were significantly higher in natalizumab-treated MS patients as compared to the control group (natalizumab median: 6 cells/mm², control median: 0 cells/mm²) (Fig. 3.1.1).
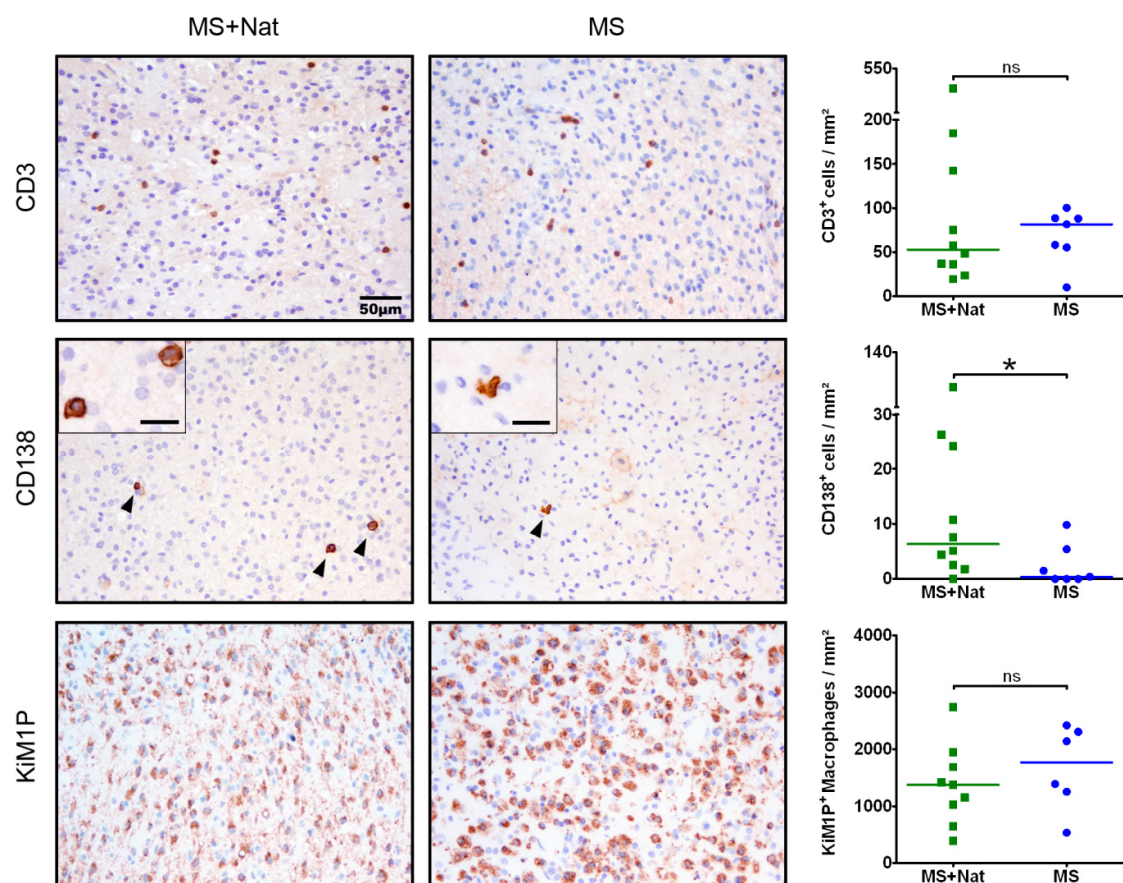
Fig. 3.1.1: Inflammatory infiltrates in natalizumab-treated MS patients (MS+Nat) and controls (MS) in *active demyelinating biopsy lesions.* Natalizumab-treated MS patients showed no significant decrease in T cell and macrophage numbers; however, significantly increased plasma cell numbers were found as compared to MS controls with no prior natalizumab therapy. Inflammatory cell infiltrates were counted in white matter lesions after immunohistochemical staining for T cells (anti-CD3, upper row), plasma

cells (anti-CD138 middle row) and macrophages / microglial cells (KiM1P, lower row). Plasma cells are indicated by black arrowheads. Scale bar in inset = 20 μm.

Analysis of inactive demyelinated autopsy lesions showed similar results. T cell numbers and macrophage numbers after natalizumab therapy were not significantly different compared to the control group (natalizumab median: 14 cells/mm², control median: 17 cells/mm²) (natalizumab median: 267 cells/mm², control median: 109 cells/mm²). By contrast the quantification of plasma cells showed significantly higher numbers in natalizumab-treated patients as compared to controls (natalizumab median: 8 cells/mm², control median: 1 cells/mm²) (Fig. 3.1.2).
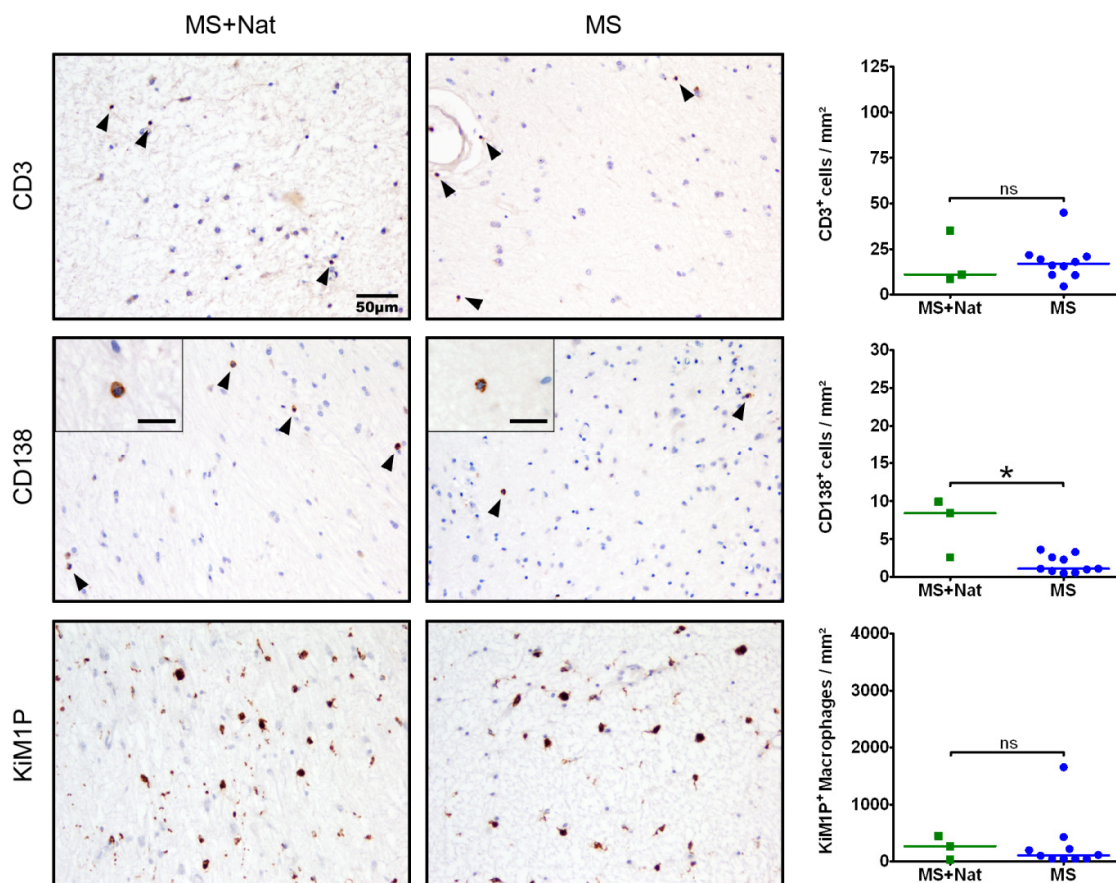
Fig. 3.1.2: Inflammatory infiltrates in natalizumab-treated MS patients (MS+Nat) and controls (MS) in *inactive demyelinated autopsy lesions.* Natalizumab-treated MS patients showed no significant decrease in T cell numbers and no significant increase in macrophage numbers. However, significantly increased plasma cell numbers were found as compared to MS controls with no prior natalizumab therapy. Inflammatory cell infiltrates were counted in white matter lesions after immunohistochemical staining for T cells (anti-CD3, upper row), plasma cells (anti-CD138 middle row) and macrophages / microglia cells (KiM1P, lower row). Plasma cells are indicated by black arrowheads. Scale bar in inset = 20 μm.

The comparison of results obtained from inactive demyelinated biopsy lesions was limited due to the low patient number in the natalizumab-treated group (n=2). Values are shown in Fig. 3.1.3. Plasma cell numbers were increased in the natalizumab-treated group with one patient showing high and the other no plasma cells. Of note, the last natalizumab infusion of the patient with no plasma cells (patient #4) was around 5 years before the biopsy, whereas the biopsy in the patient with high plasma cell numbers (patient #2) was taken 22 days after the last natalizumab infusion (Tab. 2.1).
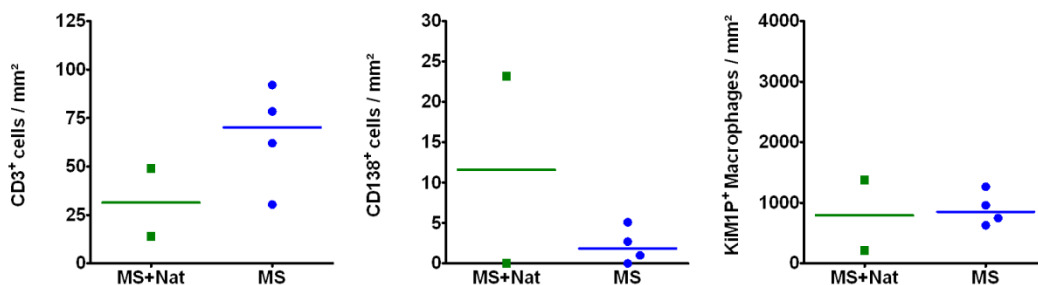
Fig. 3.1.3: Inflammatory infiltrates in natalizumab-treated MS patients (MS+Nat) and controls (MS) in *inactive demyelinated biopsy lesions*. Natalizumab-treated patients showed similar macrophage numbers, decreased T cell numbers and increased plasma cell numbers as compared to MS controls with no prior natalizumab therapy. Inflammatory cell infiltrates were counted in white matter lesions after immunohistochemical staining for T cells (anti-CD3), plasma cells (anti-CD138) and macrophages / microglia cells (KiM1P). Plasma cells are indicated by black arrowheads. Scale bar in inset = 20 µm.

The control group was matched for disease duration, as it is known that plasma cells increase with longer disease duration (Frischer et al., 2009). However, control groups revealed slight differences in mean disease durations as compared to the natalizumab-treated groups. In active demyelinating biopsies as well as in inactive demyelinated autopsies the mean disease duration of the natalizumab-treated group was slightly longer and in inactive demyelinated biopsies slightly shorter as compared to controls (Tab. 3.1.1). Moreover, all three control groups showed a similar mean age at biopsy / autopsy as compared to the respective natalizumab-treated group. All groups had more female than male patients, except for the inactive biopsies of the natalizumab-treated group with an equal distribution of female and male patients as well as the inactive autopsies of the control group with more male patients.

Tab. 3.1.1: Mean disease duration, mean age and sex distribution in natalizumab treated patients and control groups.

	Active demyelinating biopsy lesions		Inactive demyelinated biopsy lesions		Inactive demyelinated autopsy lesions	
	MS+Nat	MS	MS+Nat	MS	MS+Nat	MS
Mean disease duration ± SEM in years	12.2 ± 1.8	8.0 ± 0.9	6.5 ± 2.5	8.8 ± 2.1	13.7 ± 3.5	11.3 ± 2.1
Mean age at biopsy / autopsy ± SEM in years	38.9 ± 1.9	33.3 ± 4.8	28.0 ± 5.0	34.5 ± 3.8	48.0 ± 7.1	48.3 ± 4.0
Sex ♀ / ♂	8 / 2	5 / 2	1 / 1	4 / 0	2 / 1	4 / 6

3.1.2 Higher plasma cell numbers are not dependent on disease duration

To examine whether increased plasma cell numbers in natalizumab-treated patients are due to a longer duration of the disease and therefore are a disease-related effect, plasma cell numbers were investigated dependent of the disease duration. The correlation revealed no dependence between plasma cells and disease duration in active demyelinating lesions (Fig. 3.1.4, Suppl. Tab. 1). Investigation of plasma cells in the parenchyma and perivascular spaces separately also showed no increase with longer disease duration. A statistical correlation was only performed in active demyelinating biopsy lesions, due to the low patient number of inactive demyelinated biopsy lesions as well as active- and inactive demyelinated autopsy lesions.

Macrophages / microglia cells showed no correlation with disease duration. However, CD3^{+} and CD4^{+} T cell numbers were higher with a longer disease duration (CD3^{+} T cells $p = 0.011$, CD4^{+} T cells $p = 0.006$) (Suppl. Tab. 1).
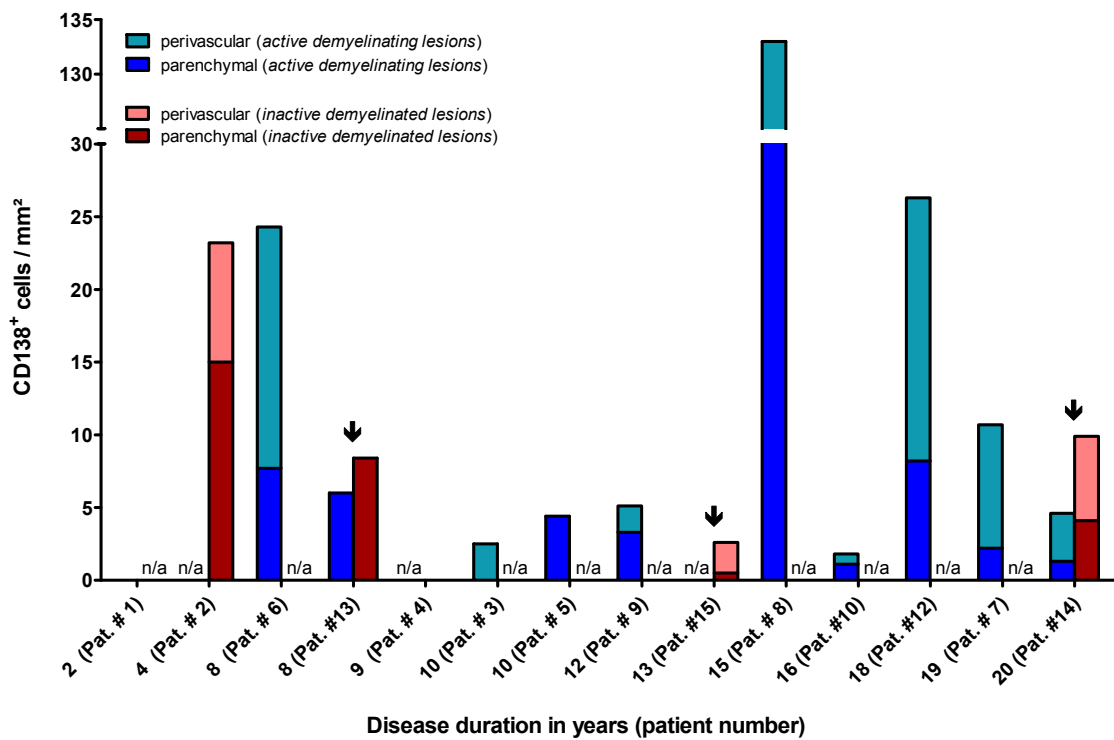
Fig. 3.1.4: Plasma cell numbers in natalizumab-treated patients in relation to disease duration. Plasma cell numbers in the parenchyma, perivascular space as well as plasma cell numbers in total revealed no correlation with longer disease duration. Plasma cell numbers were quantified in active demyelinating and inactive demyelinated lesions in natalizumab-treated patients and are shown in relation to the disease duration in years. Plasma cell numbers in active demyelinating lesions are depicted in blue and in inactive demyelinated lesions in red, whereby cells in the parenchyma are shown in dark color and perivascular cells in light color. Autopsies are indicated by black arrows. The abbreviation n/a was used if no data were available.

3.1.3 Therapy duration has no effect on plasma cell numbers

To address whether a longer natalizumab therapy duration results in plasma cell accumulation, plasma cell numbers were investigated dependent of the therapy duration.

No correlation was found between perivascular, parenchymal or total plasma cell numbers and therapy duration in active demyelinating biopsy lesions (Fig. 3.1.5, Suppl. Tab. 2).

T cells and macrophage numbers were increased with longer therapy duration (CD3^{+} T cells p = 0.031, CD4^{+} T cells p = 0.031, CD8^{+} T cells p = 0.049, macrophages p = 0.043) (Suppl. Tab. 2).
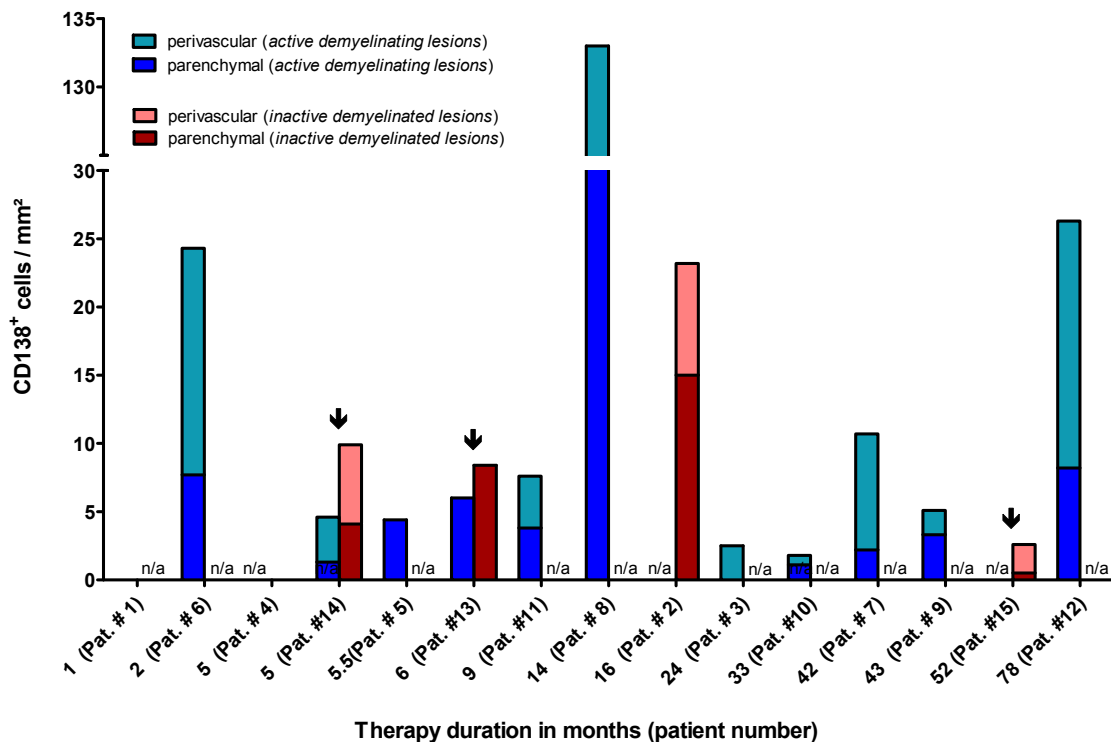
Fig. 3.1.5: Plasma cell numbers in natalizumab-treated patients in relation to therapy duration. Plasma cell numbers in the parenchyma, perivascular space as well as total number of plasma cells revealed no correlation with longer ongoing therapy duration. Plasma cell numbers were quantified in active demyelinating and inactive demyelinated lesions in natalizumab-treated patients and correlated with therapy duration. Plasma cell numbers in active demyelinating lesions are depicted in blue and in inactive demyelinated lesions in red, whereby cells in the parenchyma are shown in a dark color and perivascular cells in a light color. Autopsies are indicated by black arrows. The abbreviation n/a was used if no data were available.

3.1.4 Is there a decrease in plasma cells and an increase in T cells when the natalizumab treatment effect ceases?

To examine whether plasma cell numbers in natalizumab-treated patients are dependent on the time interval since the last natalizumab application, cell numbers were analyzed in correlation to the time interval between last natalizumab infusion and biopsy or death.

No correlation between perivascular, parenchymal or total plasma cell numbers and the time interval between the last natalizumab injection and biopsy or death was found (Fig. 3.1.6, Suppl. Tab. 3).
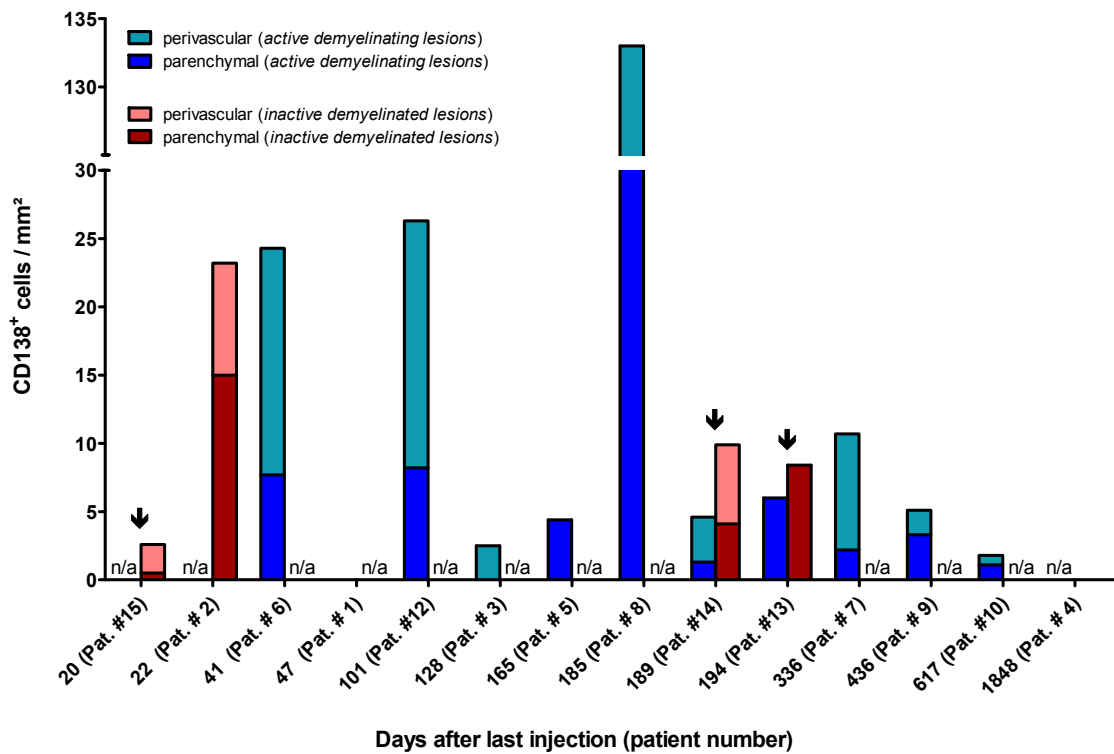
Fig. 3.1.6: Plasma cell numbers in natalizumab-treated patients in relation to the time interval between last natalizumab infusion and biopsy or death. Plasma cell numbers in the parenchyma, perivascular space as well as total plasma cell numbers showed no dependence on this time interval. Plasma cell numbers were quantified in active demyelinating and inactive demyelinated lesions in natalizumab-treated patients and correlated with the time interval between last natalizumab infusions and biopsy / autopsy. Plasma cell numbers in active demyelinating lesions are depicted in blue and in inactive demyelinated lesions in red, whereby cells in the parenchyma are shown in a dark color and perivascular cells in a light color. Autopsies are indicated by black arrows. The abbreviation n/a was used if no data were available.

CD3^{+} T cells (Fig. 3.1.7, Suppl. Tab. 3) and macrophages / microglial cells (Fig. 3.1.8, Suppl. Tab. 3) also did not correlate with the time interval after the last natalizumab infusion. However, perivascular CD4^{+} T cell numbers were increased with longer interruption of natalizumab therapy (p = 0.043) (Suppl. Tab. 3).

After discontinuing natalizumab treatment, a decrease in free CD49d receptor binding sites on PBMCs was described for a further 3½ months as compared to levels before the first injection (Wipfler et al. 2011). To determine whether the natalizumab activity has an influence on plasma cell numbers, cell numbers of all active demyelinating biopsies until 3½ months after the last injection were compared to cell numbers of all remaining active demyelinating biopsies. The comparison of both groups showed a

tendency for increased plasma cell numbers during the first 3½ months after halting natalizumab treatment compared to the other group in which no natalizumab activity was expected (Fig. 3.1.9). By contrast T cell numbers tended to be lower in the first 3½ months compared to later time points. Analysis was hampered by low patient numbers for different groups.
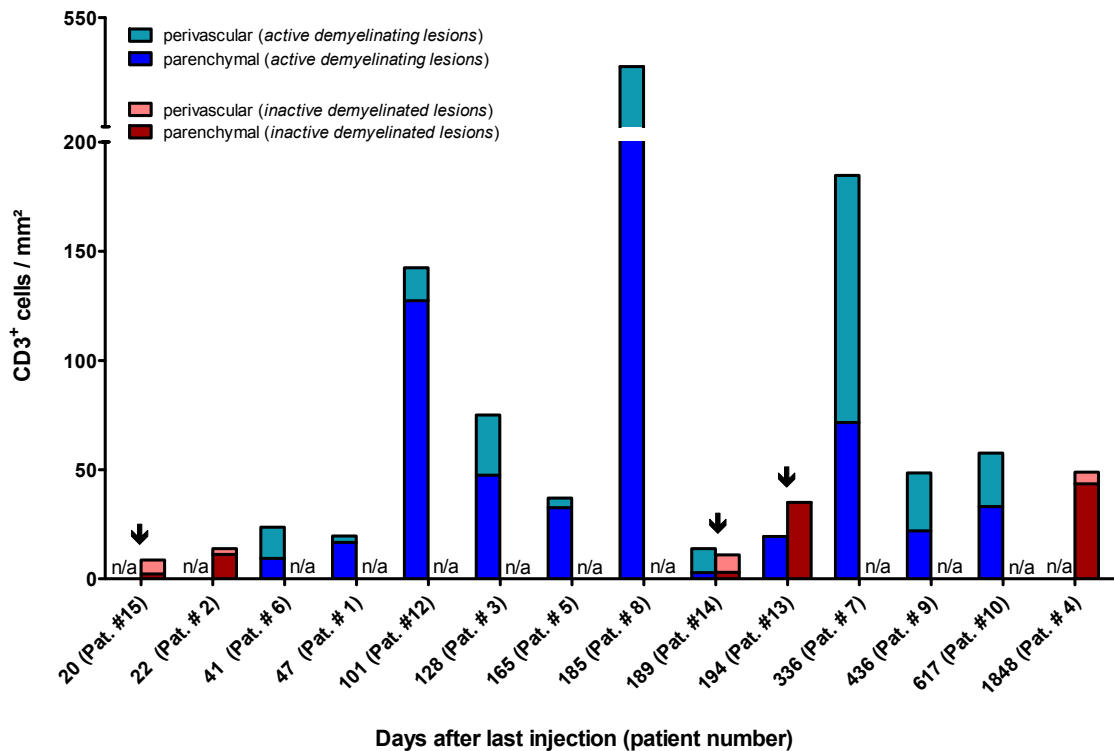
Fig. 3.1.7: T cell numbers in natalizumab-treated patients in relation to the time interval between last natalizumab infusion and biopsy or death. CD3^{+} T cell numbers in the parenchyma, perivascular space as well as total CD3^{+} T cell numbers showed no dependence on this time interval. CD3^{+} T cell numbers were quantified in active demyelinating and inactive demyelinated lesions in natalizumab-treated patients and correlated with the time interval between last natalizumab infusions and biopsy / autopsy. CD3^{+} T cell numbers in active demyelinating lesions are depicted in blue and in inactive demyelinated lesions in red, whereby cells in the parenchyma are shown in a dark color and perivascular cells in a light color. Autopsies are indicated by black arrows. The abbreviation n/a was used if no data were available.
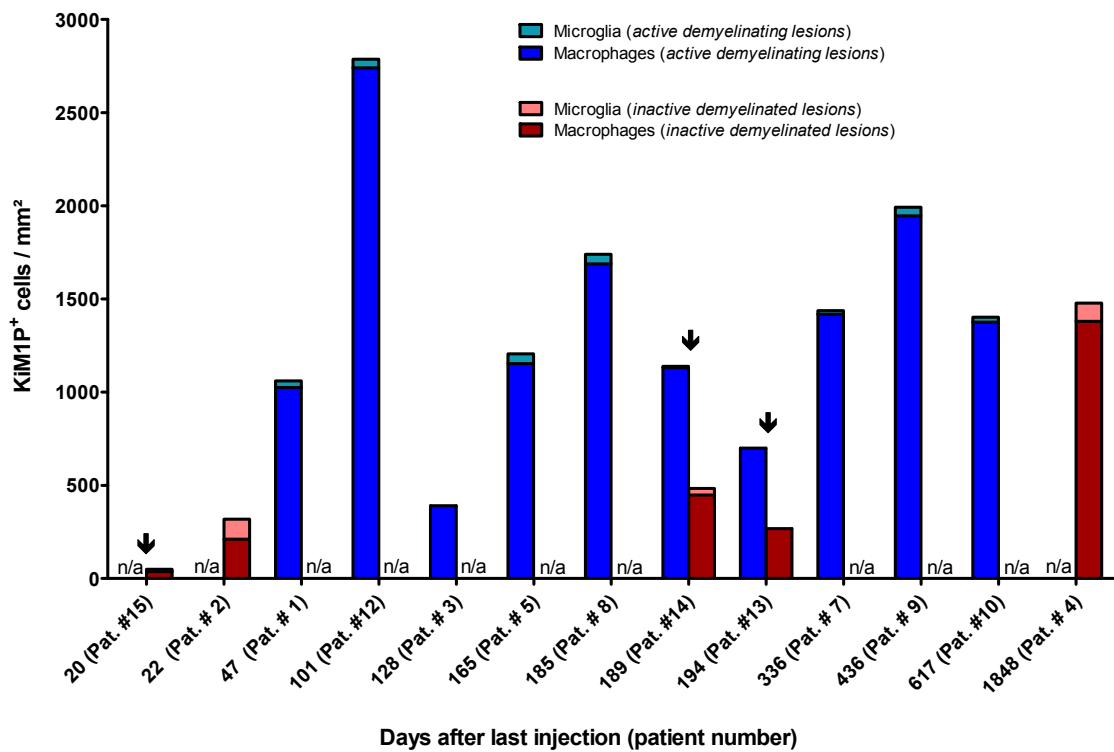
Fig. 3.1.8: Number of macrophages and microglia in natalizumab-treated patients in relation to the time interval between last natalizumab infusion and biopsy or death. Macrophage numbers showed no dependence on this time interval. Macrophage / microglia numbers were quantified in active demyelinating and inactive demyelinated lesions in natalizumab-treated patients and correlated with the time interval between last natalizumab infusions and biopsy / autopsy. Cell numbers in active demyelinating lesions are depicted in blue and in inactive demyelinated lesions in red, whereby macrophages are shown in a dark color and microglia in a light color. Autopsies are indicated by black arrows. The abbreviation n/a was used if no data were available.
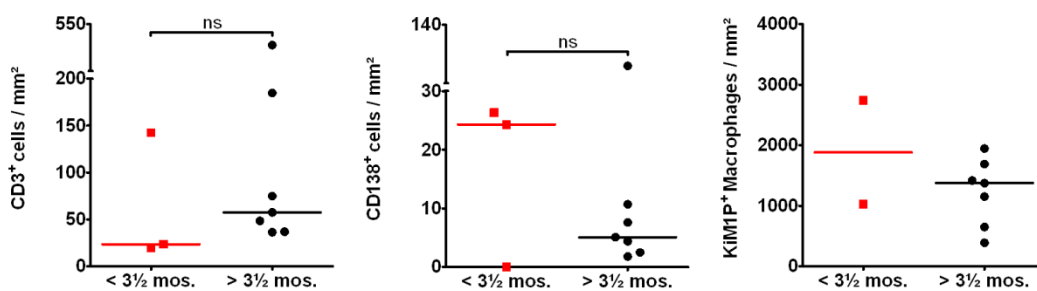
Fig. 3.1.9: Number of inflammatory cell infiltrates in active demyelinating biopsy lesions during the activity period of natalizumab. Analysis showed a tendency toward increased plasma cell numbers as well as decreased T cell numbers during the first 3½ months after discontinuing natalizumab treatment, in comparison to the other group in which no natalizumab activity was expected. Inflammatory cell infiltrates were counted in white matter lesions after immunohistochemical staining for T cells (anti-CD3), plasma cells (anti-CD138) and macrophages / microglia cells (KiM1P). Cell numbers during natalizumab activity (< 3½ mos.) were compared to cell numbers where no more natalizumab activity was expected (> 3½ mos.). < 3½ mos. = cell numbers of natalizumab-treated patients with a treatment interruption of less than 3½ months. > 3½ mos. = cell numbers of natalizumab-treated patients with a treatment interruption of more than 3½ months.

In summary, inflammatory cells are present in demyelinating lesions of natalizumab-treated patients. T cell numbers were not significantly different compared to MS patients without natalizumab treatment. Natalizumab-treated MS patients showed significantly higher plasma cell numbers in active demyelinating as well as in inactive demyelinated lesions as compared to MS patients with no natalizumab therapy. Higher plasma cell numbers did not correlate with the disease duration or the therapy duration. Plasma cells tended to be higher and T cells to be lower when natalizumab was still pharmacologically active compared to later time points.

3.2 Part two: Treatment effects with the natalizumab-analogon PS/2 in a B cell-dependent mouse model of demyelination

In the second part of the work, the results of the natalizumab therapy in humans were reviewed in an EAE model of MS. Due to the clinical relevance of B cells in MS pathogenesis, the high frequency of lesions with immune pattern II as well as the noteworthy findings on plasma cells in this present study, therapy effects were analyzed in a B cell-dependent mouse model of demyelination. For medication the natalizumab-analogon with the clone name PS/2 was used. It is a monoclonal antibody specifically binding CD49d receptors in mice.

3.2.1 Determination of an appropriate treatment dosage and treatment interval

To study the effects after treatment with the α-CD49d (PS/2) antibody, an appropriate dosage was determined (Fig. 3.2.1). The intraperitoneal injection of 75 μg of the α-CD49d (PS/2) antibody in adult mice revealed a strong saturation of the CD49d receptors on WBCs by about 90% for at least 72 hours. 144 hours after the injection, a decrease in free CD49d binding sites by about 15% as compared to levels before the injection was found (Fig. 3.2.1, green curve). Up to 72 hours after injection about 80% of the PS/2 antibody was bound to CD49d receptors compared to measurements directly after treatment. The amount of bound antibody then declined, reaching about 10% of PS/2 antibody bound to the CD49d receptors 144 hours after the injection (Fig. 3.2.1, blue curve).

In natalizumab-treated patients a strong and continuous decrease in unblocked CD49d receptors in PBMCs was shown (Wipfler et al., 2011). The results showed that the saturation achieved with an intraperitoneal injection of 75 μg PS/2 antibody every other day corresponds best with the data in humans, and thus this regimen was chosen for the subsequent experiments.
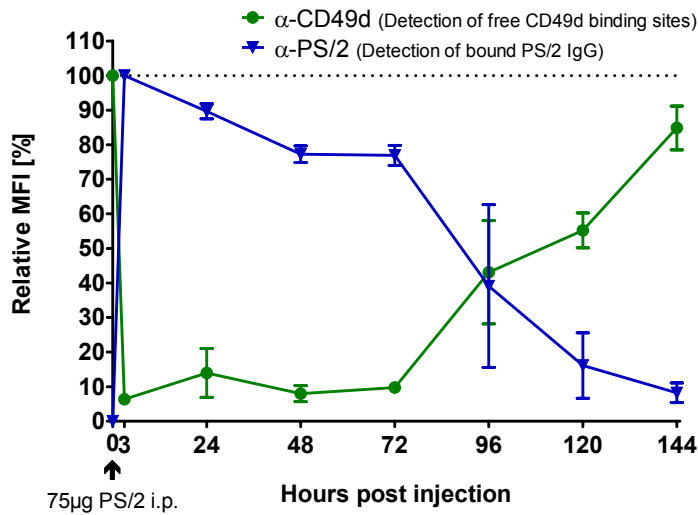
Fig. 3.2.1: Detection of free CD49d binding sites as well as the proportion of bound PS/2 antibody to CD49d receptors upon a single intraperitoneal injection. Before and at definite time points after a single intraperitoneal injection of 75 µg of the α-CD49d (PS/2) antibody in adult mice, blood was collected and flow cytometry analysis was performed. The detection of free CD49d binding sites occurred with a fluorophore-conjugated α-CD49d (PS/2) antibody (green curve). To measure the proportion of bound PS/2 antibody to CD49d receptors a fluorophore-conjugated α-PS/2 antibody was used (blue curve). Relative MFI is given for all WBCs and was calculated by the median fluorescence intensity of interest minus the median fluorescence intensity of the isotype control. Data are mean ± SEM, n = 3-10.

3.2.2 Treatment effects in the peripheral blood

To assess whether the PS/2 antibody therapy has an effect on peripheral blood cells, blood samples were collected before antibody injection as well as on the day animals were sacrificed. Flow cytometry analysis of WBCs was performed. Data from short-term therapy experiments are shown. Similar findings were found in long-term treatment experiments (data not shown).

3.2.2.1 Reduction of free CD49d receptor binding sites on WBCs as well as the proportion of CD49d-positive cells in the blood after treatment with PS/2 antibody

Before α-CD49d (PS/2) antibody injection flow cytometry analysis showed different CD49d expression levels in different cells subsets (Fig. 3.2.2). The lowest MFI was observed for Gr-1$^+$ cells (4.4 ± 0.2), followed by CD4$^+$ cells (10.2 ± 0.4) and CD8$^+$ cells (13.7 ± 3.3). Higher MFIs were measured for Syndecan-1$^+$ cells (25.9 ± 1.0) and B220$^+$ cells (30.3 ± 0.7). Highest MFIs were noticed on NK1.1$^+$ cells (48.7 ± 2.2) and CD11b$^+$ cells (62.6 ± 1.3) (Fig. 3.2.2 A, C). At the end of the experiment, two days after the last PS/2 antibody injection, the CD49d MFI was significantly reduced in all immune cell subsets (Fig. 3.2.2 A, C). The reduction of free CD49d receptor binding sites exceeded 90% in all cell subsets as compared to before therapy (Fig. 3.2.2 D).
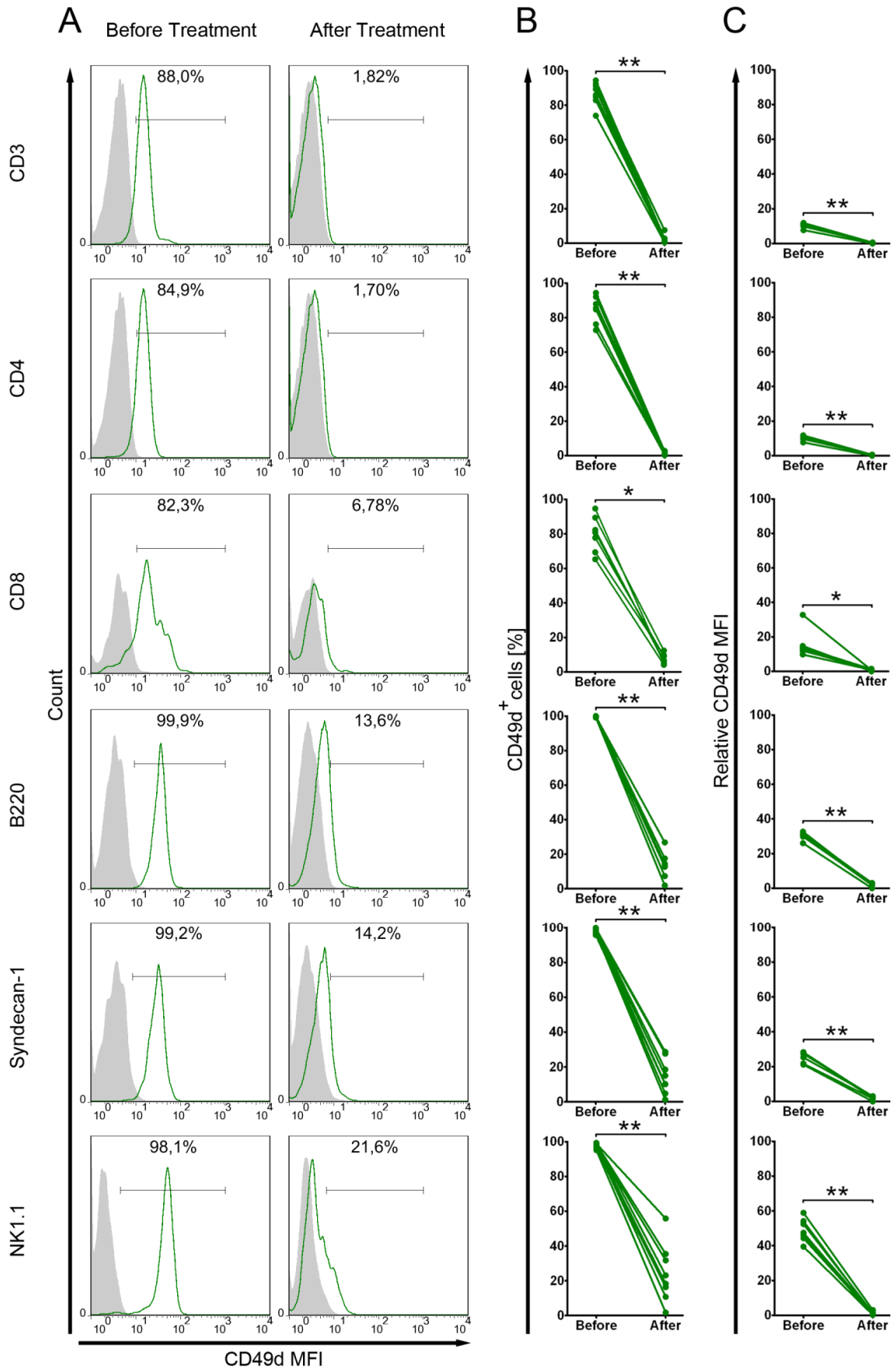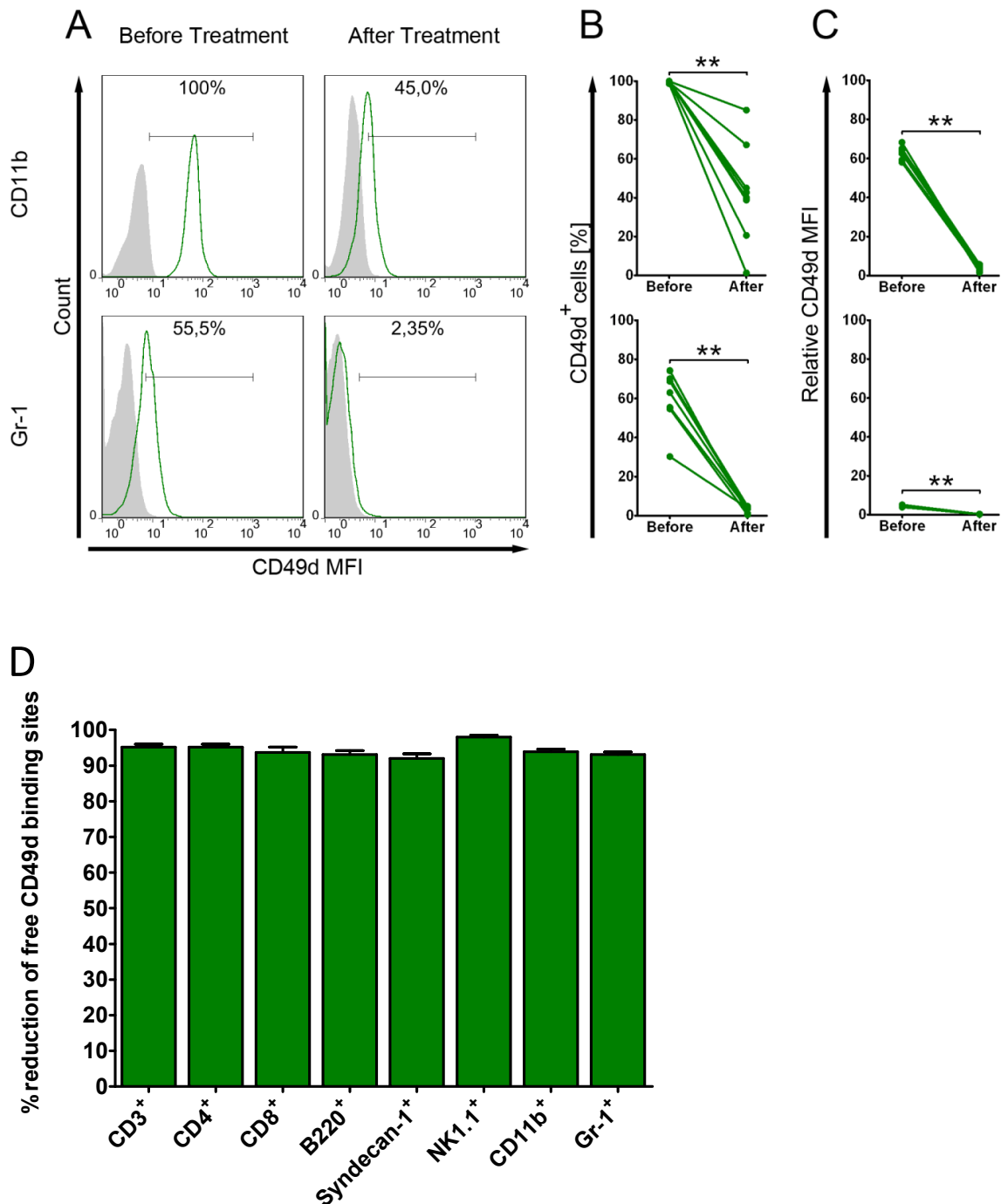
CD49d MFI

Fig. 3.2.2: Percentage of CD49d$^+$ cells and relative CD49d MFI before and after short-term treatment with α-CD49d (PS/2) antibody. A strong reduction of CD49d-free binding sites as well as a decrease in CD49d-positive cells in all investigated immune cell subsets after the short-term treatment with α-CD49d (PS/2) antibody was found. Before and after the treatment blood was collected and flow cytometry analysis on WBCs was performed. The CD49d MFI on CD3$^+$, CD4$^+$, CD8$^+$, B220$^+$, Syndecan-1$^+$ and NK1.1$^+$ cells was determined while gating on the lymphocyte population in SSC/FSC. By contrast, the CD49d MFI on CD11b$^+$ and Gr-1$^+$ cells was investigated by gating on the monocyte and granulocyte population, respectively. Connected dots before and after treatment in (B) and (C) represent data obtained from one mouse. Relative MFI in (C) is given as the median fluorescence intensity of CD49d minus the median fluorescence intensity of the isotype control. (D) Percentage reduction of free CD49d binding sites after the treatment was calculated as follows: relative median fluorescence intensity before treatment divided by the relative median fluorescence intensity after treatment.

Furthermore, the immune cell subsets in blood showed different percentage proportions of CD49d$^+$ cells before the α-CD49d (PS/2) antibody injection. The lowest percentage proportion of CD49d$^+$ cells was found in the Gr-1$^+$ population (61.4 ± 4.9%) followed by the CD8$^+$ population (80.0 ± 3.7%) and the CD4$^+$ population (84.8 ± 2.6%). In all remaining cell subsets the percentage proportion of CD49d$^+$ cells was higher than 97% (NK1.1$^+$ population = 97.6 ± 0.5%, Syndecan-1$^+$ population = 98.4 ± 0.5%, CD11b$^+$ population = 99.8 ± 0.2%, B220$^+$ population = 99.8 ± 0.1%) (Fig. 3.2.2 A, B). Two days after the last injection the percentage proportion of CD49d$^+$ cells was significantly reduced in all immune cell subsets (Fig. 3.2.2 A, B). Almost no CD49d$^+$ cells were observed in the CD4$^+$ population (1.3 ± 0.3%) and Gr-1$^+$ population (2.9 ± 0.6%). About one-tenth of CD49d$^+$ cells were seen in the CD8$^+$ population (7.6 ± 1.0%), the B220$^+$ population (13.5 ± 2.4%) and the Syndecan-1$^+$ population (14.5 ± 3.3%). The highest proportion of CD49d$^+$ cells were found in the NK1.1$^+$ population (24.1 ± 5.5%) as well as the CD11b$^+$ population (42.6 ± 8.5%).

The control group showed no significant differences regarding the CD49d MFI as well as a similar proportion of CD49d positive cells before as compared to after the treatment ruling out a disease-dependent effect on the CD49d expression (Fig. 3.2.3 A, B, C and Suppl. Tab. 4).
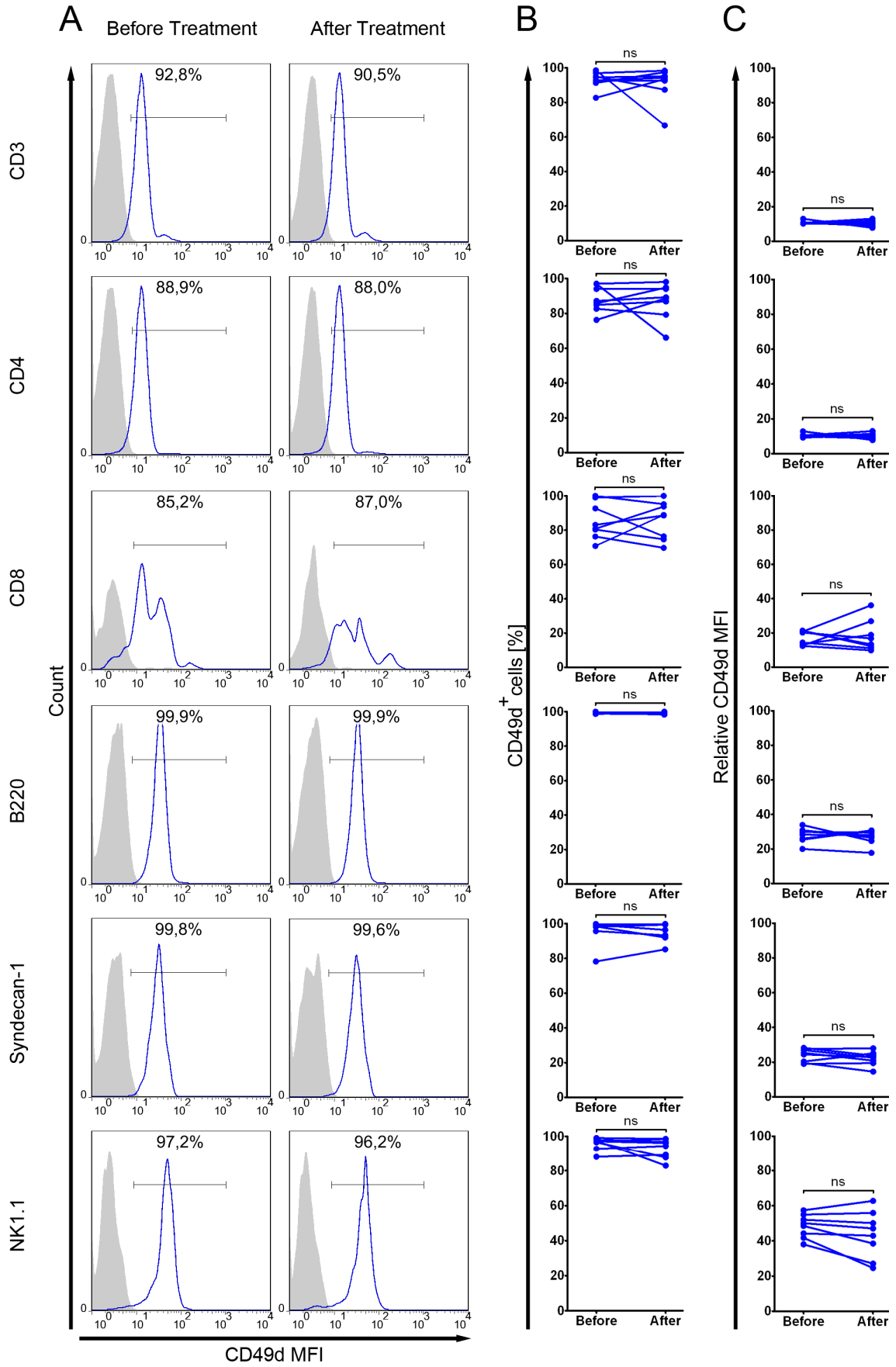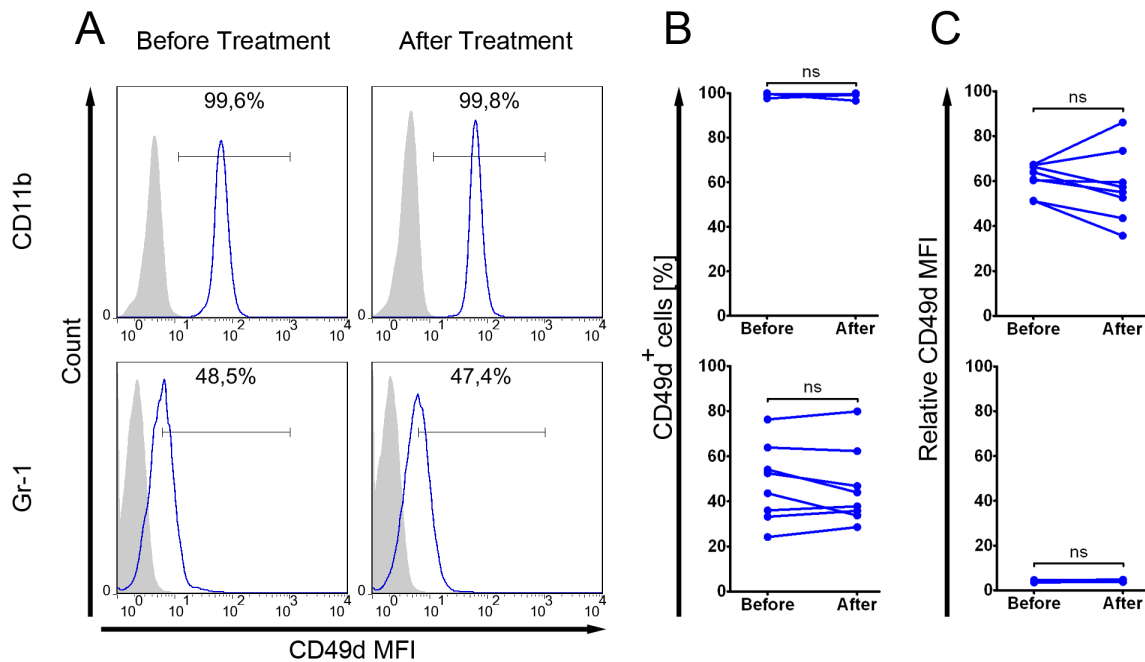
Fig. 3.2.3: Percentage of CD49d$^+$ cells and relative CD49d MFI before and after short-term treatment with PBS. Within the control group no significant differences in regard to the CD49d MFI as well as similar proportions of CD49d-positive cells before as compared to after the PBS treatment were evident. Before and after the treatment, blood was collected and flow cytometry analysis on WBCs was performed. For more information regarding gating of the WBC subpopulations see figure description Fig. 3.2.2. Connected dots before and after treatment in (B) and (C) represent data obtained from one mouse. Relative MFI in (C) is given as the median fluorescence intensity of CD49d minus the median fluorescence intensity of the isotype control.

3.2.2.2 Increase in absolute WBC numbers after treatment with the PS/2 antibody

To examine whether PS/2 antibody therapy has an effect on absolute WBC numbers, blood samples were collected before the antibody injection as well as on the sacrifice day and the absolute cell number of blood cells was determined with the Neubauer counting chamber. The absolute number of immune cell subsets was then calculated based on the percentages investigated with the flow cytometry analysis. The data described here for the short-term therapy.

The α-CD49d (PS/2) antibody therapy resulted in a significant increase in the WBC numbers (before treatment: 4061 ± 404 cells/µl, after treatment: 13329 ± 1969 cells/µl) (Fig. 3.2.4 A). Investigation of a different cell subpopulation showed a significant increase in cell number after therapy, albeit to a different extent (Fig. 3.2.4 A).

A
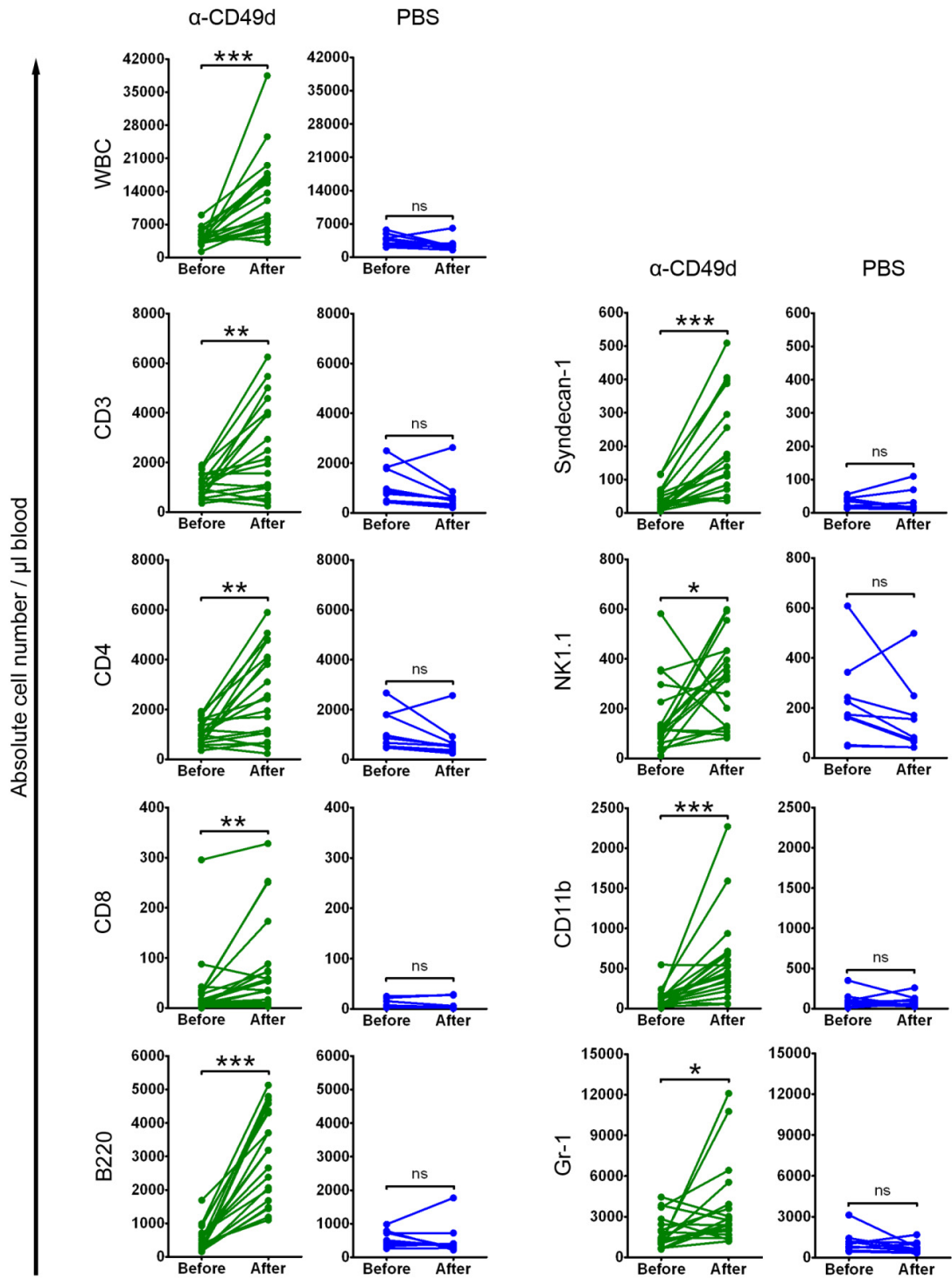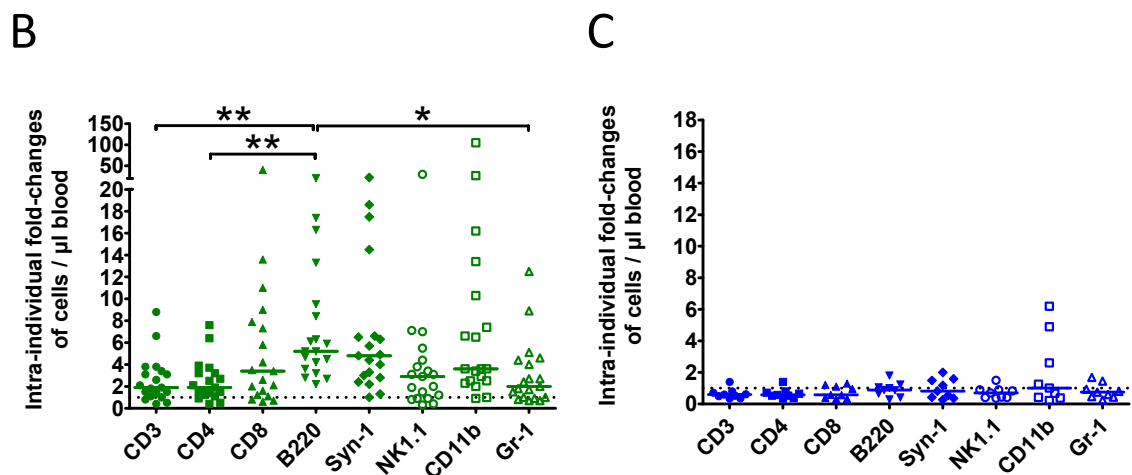
Fig. 3.2.4: Absolute cell numbers of WBCs before and after short-term treatment with the α-CD49d (PS/2) antibody or PBS. α-CD49d (PS/2) antibody therapy resulted in a significant increase in the absolute number of all investigated WBCs but not after the treatment with PBS. The highest intra-individual fold-change in cell numbers was observed for B220^{+} cells. Before and after treatment blood was collected and the absolute cell number determined with the Neubauer counting chamber. The absolute number of immune cell subsets was then calculated based on the percentages of cell subsets determined by flow cytometry analysis. (A) Connected dots before and after treatment represent data obtained from one mouse. Mice treated with α-CD49d (PS/2) antibody are shown in green and with PBS in blue. (B) and (C) intra-individual fold-change of cell subsets were calculated as follows: The absolute cell number after treatment was divided by the absolute cell number before treatment. Treatment results with α-CD49d (PS/2) antibody are depicted in (B) and with PBS in (C). Data are given as median.

To investigate the increase in cell numbers of different WBC subpopulations in more detail, an intra-individual fold-change was determined. The lowest intra-individual increase in absolute cell numbers was observed for the Gr-1^{+} population (median increase: 1.7-fold), followed by the CD4^{+} population (median increase: 1.9-fold) (Fig. 3.2.4 B). Higher intra-individual increases were noticed in the NK1.1^{+} population (median increase: 2.9-fold), the CD8^{+} population (median increase: 3.4-fold) and the CD11b^{+} population (median increase: 3.6-fold). The highest intra-individual increases were found in the Syn-1^{+} population (median: 4.8-fold) and B220[+] population (median: 5.2-fold). The intra-individual fold-change of the B220^{+} population was significantly higher as compared to the Gr-1^{+} population ($p \leq 0.05$) and the CD4^{+} population ($p \leq 0.01$) (Fig. 3.2.4 B).

As expected, the control group showed no significant differences in either the absolute cell number or in the intra-individual fold-change of cell numbers (Fig. 3.2.4 A, C and Suppl. Tab. 5).

In summary, PS/2 therapy strongly reduced free CD49d receptor binding sites on different immune cell subsets and increased leukocyte numbers in blood.

3.2.3 Treatment effects in the CNS

3.2.3.1 Short-term therapy

To address the question as to whether the PS/2 antibody therapy has a therapeutic effect when applied early, short-term treatment experiments were performed. Upon first clinical symptoms, at least a tail paralysis (clinical score ≥ 1.0), mice were treated twice either with 75 µg of α-CD49d (PS/2) antibody or PBS every other day (Fig. 3.2.5). Two days after the last injection, pathology of the CNS was investigated.

3.2.3.1.1 Decreased clinical severity after treatment with the PS/2 antibody

As the OSE mouse model is a spontaneous, genetically caused EAE model, mice develop symptoms at different ages and clinical courses with a varying severity. Thus, a careful randomization of animals to the study and control group was necessary. Randomization was performed in regard to age, sex as well as clinical score at therapy onset to obtain comparable results (Tab. 3.2.1). Both groups had the same average age (PS/2: 40.5 ± 3.6d, PBS: 40.5 ± 2.9d), a similar sex ratio (PS/2 f/m: 1.2, PBS f/m: 1.6) and the same mean clinical score at therapy onset (PS/2: 1.5 ± 0.1, PBS: 1.5 ± 0.1).

A therapeutic effect was already evident one day after the first injection of the α-CD49d (PS/2) antibody with a reduced clinical severity as compared to the control group (day 2: PS/2 1.8 ± 0.2, PBS 2.1 ± 0.1) (Fig. 3.2.5). On day 1 and day 2 after the second α-CD49d (PS/2) injection the clinical scores in treated animals were significantly lower as compared to the control group (day 4: PS/2 2.1 ± 0.2, PBS 2.9 ± 0.2; day 5: PS/2 2.0 ± 0.3, PBS 2.9 ± 0.2).

Tab. 3.2.1: Randomization of mice for the short-term therapy. Data are shown as mean ± SEM.
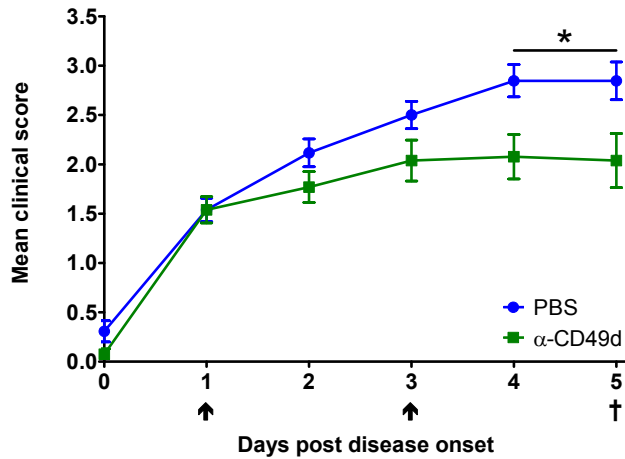
	α-CD49d (PS/2)	PBS
Mean age at therapy onset in days	40.5 ± 3.6	40.5 ± 2.9
Sex ratio ♀ / ♂	7 / 6	8 / 5
Mean clinical score at therapy onset in days	1.5 ± 0.1	1.5 ± 0.1

Fig. 3.2.5: Disease course of OSE mice during short-term therapy with the α-CD49d (PS/2) antibody or PBS. Therapy with the α-CD49d (PS/2) antibody resulted in a reduced clinical severity as compared to controls. Therapy was started at a clinical score ≥ 1.0 either with 75 μg α-CD49d (PS/2) antibody or PBS intraperitoneally. Medication time points are indicated by black arrows. Clinical scores were monitored every day. Two days after the last injection CNS pathology was investigated, as indicated by the dagger. Data are mean ± SEM, n = 13 per group.

3.2.3.1.2 Reduction of white matter demyelination in the spinal cord after treatment with the PS/2 antibody

To assess the histopathological treatment effects, the area of demyelinated white matter in the spinal cord was determined. In general, demyelinated areas in the spinal cord were located in the parenchyma close to the meninges, whereas a diffuse demyelination was observed in the optic nerve. A significantly reduced percentage of demyelinated white matter after the therapy with α-CD49d (PS/2) antibody (median: 14.4%) as compared to the control group (median: 25.1%) was found (Fig. 3.2.6).
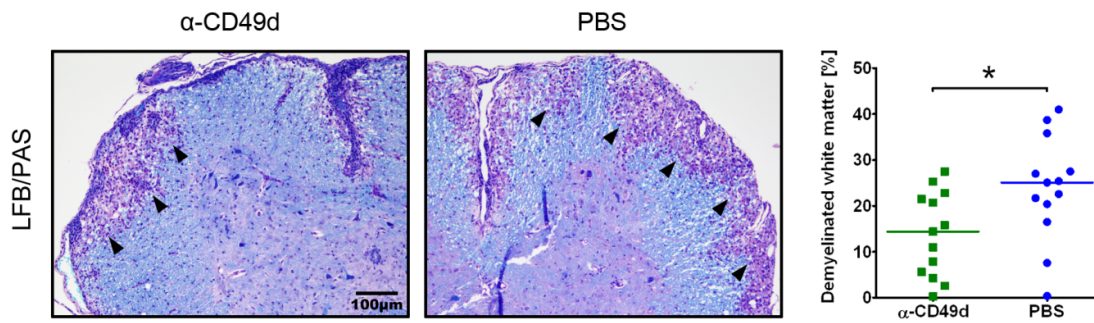
Fig. 3.2.6: Spinal white matter demyelination in OSE mice after short-term therapy with the α-CD49d (PS/2) antibody or PBS. Less demyelination was observed after the α-CD49d (PS/2) therapy as compared to controls. Myelinated as well as demyelinated white matter areas were measured in the spinal cord after LFB/PAS staining. The percentage of demyelinated white matter was calculated relative to the whole white matter area. Black arrowheads indicate demyelinated white matter.

3.2.3.1.3 Less inflammation in the spinal cord and the optic nerve after treatment with the PS/2 antibody

To investigate whether the PS/2 antibody therapy has an influence on the inflammatory cell infiltrate, the numbers of T cells (CD3), B cells (B220), plasma cells (IgG) and macrophages (Mac-3) were quantified.

In the spinal cord parenchyma reduced numbers of T cells (PS/2 median: 1132 cells/mm², PBS median: 1814 cells/mm²) and significantly decreased plasma cell numbers (PS/2 median: 0 cells/mm², PBS median: 2.2 cells/mm²) were found after the α-CD49d (PS/2) antibody therapy. However, similar numbers of macrophages (PS/2 median: 7167 cells/mm², PBS median: 7374 cells/mm²) as well as B cells (PS/2 median: 182 cells/mm², PBS median: 227 cells/mm²) as compared to the controls (Fig. 3.2.7) were also seen. Furthermore, medication with the α-CD49d (PS/2) antibody resulted in a significant reduction in B cell aggregates (PS/2 median: 0 aggregates/spinal cord section, PBS median: 1.6 aggregates/spinal cord section) (Fig. 3.2.8) and plasma cell numbers (PS/2 median: 0.1 plasma cells/spinal cord section, PBS median: 0.8 plasma cells/spinal cord section) in the spinal cord meninges as compared to the control group (Fig. 3.2.9).
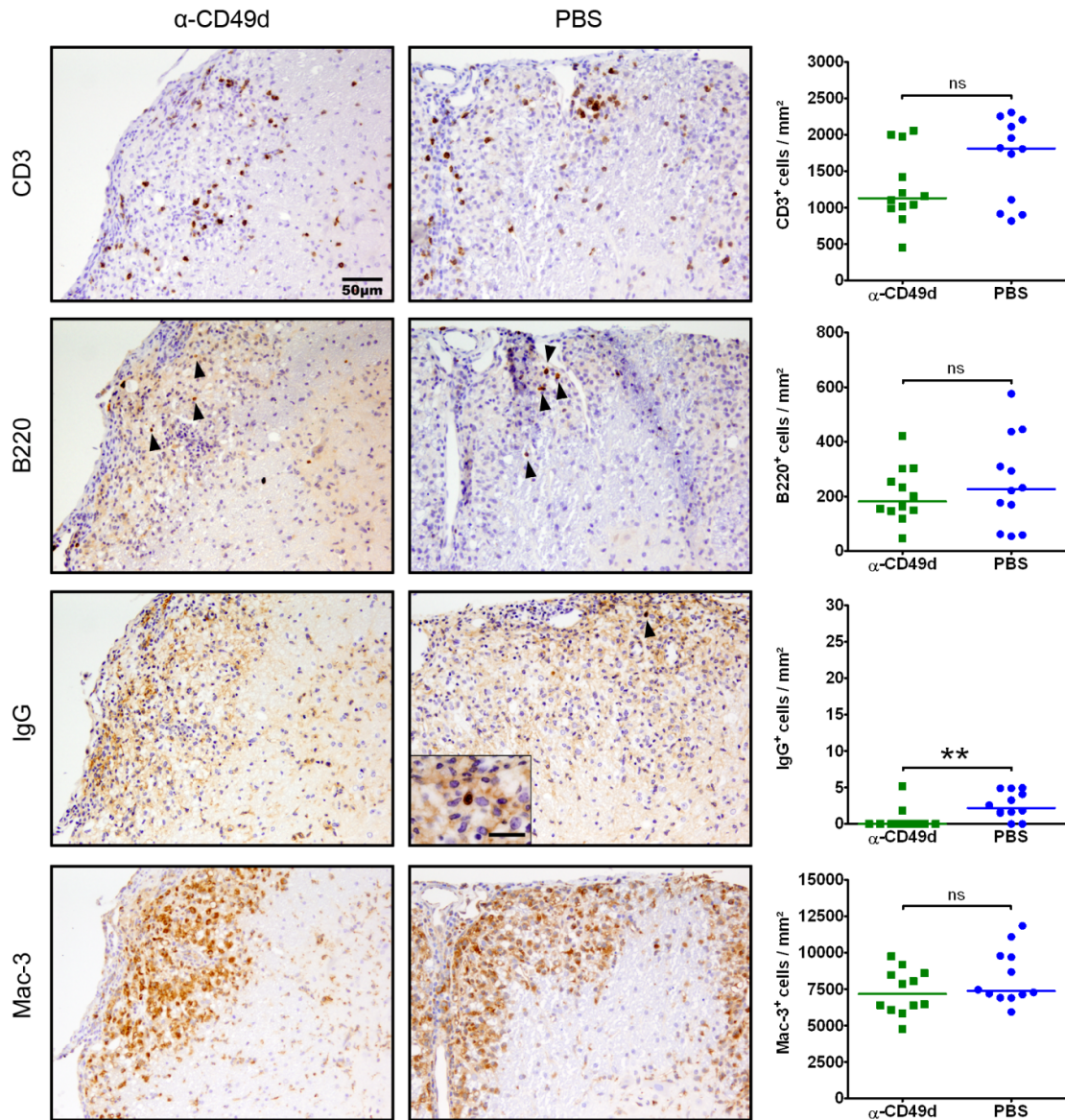
Fig. 3.2.7: Spinal cord infiltration in OSE mice after short-term therapy with the α-CD49d (PS/2) antibody or PBS. Therapy with the α-CD49d (PS/2) antibody showed reduced T cell numbers and significantly decreased plasma cell numbers, but similar numbers of B cells and macrophages as compared to the controls. Inflammatory cell infiltrates were counted in the white matter lesions of the spinal cord after the respective immunohistochemical staining procedures. B cells and plasma cells are indicated by black arrowheads. Scale bar in inset = 20 μm.
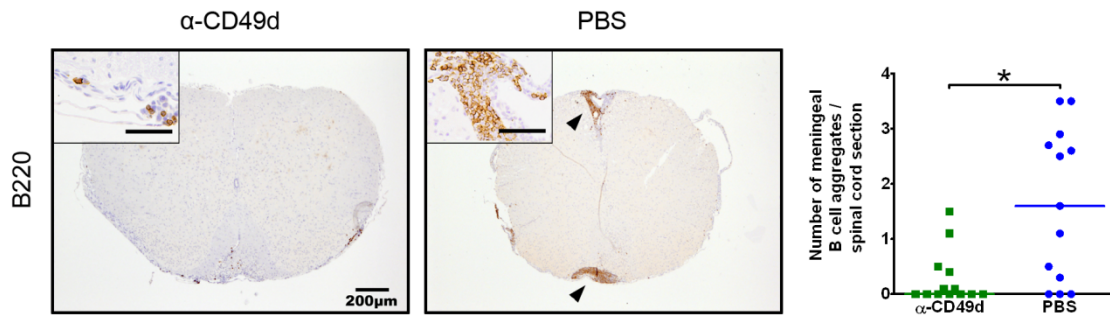
Fig. 3.2.8: Number of B cell aggregates in spinal cord meninges of OSE mice after short-term therapy with the α-CD49d (PS/2) antibody or PBS. Treatment with the α-CD49d (PS/2) antibody resulted in a significant reduction of B cell aggregates in the spinal cord meninges as compared to the control group. B cell aggregates were counted after the immunohistochemical staining procedure with an α-B220 antibody. More than 20 accumulated B cells were considered as a B cell aggregate, indicated by black arrowheads. Scale bar in inset = 20 μm.
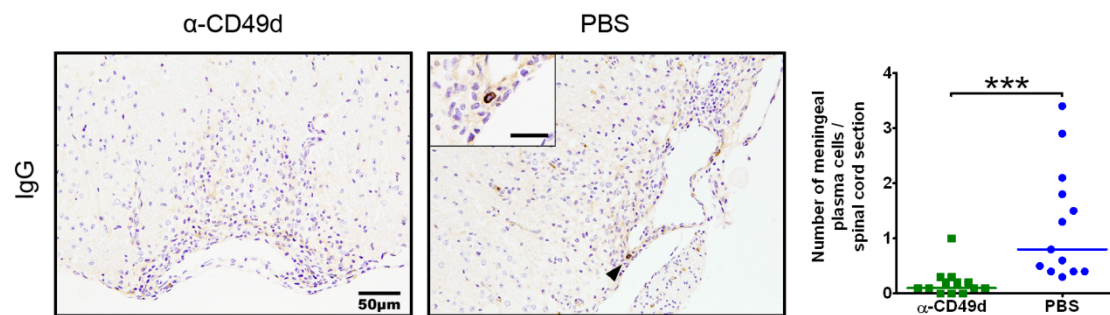
Fig. 3.2.9: Number of plasma cells in spinal cord meninges of OSE mice after short-term therapy with the α-CD49d (PS/2) antibody or PBS. Quantification showed significantly lower plasma cell numbers in the spinal cord meninges after treatment with the α-CD49d (PS/2) antibody as compared to the controls. Plasma cells were counted after the immunohistochemical staining procedure with an α-IgG antibody. Plasma cells are indicated by black arrowheads. Scale bar in inset = 20 μm.

The inflammatory cell infiltrate in the optic nerve parenchyma showed a significant reduction of T cells (PS/2 median: 17 cells/mm², PBS median: 44 cells/mm²), B cells (PS/2 median: 0 cells/mm², PBS median: 3 cells/mm²) and macrophages (PS/2 median: 24 cells/mm², PBS median: 208 cells/mm²) (Fig. 3.2.10). With the exception of one mouse in the control group, no plasma cells in the optic nerve parenchyma were observed (PS/2 median: 0 cells/mm², PBS median: 0 cells/mm²).

Fig. 3.2.10: Optic nerve inflammatory infiltration in OSE mice after short-term therapy with the α-CD49d (PS/2) antibody or PBS. Therapy with the α-CD49d (PS/2) antibody resulted in a significant decrease in T cells, B cells and macrophages. Almost no plasma cells were observed. Inflammatory cell infiltrates were counted in the optic nerve parenchyma after the respective immunohistochemical staining procedures. B cells are indicated by black arrowheads.

In summary, short-term treatment with PS/2 antibody resulted in reduced clinical severity, white matter demyelination and partly decreased infiltration in the spinal cord and optic nerve.

3.2.3.2 Long-term therapy

To investigate the treatment effects of a long-term medication, mice were treated fifteen times either with 75 µg of the α-CD49d (PS/2) antibody or with PBS every other day starting from the disease onset (clinical score ≥ 1.0). The CNS pathology was examined two days after the last administration.

3.2.3.2.1 Reduced clinical severity after treatment with the PS/2 antibody

In the same manner as for the short-term therapy, OSE mice were randomized to obtain two equally distributed groups regarding age, sex and clinical score at therapy onset. Mice showed a similar average age (PS/2: 42.1 ± 2.8d, PBS: 42.3 ± 3.2d), the same mean clinical score at therapy onset (PS/2: 1.5 ± 0.1, PBS: 1.5 ± 0.1) (Tab. 3.2.2) and the same distribution of sexes.

One day after the first injection of the α-CD49d (PS/2) antibody mice showed less clinical disability as compared to the controls (day 2: PS/2 1.8 ± 0.1, PBS 2.1 ± 0.2) (Fig. 3.2.11 A), as was already shown for the short-term treatment (see 3.2.3.1.1). Two days after the first injection the clinical scores were significantly different when comparing treated and non-treated animals (day 3: PS/2 1.9 ± 0.2, PBS 2.5 ± 0.2). The peak of the disease severity was reached 5 days post disease onset in mice treated with the α-CD49d (PS/2) antibody (clinical score of 2.0 ± 0.2) and by contrast 7 days post disease onset in the control group (clinical score of 3.0 ± 0.1). Treatment effects persisted until the end of the experiment with a lower mean clinical score in the treatment group compared to the control group (day 31: clinical score PS/2 1.4 ± 0.3, clinical score PBS 2.2 ± 0.3).

Results from monitoring body weight reflected the clinical disease severity. Treatment with the α-CD49d (PS/2) antibody resulted in a higher body weight as compared to the control group (Fig. 3.2.11 B).

A
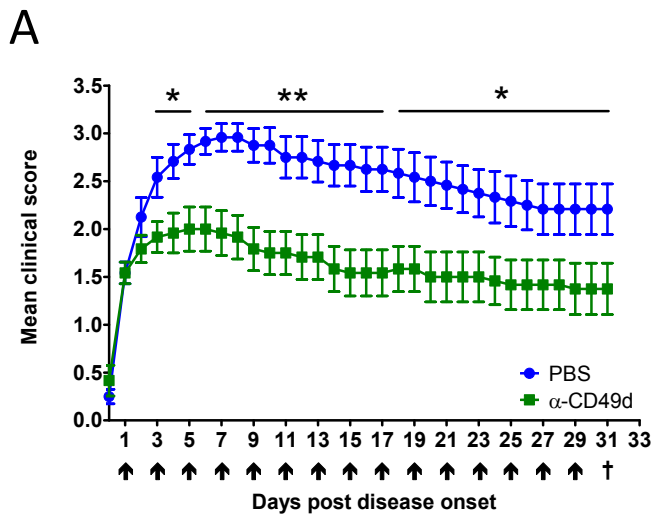
	α-CD49d (PS/2)	PBS
Mean age at therapy onset in days	42.1 ± 2.8	42.3 ± 3.2
Sex ratio ♀ / ♂	6 / 6	6 / 6
Mean clinical score at therapy onset in days	1.5 ± 0.1	1.5 ± 0.1

B
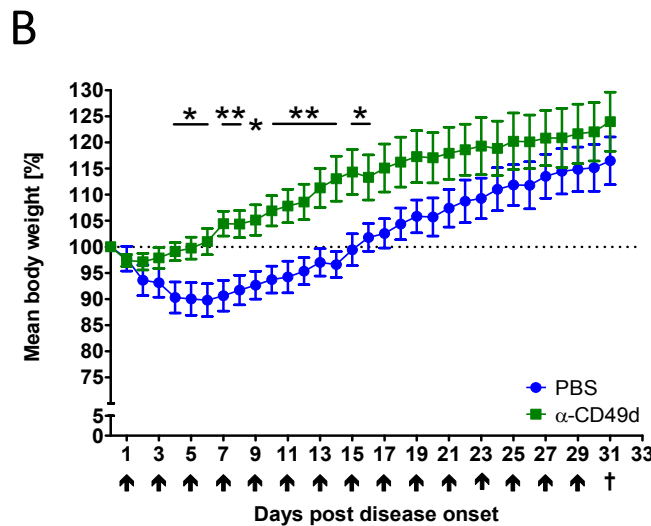
Fig. 3.2.11: Disease course and body weight of OSE mice during long-term therapy with the α-CD49d (PS/2) antibody or PBS. Therapy with the α-CD49d (PS/2) antibody resulted in decreased clinical severity and less body weight loss as compared to the control group. Therapy onset occurred at a clinical score ≥ 1.0 either with 75 µg α-CD49d (PS/2) antibody or PBS intraperitoneally. Medication time points are indicated by black arrows. Clinical scores and body weight were monitored every day. Two days after the last injection CNS pathology was investigated, as indicated by the dagger. Data are given as mean ± SEM, n = 12 per group.

3.2.3.2.2 Less white matter demyelination in the spinal cord after treatment with the PS/2 antibody

The percentage of white matter demyelination in the spinal cord correlated with the clinical symptoms (data not shown). Treatment with the α-CD49d (PS/2) antibody significantly decreased the white matter demyelination as compared to the control group (median: PS/2 3.4%, PBS 8.7%) (Fig. 3.2.12).
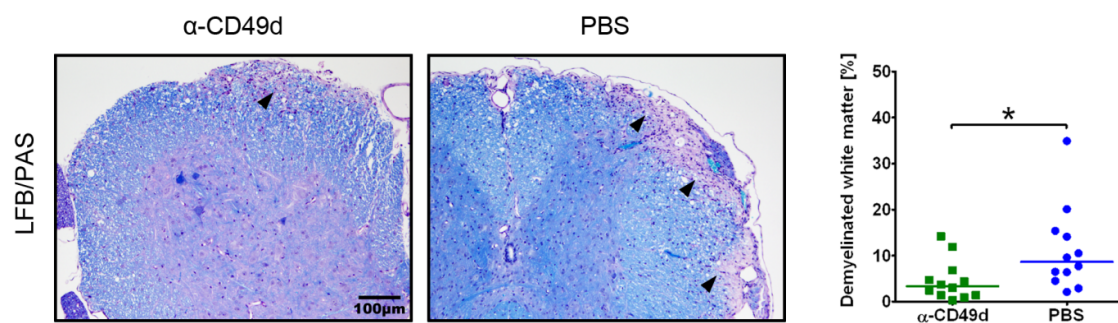

Fig. 3.2.12: White matter demyelination in OSE mice after long-term therapy with the α-CD49d (PS/2) antibody or PBS. White matter demyelination was decreased after the α-CD49d (PS/2) therapy as compared to controls. Myelinated as well as demyelinated white matter areas were measured in the spinal cord after LFB/PAS staining. The percentage of demyelinated white matter was calculated relative to the whole white matter area. Black arrowheads indicate demyelinated white matter.

3.2.3.2.3 Decreased inflammation in the spinal cord after treatment with the PS/2 antibody

To determine the extent of inflammatory cell infiltrates in the spinal cord parenchyma after treatment with the α-CD49d (PS/2) antibody or PBS, cross sections of the spinal cord were stained with the respective immunohistochemical markers. Results showed significantly reduced numbers of T cells (PS/2 median: 115 cells/mm², PBS median: 445 cells/mm²), B cells (PS/2 median: 2 cells/mm², PBS median: 74 cells/mm²), plasma cells (PS/2 median: 0 cells/mm², PBS median: 37 cells/mm²) and macrophages (PS/2 median: 110 cells/mm², PBS median: 493 cells/mm²) after treatment with α-CD49d (PS/2) antibody as compared to the controls (Fig. 3.2.13).
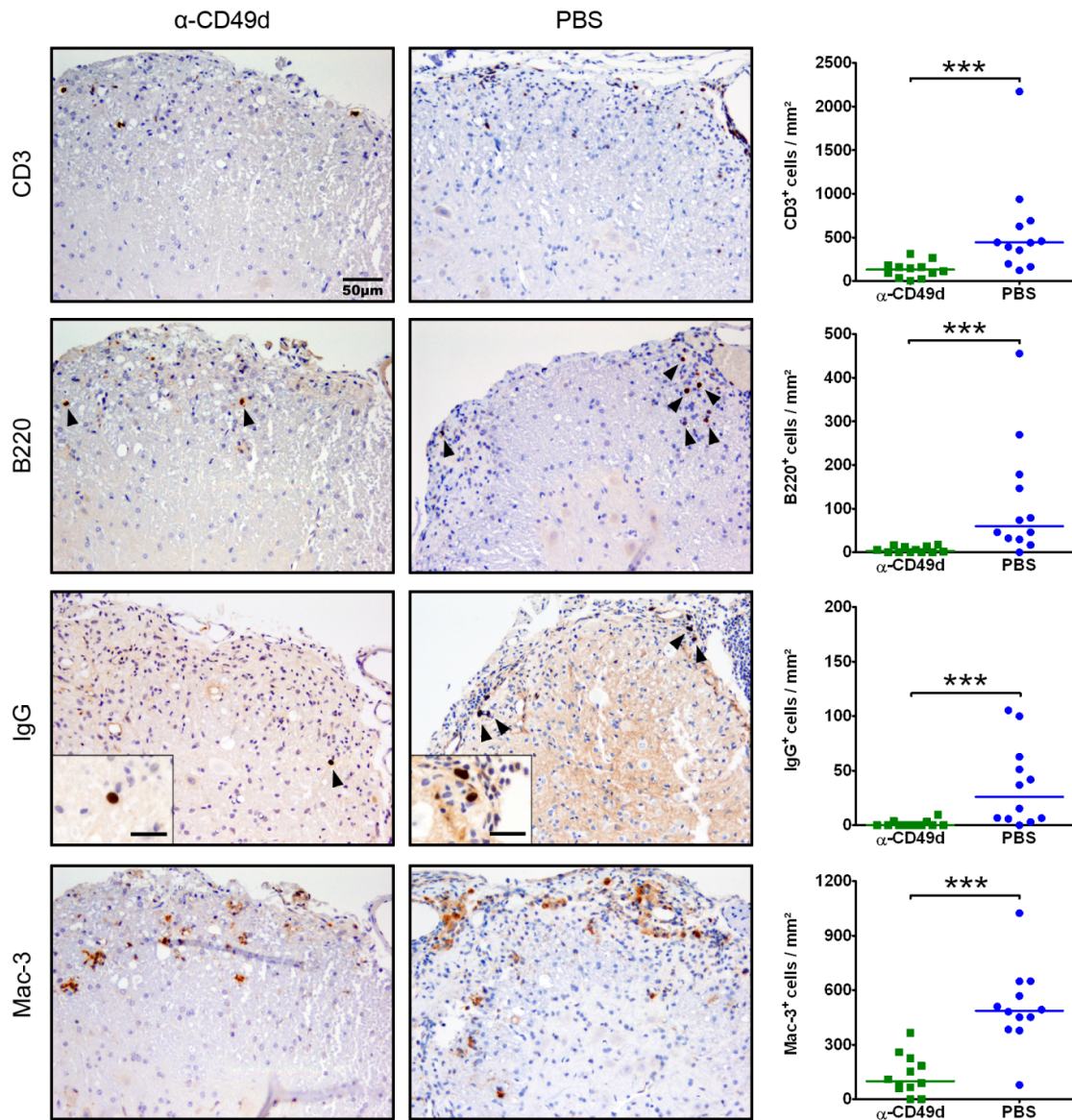
Fig. 3.2.13: Spinal cord inflammatory infiltration in OSE mice after long-term therapy with the α-CD49d (PS/2) antibody or PBS. Therapy with the α-CD49d (PS/2) antibody resulted in a significant reduction of inflammatory cell infiltrates as shown for T cells, B cells, plasma cells and macrophages as compared to the control group. Inflammatory cell infiltrates were determined in the white matter lesions of the spinal cord after the respective immunohistochemical staining procedures. B cells and plasma cells are indicated by black arrowheads. Scale bar in inset = 20 μm.
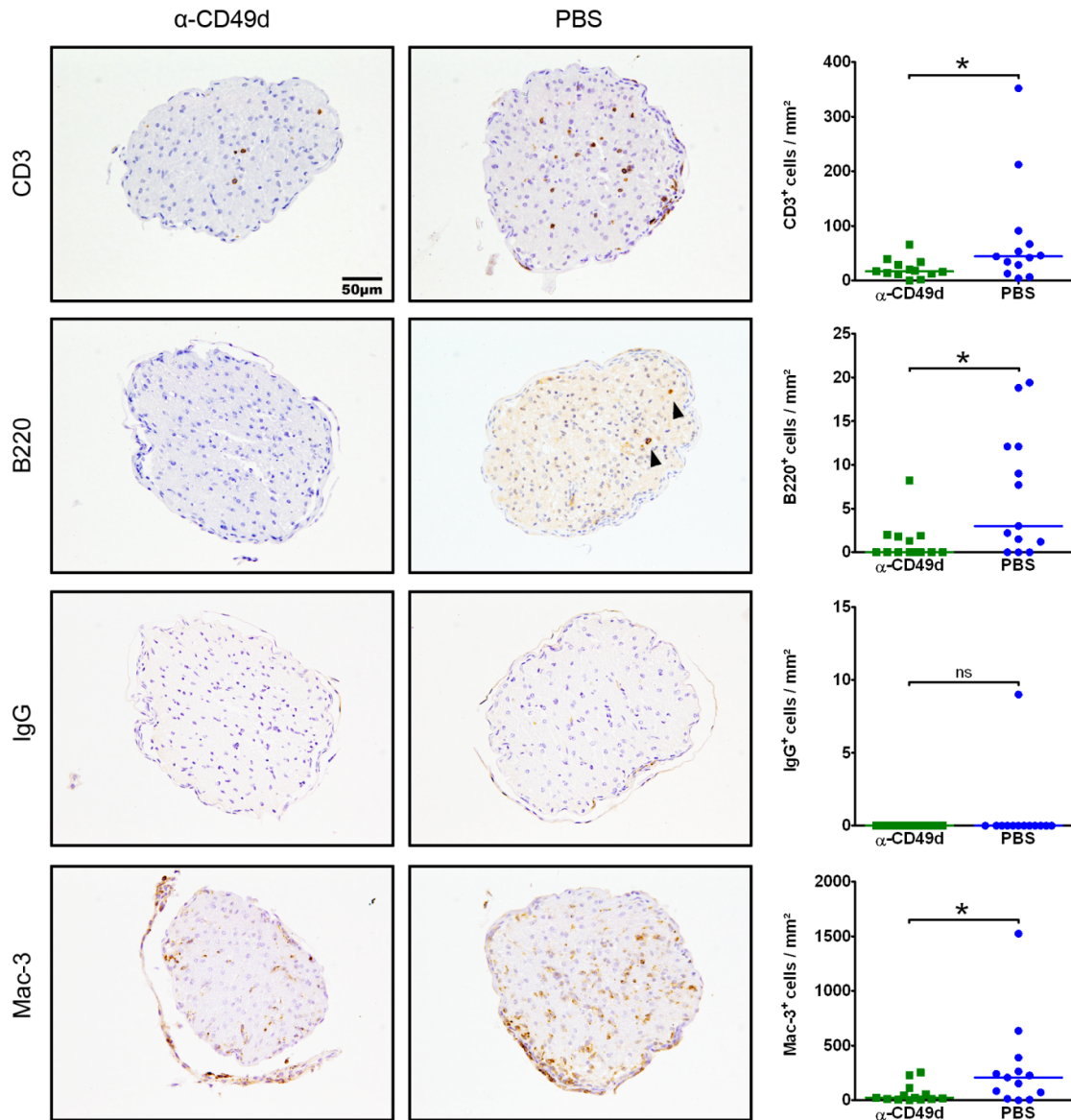
In summary, long-term treatment with PS/2 antibody resulted in reduced clinical severity, white matter demyelination and spinal cord infiltration.

3.2.3.3 Treatment in later disease phases

In an attempt to mimic chronic disease stages of multiple sclerosis mice were treated in the later disease phases. Starting at 13 days post disease onset, mice were treated nine times either with 75 µg of the α-CD49d (PS/2) antibody or with PBS every other day. The CNS pathology was examined two days after the last antibody administration.

3.2.3.3.1 No impact on clinical severity after treatment with the PS/2 antibody

The randomization of mice revealed the same mean clinical score on the first day after the disease onset for both groups (PS/2: 1.8 ± 0.2, PBS: 1.8 ± 0.1) (Tab. 3.2.3). Furthermore, both groups showed a shift of the sex ratio towards male mice. At therapy onset, the average age of antibody treated mice was slightly higher as compared to the control group (PS/2: 49.7 ± 4.1d, PBS: 44.7 ± 1.3d), but the mean clinical score was almost the same (PS/2: 2.9 ± 0.2, PBS: 2.8 ± 0.2).

Clinical scores before treatment began were, as expected, similar in both groups (Fig. 3.2.14). The peak of the disease severity was reached between day 7 (PS/2: 2.9 ± 0.3) and day 8 (PBS: 3.0 ± 0.1), respectively. Therapy with the α-CD49d (PS/2) antibody starting on day 13 showed no effect on the clinical course when compared with the controls (day 31: PS/2 2.9 ± 0.3, day 31: PBS 2.5 ± 0.2).

Tab. 3.2.3: Randomization of mice for the therapy in the late phase of the disease. Data are shown as mean ± SEM.
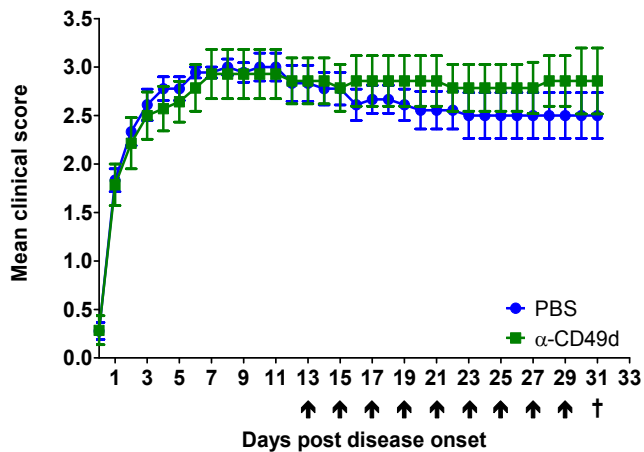
	α-CD49d (PS/2)	PBS
Mean age at therapy onset in days	49.7 ± 4.1	44.7 ± 1.3
Sex ratio ♀ / ♂	3 / 4	3 / 6
Mean clinical score on 1st day post disease onset	1.8 ± 0.2	1.8 ± 0.1
Mean clinical score at therapy onset in days	2.9 ± 0.2	2.8 ± 0.2

Fig. 3.2.14: Disease course of OSE mice during therapy with the α-CD49d (PS/2) antibody or PBS in later disease phases. Therapy with the α-CD49d (PS/2) antibody resulted in a similar clinical severity as compared to the control group. Therapy was started 13 days post disease onset either with 75 µg α-CD49d (PS/2) antibody or PBS intraperitoneally. Medication time points are indicated by black arrows. Clinical scores were monitored every day. Two days after the last injection CNS pathology was investigated, as indicated by the dagger. Data are mean values ± SEM. α-CD49d (PS/2) antibody-treated group: n = 7; control group: n = 9.

3.2.3.3.2 No influence on white matter demyelination in the spinal cord after treatment with the PS/2 antibody

Percentage of white matter demyelination in the spinal cord showed no significant difference between PS/2 antibody-treated (median: 17.9%) and PBS-treated control animals (median: 13.1%) (Fig. 3.2.15).
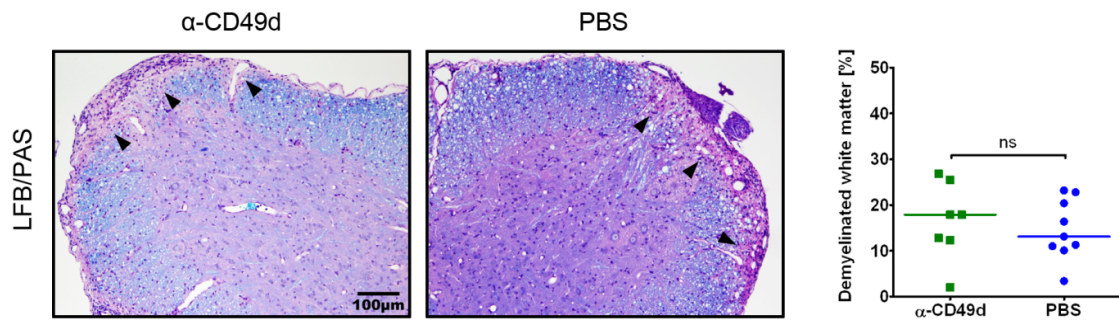
Fig. 3.2.15: White matter demyelination in OSE mice after therapy with the α-CD49d (PS/2) antibody or PBS in later disease phases. A similar percentage of white matter demyelination is found after the α-CD49d (PS/2) therapy as compared to controls. Myelinated as well as demyelinated white matter areas were measured in the spinal cord after LFB/PAS staining. The percentage of demyelinated white matter was calculated relative to the whole white matter areas. Black arrows indicate demyelinated white matter.

3.2.3.3.3 No effect on spinal cord infiltration after treatment with the PS/2 antibody

Inflammatory cell infiltrates in the spinal cord parenchyma showed similar numbers of T cells (PS/2 median: 353 cells/mm², PBS median: 361 cells/mm²), B cells (PS/2 median: 13 cells/mm², PBS median: 17 cells/mm²), plasma cells (PS/2 median: 60 cells/mm², PBS median: 57 cells/mm²) as well as macrophages (PS/2 median: 326 cells/mm², PBS median: 258 cells/mm²) in antibody-treated and control groups (Fig. 3.2.16).
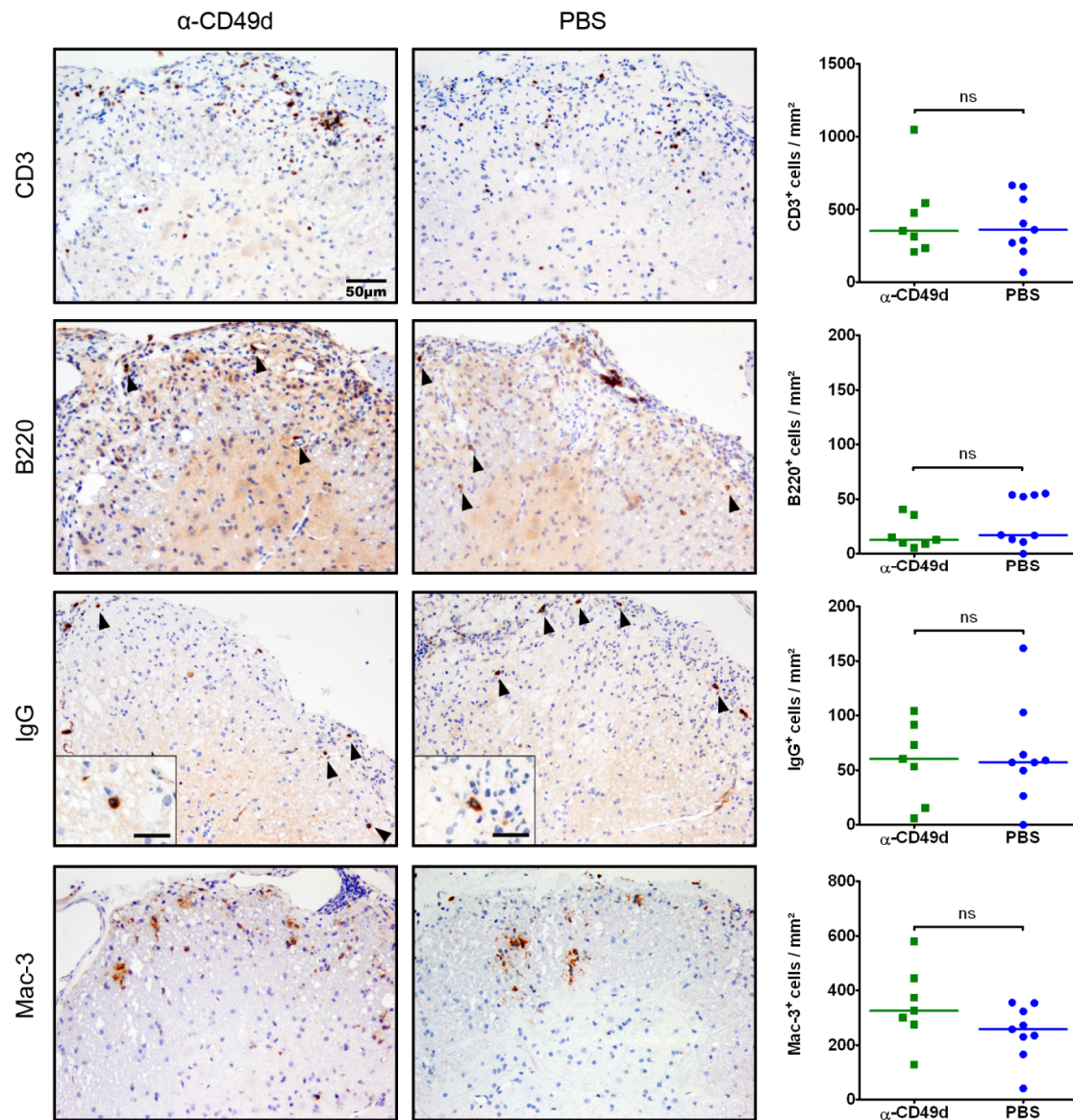
Fig. 3.2.16: Spinal cord inflammatory infiltration in OSE mice after therapy with the α-CD49d (PS/2) antibody or PBS in the later disease phases. Therapy with the α-CD49d (PS/2) antibody showed similar numbers in all investigated inflammatory cell subsets as compared to the controls. Inflammatory cell infiltrates were counted in the white matter lesion of the spinal cord after the respective immunohistochemical staining procedures. B cells and plasma cells are indicated by black arrowheads. Scale bar in inset = 20 μm.

In summary, PS/2 treatment in late phase of the disease revealed no difference in clinical severity, white matter demyelination and spinal cord infiltration as compared to untreated controls.

3.2.3.4 Long-term therapy with an additional observation period after the last PS/2 antibody administration

To address the question whether the cessation of the PS/2 antibody therapy leads to a return of disease activity (rebound), mice were treated fifteen times either with 75 µg of the α-CD49d (PS/2) antibody or with PBS every other day starting from disease onset (clinical score ≥ 1.0). After the fifteenth injection, mice were observed for another 15 days before CNS pathology was examined.

3.2.3.4.1 No clinical worsening after stopping the PS/2 therapy

Randomization resulted in a nearly equal distribution of mice regarding the average age at therapy onset (PS/2: 35.0 ± 3.3d, PBS: 34.3 ± 3.2d) (Tab. 3.2.4). Moreover, the mean clinical score at therapy onset was the same in mice treated with α-CD49d (PS/2) antibody (1.3 ± 0.1) and controls (1.3 ± 0.2). Both groups showed a shift of the sex ratio towards male mice.

As shown in prior experiments a clear therapy effect with decreased clinical disability in antibody-treated versus PBS-treated animals was evident (Fig. 3.2.17). On the day of the last injection, the difference in clinical scores averaged 1.3 between both groups (PS/2: 1.5 ± 0.3, PBS: 2.8 ± 0.1). After stopping therapy, clinical scores remained nearly unchanged in both groups, with no evidence of rebound activity.

Tab. 3.2.4: Randomization of mice for the experiment with an additional observation period after the last injection. Data are shown as mean ± SEM.

	α-CD49d (PS/2)	PBS
Mean age at therapy onset in days	35.0 ± 3.3	34.3 ± 3.2
Sex ratio ♀ / ♂	2 / 4	0 / 6
Mean clinical score at therapy onset in days	1.3 ± 0.1	1.3 ± 0.2
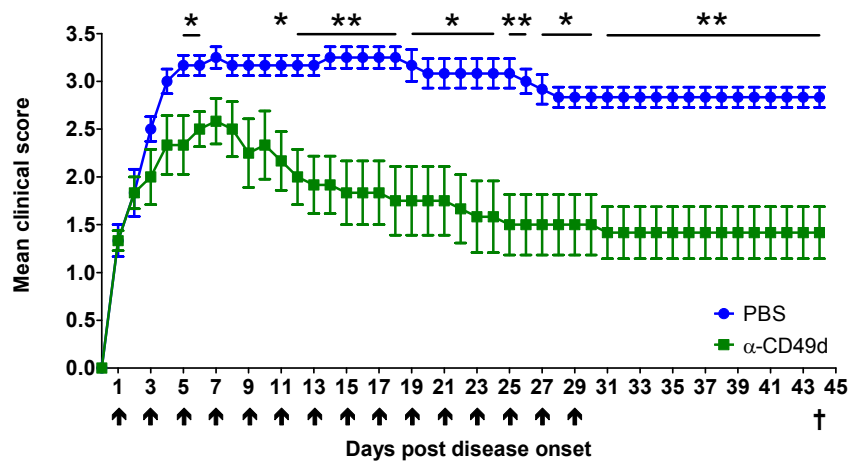
Fig. 3.2.17: Disease course of OSE mice during long-term therapy with the α-CD49d (PS/2) antibody or PBS and after therapy was stopped. Therapy with the α-CD49d (PS/2) antibody resulted in a better clinical course as compared to the controls. No worsening of the clinical disability was observed after the therapy was stopped. Therapy was started at a clinical score ≥ 1.0 either with 75 µg α-CD49d (PS/2) antibody or PBS intraperitoneally. Medication time points are indicated by black arrows. Clinical scores were monitored every day. Fifteen days after the last injection CNS pathology was investigated, indicated by a dagger. Data are mean values ± SEM, n = 6 per group.

3.2.3.4.2 No increased white matter demyelination in the spinal cord after cessation of the PS/2 therapy

The percentage of demyelinated white matter was significantly reduced after therapy with the α-CD49d (PS/2) antibody (median: 4.9%) as compared to the control group (median: 15.4%) (Fig. 3.2.18). Furthermore, no difference was observed in the extent of white matter demyelination two days (median: 3.4) as compared to 15 days after the last PS/2 injection (median: 4.9%) (Fig. 3.2.12, Fig. 3.2.18).
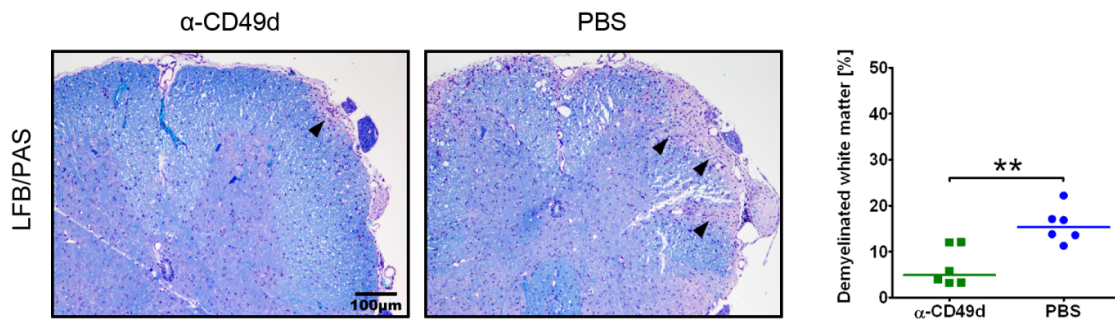
Fig. 3.2.18: White matter demyelination in OSE mice 15 days after stopping the long-term therapy with the α-CD49d (PS/2) antibody or PBS. α-CD49d (PS/2) therapy discontinuation did not increase white matter demyelination in the spinal cord parenchyma. The extent of white matter demyelination was similar 15 days as compared to two days after the last PS/2 injection. Myelinated as well as demyelinated white matter was measured in the spinal cord after LFB/PAS staining. The percentage of demyelinated white matter was calculated relative to the whole white matter area. Black arrowheads indicate demyelinated white matter.

3.2.3.4.3 No impact on the inflammatory infiltration in the spinal cord after stopping the PS/2 antibody therapy

To examine whether the discontinuation of the α-CD49d (PS/2) therapy has an influence on the inflammatory cell infiltrate in the spinal cord parenchyma, the number of T cells (CD3), B cells (B220), plasma cells (IgG) and macrophages (Mac-3) was evaluated.

The quantification showed lower numbers of T cells (PS/2 median: 55 cells/mm², PBS median: 90 cells/mm²), B cells (PS/2 median: 4 cells/mm², PBS median: 32 cells/mm²) and plasma cells (PS/2 median: 4 cells/mm², PBS median: 14 cells/mm²) after the treatment with α-CD49d (PS/2) antibody as compared to the control group, but the cell number differences were not statistically significant (Fig. 3.2.19). By contrast, the macrophage numbers were similar in both groups (PS/2 median: 105 cells/mm², PBS median: 122 cells/mm²) (Fig. 3.2.19). Furthermore, a tendency toward decreased T cell numbers and similar B cell, plasma cell as well as macrophage numbers was observed 15 days (T cells median: 55 cells/mm², B cells median: 4 cells/mm², plasma cells median: 4 cells/mm², macrophages median: 105 cells/mm²) as compared to two days after the last PS/2 injection (T cells median: 115 cells/mm², B cells median: 2 cells/mm², plasma cells median: 0 cells/mm², macrophages median: 110 cells/mm²) (Fig. 3.2.19, Fig. 3.2.13).
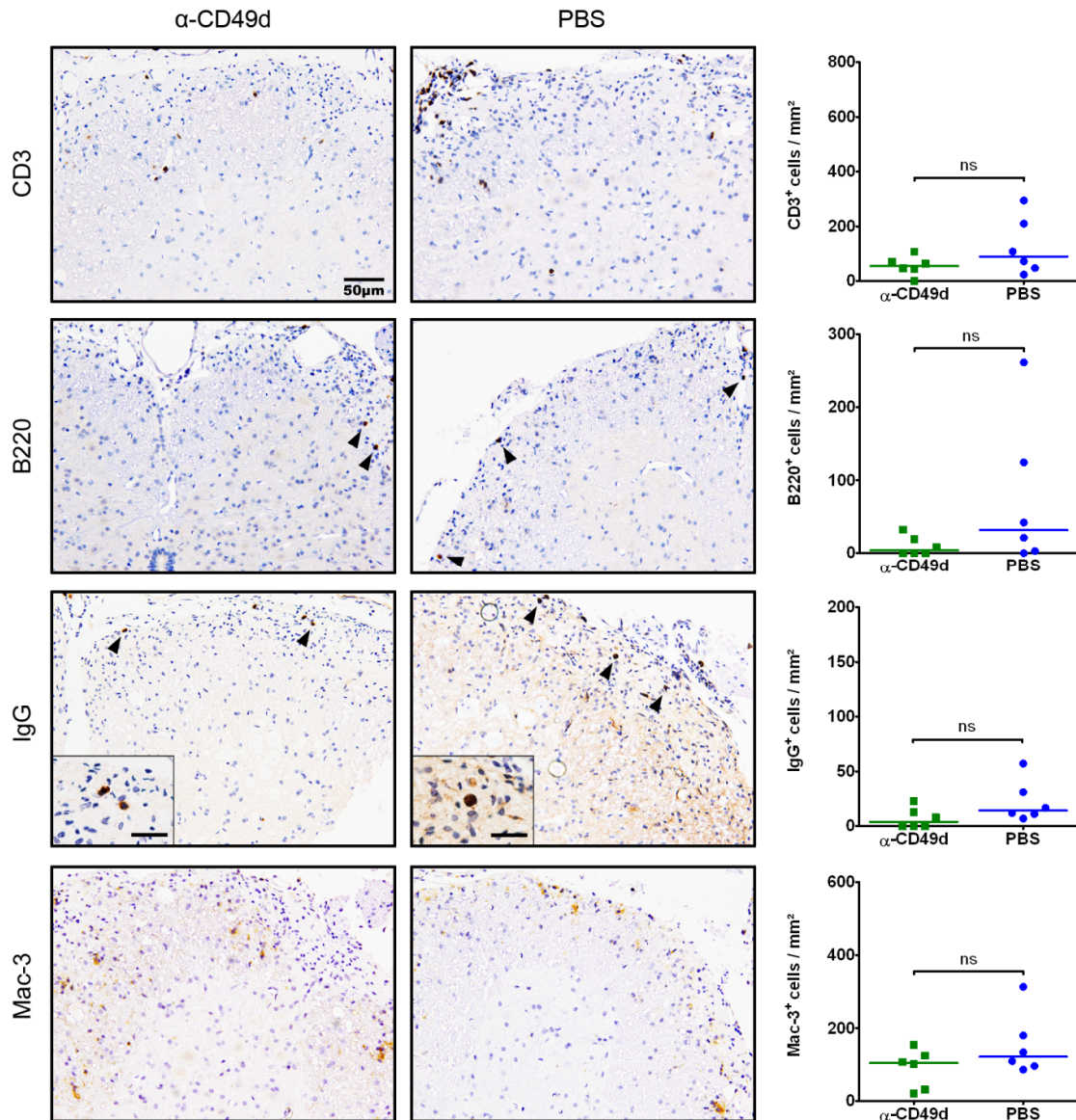
Fig. 3.2.19: Spinal cord inflammatory infiltration in OSE mice 15 days after stopping the long-term therapy with the α-CD49d (PS/2) antibody or PBS. α-CD49d (PS/2) antibody therapy discontinuation did not result in an increase of inflammatory cell infiltrates in the spinal cord parenchyma. T cells tended to be decreased and all other inflammatory infiltrates were similar 15 days as compared to two days after the last PS/2 injection. Inflammatory cell infiltrates were counted in the white matter lesion of the spinal cord after the respective immunohistochemical staining procedures. B cells and plasma cells are indicated by black arrowheads. Scale bar in inset = 20 μm.

In summary, cessation of the PS/2 therapy resulted in similar clinical severity as well as white matter demyelination and a tendency toward decreased spinal cord infiltration 15 days as compared to 2 days after the last PS/2 injection.

Of all the treatment effects in CNS observed here, PS/2 antibody therapy improved the clinical outcome and decreased spinal cord demyelination as well as immune cell infiltrations if given early in the disease course. Therapy with the PS/2 antibody in later disease stages did not show any therapeutic benefit. Discontinuation of therapy did not result in a return of disease activity.

3.2.4 Mode of action

3.2.4.1 Therapeutic effects without the involvement of Fc regions during the PS/2 antibody therapy

The α-CD49d (PS/2) antibody was generated in rats and belongs to the IgG class 2b. Some effector functions are described for this isotype class such as, for instance, the ability to bind to complement component C1q (Hughes-Jones et al., 1983) as well as the interaction with FcRI (Woof et al., 1986) and FcRII (Haagen et al., 1995). To address the question whether the beneficial therapeutic effects of the α-CD49d (PS/2) antibody are caused by blocking the CD49d receptors and not by effector functions related to the Fc region, the Fc region of the antibody was cleaved off by pepsin digestion. Afterwards F(ab')$_2$ fragments were purified and used for the short-term therapy.

3.2.4.1.1 Generation of PS/2 F(ab')$_2$ fragments

The fragmentation of the α-CD49d (PS/2) antibody with pepsin was performed in a substrate to enzyme ratio of 10:1 for 24 hours. Thereafter, the α-CD49d (PS/2) digest was purified and investigated by SDS-PAGE. An intact antibody (IgG) was used as a control and the separation by SDS-PAGE led to a band at about 150kDa (Fig. 3.2.20 A I, indicated by red frame). Under reducing conditions the disulfide bonds of the antibody were cleaved and resulted in an accumulation of heavy chains at about 50kDa and light chains at about 25kDa (Fig. 3.2.20 A III, indicated by hc and lc respectively). The separation of the α-CD49d (PS/2) digest by SDS-PAGE revealed neither a fraction of

intact antibody (Fig. 3.2.20 B I, indicated by black arrowhead) nor a fraction of the intact heavy chain under reducing conditions (Fig. 3.2.20 B III, indicated by black arrowhead). However, a fraction at about 100kDa was observed which represents the F(ab')$_2$ fragments (Fig. 3.2.20 B I, indicated by red frame) as well as a fraction at about 25kDa under reducing conditions which contain the cleaved heavy chains (Fig. 3.2.20 B III, indicated by hc). The molecular weight of the cleaved heavy chains was slightly higher as compared to the light chains (Fig. 3.2.20 B III, indicated by lc). The α-CD49d (PS/2) digest contained also some other fractions such as a fraction at about 50kDa under non-reducing conditions (Fig. 3.2.20 B I and II) and a fraction at about ≤ 15kDa both under non-reducing and reducing conditions (Fig. 3.2.20 B II and III). It is highly likely that the 50kDa product represents Fab fragments which were also generated with the digesting procedure, because this fraction shows half the molecular weight of F(ab')$_2$ fragments and because of its absence under reducing conditions, indicating that this fraction must have disulfide bounds. The fraction ≤ 15kDa presumably contains the cleaved Fc fragments which remained after the purification procedure. The isotype control was digested accordingly and showed the same results (Fig. 3.2.20 C I, II, III). For the following in vivo experiments the α-CD49d (PS/2) digest as well as the isotype control digest were used and referred to as α-CD49d (PS/2) F(ab')$_2$ fragments and isotype control F(ab')$_2$ fragments respectively.
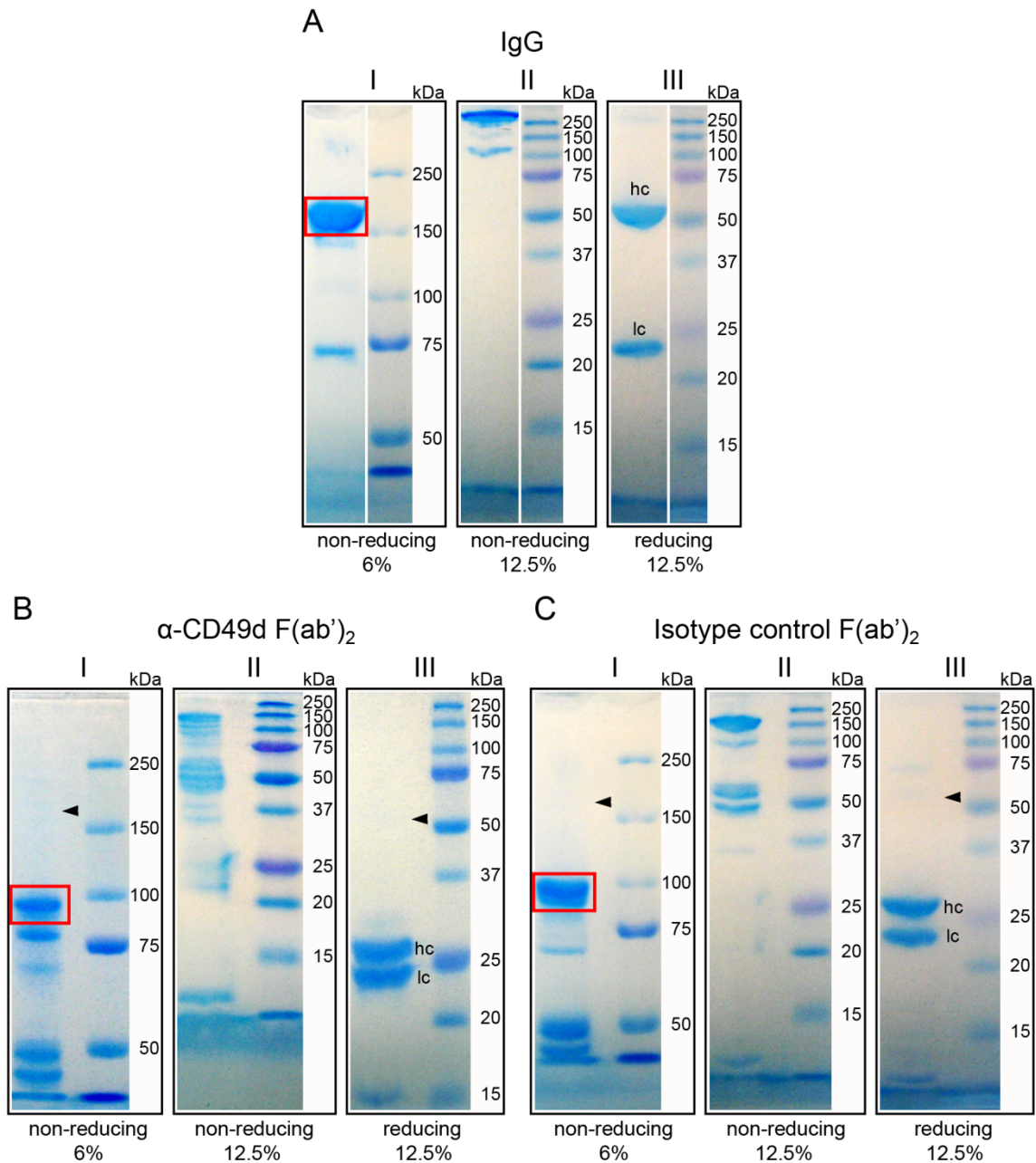
Fig. 3.2.20: Separation of F(ab')₂ fragments after pepsin digestion by SDS-PAGE. α-CD49d (PS/2) antibody and isotype control were incubated with pepsin in a substrate to enzyme ratio 10:1 for 24 hours at 37°C. After the purification procedure the digest was separated by SDS-PAGE and visualized by Coomassie brilliant blue staining. (A) An intact antibody (IgG) with a molecular weight of ~150kDa is indicated by a red frame in (A I). (B) α-CD49d (PS/2) F(ab')₂ fragments with a molecular weight of ~100kDa are indicated by a red frame in (B I). No remaining intact antibody (B I, black arrowhead) as well as intact heavy chain (B III, black arrowhead) was observed after the digestion. (C) Isotype control F(ab')₂ fragments with a molecular weight of ~100kDa are indicated by a red frame in (C I). No remaining intact antibody (C I, black arrowhead) as well as intact heavy chain (C III, black arrowhead) were observed after the digestion. A-C I: 6% gel, non-reducing conditions; A-C II: 12.5% gel, non-reducing conditions; A-C III: 12.5% gel, reducing conditions; hc = heavy chain, lc = light chain.

3.2.4.1.2 Determination of an appropriate treatment dosage and treatment interval

Similar to the treatment with the intact antibody it was necessary to determine an appropriate α-CD49d (PS/2) F(ab')$_2$ fragment treatment dosage as well as treatment interval. The intraperitoneal injection of 200 μg α-CD49d (PS/2) F(ab')$_2$ fragments every day revealed a persistent strong saturation of the CD49d receptors on WBCs by more than 80% (Fig. 3.2.21, green curve). Furthermore, in accordance with the results obtained by SDS-PAGE almost no intact bound PS/2 antibody was detected after treatment (Fig. 3.2.21, blue curve). Due to the comparable CD49d receptor saturation as observed when treating with the intact α-CD49d (PS/2) antibody, the α-CD49d (PS/2) F(ab')$_2$ fragments were administered in a dosage of 200 μg intraperitoneally every day.
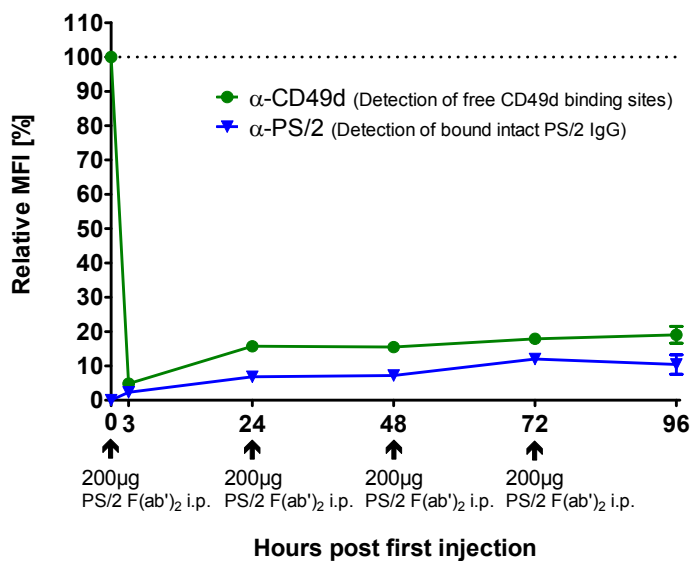
Fig. 3.2.21: Detection of free CD49d binding sites as well as the proportion of bound intact PS/2 antibody to CD49d receptors after treatment with α-CD49d (PS/2) F(ab')$_2$ fragments. The daily administration of 200 μg α-CD49d (PS/2) F(ab')$_2$ fragments turned out to be suitable to study therapeutic effects in this mouse model of demyelination. Before and at definite time points during the daily administration of 200 μg of α-CD49d (PS/2) F(ab')$_2$ fragments in adult mice, blood was collected and flow cytometry analysis performed. The detection of free CD49d binding sites occurred with a fluorophore-conjugated α-CD49d (PS/2) antibody (green curve). To measure the proportion of bound intact PS/2 antibody to CD49d receptors a fluorophore-conjugated α-PS/2 antibody was used (blue curve). Relative MFI is given for all WBCs and was calculated by the median fluorescence intensity of interest minus the median fluorescence intensity of the isotype control. Data are mean values ± SEM. N = 1 3h, 24h, 48h, 72h post first injection; n = 5 before and 96 hours post first injection.

3.2.4.1.3 Reduction of free CD49d receptor binding sites on WBCs as well as the proportion of CD49d-positive cells in the blood after treatment with the PS/2 F(ab')$_2$ fragments

To examine whether the short-term therapy with the α-CD49d (PS/2) F(ab')$_2$ fragments has the same effects on peripheral blood cells as observed with the α-CD49d (PS/2) antibody medication, blood samples were collected before therapy as well as on the sacrifice day. Flow cytometry analysis was performed.

At the end of the experiment, one day after the last α-CD49d (PS/2) F(ab')$_2$ fragments injection, the CD49d MFI was significantly reduced in all immune cell subsets as compared to before the therapy (Fig. 3.2.22 A, C). The strongest reduction of free CD49d binding sites by about 90 percent was found on Syndecan-1$^+$ cells (91.1 ± 2.1%), B220$^+$ cells (90.2 ± 2.7%), CD4$^+$ cells (89.6 ± 3.4%) and NK1.1$^+$ cells (88.2 ± 4.5%), followed by CD8$^+$ cells (82.2 ± 7.2%), Gr-1$^+$ cells (77.2 ± 5.5%) and CD11b$^+$ cells (73.7 ± 3.2%) (Fig. 3.2.22 D). It should be noted that the CD49d expression on Gr-1$^+$ cells was already very low before the therapy (Fig. 3.2.22 A, C).

Furthermore, the immune cell subsets in blood showed different percentage proportions of CD49d$^+$ cells after the injection of α-CD49d (PS/2) F(ab')$_2$ fragments. The lowest percentage proportion of CD49d$^+$ cells was found for the CD4$^+$ population (5.5 ± 1.6%) and Gr-1$^+$ population (9.1 ± 3.0%), followed by the B220$^+$ population (13.5 ± 5.5%) and Syndecan-1$^+$ population (14.6 ± 4.4%). A higher proportion of CD49d$^+$ cells was observed in the CD8$^+$ population (35.3 ± 9.8%) and in the NK1.1$^+$ population (47.3 ± 9.2%). Most CD11b$^+$ cells were positive for CD49d (89.5 ± 3.4%) (Fig. 3.2.22 A, B).

Thus, similar to the therapy with the intact α-CD49d (PS/2) antibody (Fig. 3.2.2 A, B, C, D) the flow cytometry analysis revealed also a strong reduction of free CD49d binding sites on WBCs after the medication with the α-CD49d (PS/2) F(ab')$_2$ fragments. However, a higher proportion of CD49d positive cells especially in the CD11b$^+$ population was present.
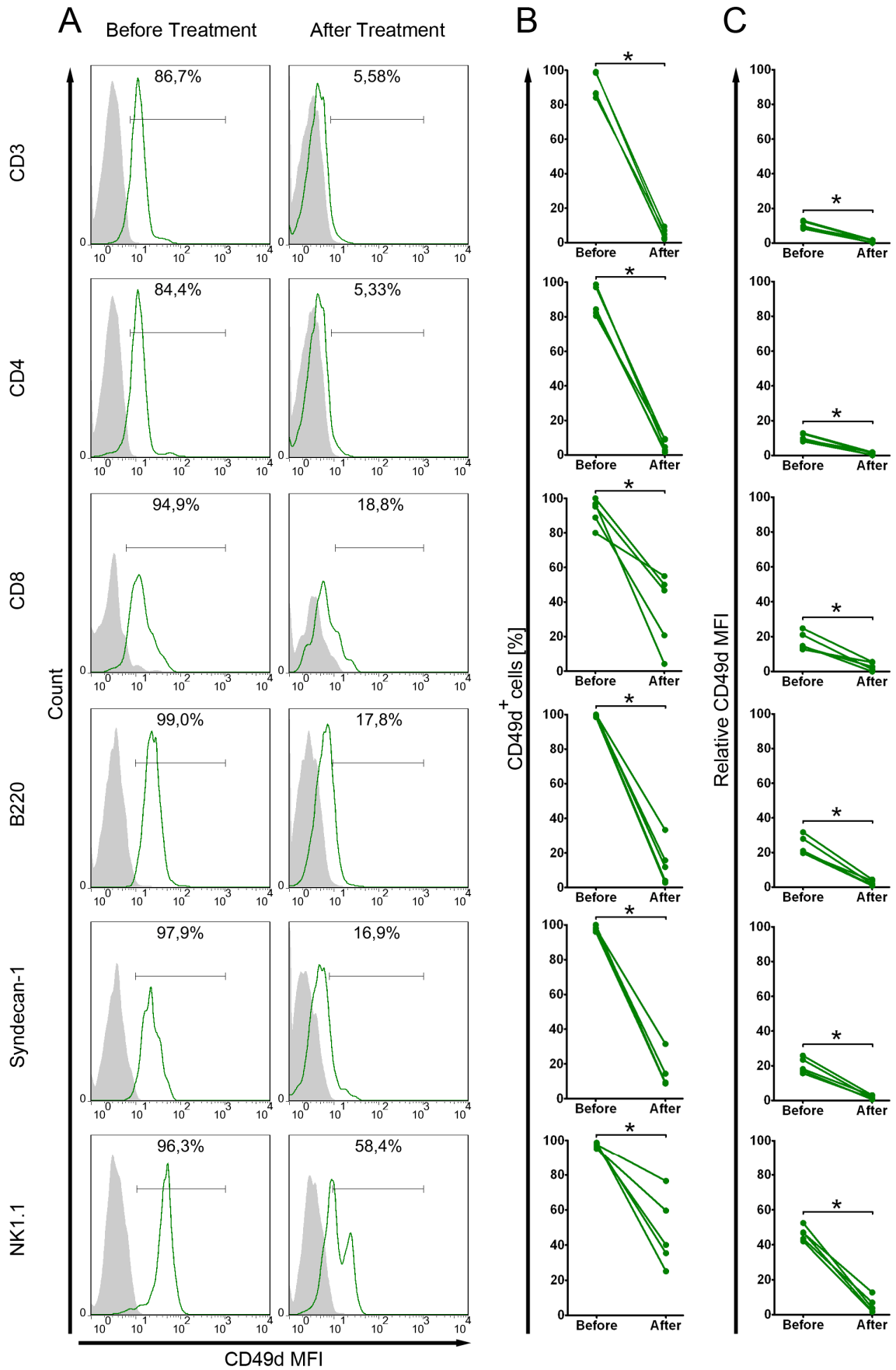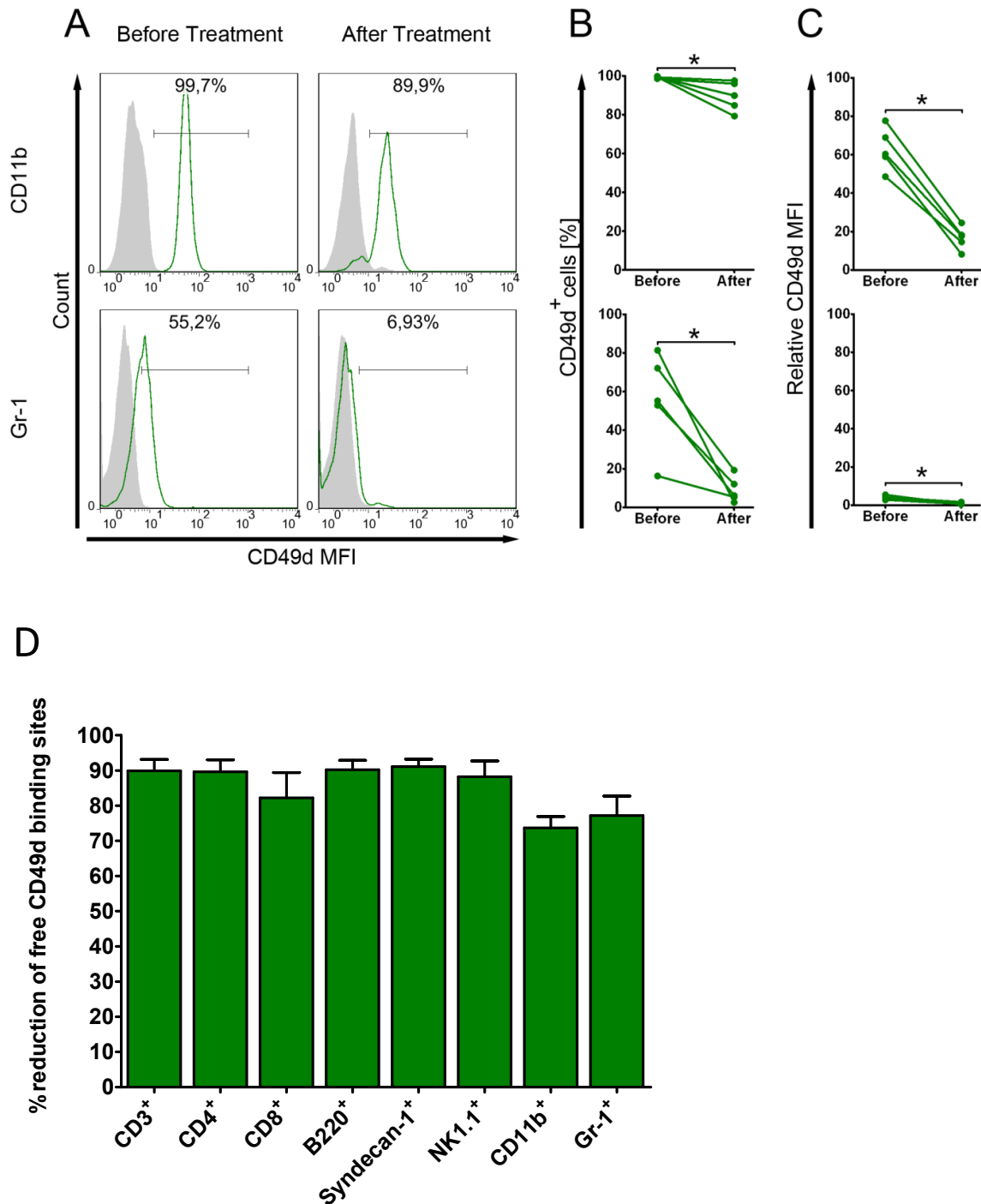
Fig. 3.2.22: Percentage of CD49d$^+$ cells and relative CD49d MFI before and after short-term treatment with the α-CD49d (PS/2) F(ab')$_2$ fragments. After short-term treatment with the α-CD49d (PS/2) F(ab')$_2$ fragments free CD49d binding sites as well as the proportion of CD49d positive cells were significantly reduced as compared to before the therapy. Before and after treatment, blood was collected and flow cytometry analysis performed. The CD49d MFI for CD3$^+$, CD4$^+$, CD8$^+$, B220$^+$, Syndecan-1$^+$ and NK1.1$^+$ cells was determined while gating on the lymphocyte population in SSC/FSC. The CD49d MFI for CD11b$^+$ and Gr-1$^+$ cells was investigated by gating on the monocyte and granulocyte population, respectively. Connected dots before and after treatment in (B) and (C) represent data obtained from one mouse. Relative MFI in (C) is given as the median fluorescence intensity of CD49d minus the median fluorescence intensity of the isotype control. (D) Percentage reduction of free CD49d binding sites after the treatment was calculated as follows: relative median fluorescence intensity before treatment divided by the relative median fluorescence intensity after treatment.

3.2.4.1.4 Increase in absolute WBC numbers after treatment with the PS/2 F(ab')$_2$ fragments

To assess whether the α-CD49d (PS/2) F(ab')$_2$ fragments also have an effect on absolute WBC numbers, blood samples were collected before the injection of F(ab')$_2$ fragments as well as on the sacrifice day, and the absolute blood cell number was determined with the Neubauer counting chamber. The absolute number of immune cell subsets was then calculated based on the percentage numbers determined with the flow cytometry analysis.

Similar to the medication with the intact α-CD49d (PS/2) antibody (Fig. 3.2.4 A) the quantification of absolute cell numbers after therapy with the α-CD49d (PS/2) F(ab')$_2$ fragments showed a significant increase in WBC numbers (before therapy: 4061 ± 404 cells/µl, after therapy: 13329 ± 1969 cells/µl). An absolute increase in cell numbers could be shown for all investigated cell subsets (Fig. 3.2.23).
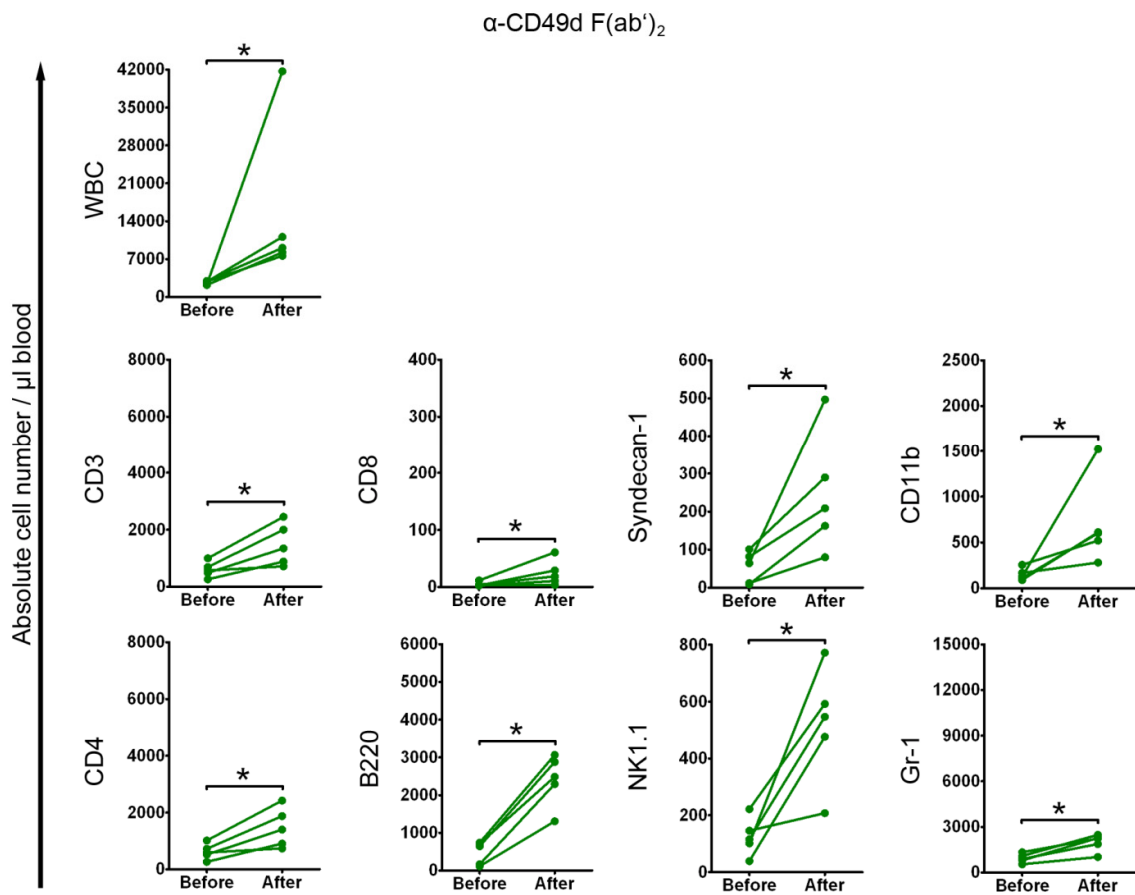
Fig. 3.2.23: Absolute cell numbers of WBCs before and after short-term treatment with the α-CD49d (PS/2) F(ab')₂ fragments. α-CD49d (PS/2) F(ab')₂ fragment therapy resulted in a significant increase in the absolute cell number of all investigated cell subsets. Before and after treatment blood was collected and absolute blood cell numbers determined with the Neubauer counting chamber. The absolute number of immune cell subsets was then calculated based on the percentage numbers evaluated with the flow cytometry analysis. Connected dots before and after treatment represent data obtained from one mouse. Data are given as median.

3.2.4.1.5 Decreased clinical severity after the treatment with PS/2 F(ab')₂ fragments

To determine whether the α-CD49d (PS/2) F(ab')₂ fragments have the same therapeutic effect as the intact α-CD49d (PS/2) antibody, short-term treatment experiments were performed. Upon first clinical symptoms, at least a tail paralysis (clinical score ≥ 1.0), mice were treated daily either with 200 µg of α-CD49d (PS/2) F(ab')₂ fragments or isotype control F(ab')₂ fragments intraperitoneally for four days. One day after the last injection the CNS pathology was investigated.

Randomization of mice showed a similar average age (PS/2 F(ab')$_2$: 30.8 ± 1.2d, isotype control F(ab')$_2$: 32.3 ± 2.5d) as well as a similar clinical score at therapy onset for both groups (PS/2 F(ab')$_2$: 1.4 ± 0.1, isotype control F(ab')$_2$: 1.5 ± 0.2), but a different sex ratio (Tab. 3.2.5).

Clinical scores were already significantly lower one day after the first injection of α-CD49d (PS/2) F(ab')$_2$ fragments as compared to the control group (day 2: PS/2 F(ab')$_2$ 1.5 ± 0.2, control F(ab')$_2$ 2.2 ± 0.1) (Fig. 3.2.24). This effect was sustained during the treatment experiment, with significant differences found on days 2-4. Furthermore, clinical courses during treatment with α-CD49d (PS/2) F(ab')$_2$ fragments were comparable to the clinical courses of the intact α-CD49d (PS/2) antibody. At the end of the short-term therapy both groups showed the same mean clinical scores (PS/2 F(ab')$_2$: 2.0 ± 0.4, PS/2 IgG: 2.0 ± 0.3) (Fig. 3.2.24).

Tab. 3.2.5: Randomization of mice for the short-term therapy with F(ab')$_2$ fragments. Data are shown as mean ± SEM.

	α-CD49d (PS/2) F(ab')$_2$	Iso. ctrl. F(ab')$_2$
Mean age at therapy onset in days	30.8 ± 1.2	32.3 ± 2.5
Sex ratio ♀ / ♂	3 / 2	3 / 4
Mean clinical score at therapy onset in days	1.4 ± 0.1	1.5 ± 0.2
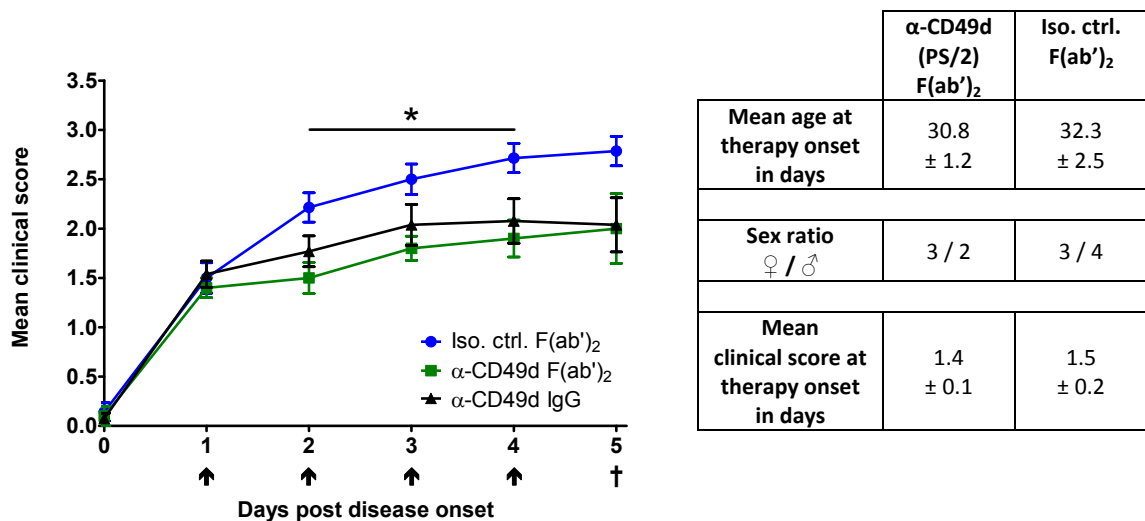
Fig. 3.2.24: Disease course of OSE mice during short-term therapy with the α-CD49d (PS/2) F(ab')$_2$ fragments or isotype control F(ab')$_2$ fragments. Therapy with the α-CD49d (PS/2) F(ab')$_2$ fragments resulted in lower clinical scores as compared to the control group. Clinical courses after therapy with α-CD49d (PS/2) F(ab')$_2$ fragments were comparable to the clinical courses after the therapy with intact α-CD49d (PS/2) antibody. Therapy was started at a clinical score ≥ 1.0 either with 200 µg α-CD49d (PS/2) F(ab')$_2$ fragments or isotype control F(ab')$_2$ fragments intraperitoneally. Medication time points are indicated by black arrows. Clinical scores were monitored every day. One day after the last injection CNS pathology was investigated, indicated by a dagger. Data are mean values ± SEM. α-CD49d (PS/2) F(ab')$_2$ treated group: n = 5; control group: n = 7.

3.2.4.1.6 Reduced white matter demyelination in the spinal cord after treatment with PS/2 F(ab')₂ fragments

The percentage of demyelinated white matter was significantly reduced after therapy with the α-CD49d (PS/2) F(ab')₂ fragments (median: 11.9%) as compared to the control group (median: 29.2%) (Fig. 3.2.25). Furthermore, the extent of white matter demyelination after treatment with α-CD49d (PS/2) F(ab')₂ fragments (median: 11.9%) were comparable to the white matter demyelination after treatment with intact α-CD49d (PS/2) antibody (median: 14.4%) (Fig. 3.2.25).
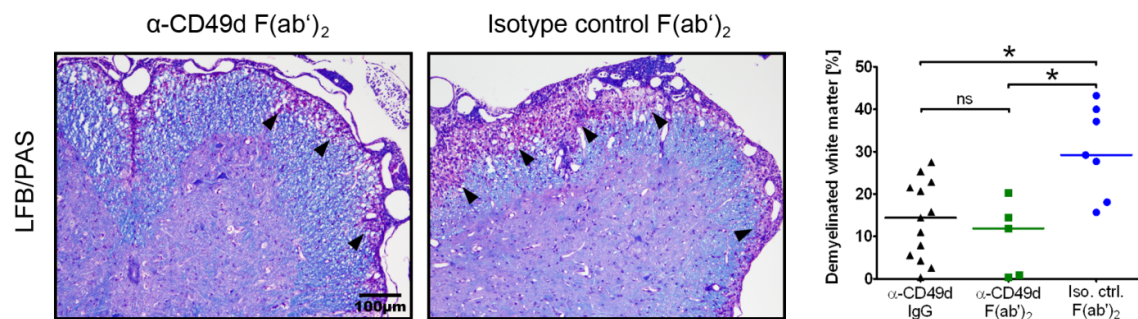
Fig. 3.2.25: White matter demyelination in OSE mice after short-term therapy with the α-CD49d (PS/2) F(ab')₂ fragments or isotype control F(ab')₂ fragments. The white matter demyelination was significantly decreased after the α-CD49d (PS/2) F(ab')₂ fragment therapy as compared to the control group and was similar to the white matter demyelination after therapy with intact α-CD49d (PS/2) antibody. Myelinated as well as demyelinated white matter was determined in the spinal cord after LFB/PAS staining. The percentage of demyelinated white matter was calculated relative to the whole white matter area. Black arrowheads indicate demyelinated white matter.

3.2.4.1.7 Diminished inflammatory cell infiltration in the spinal cord after treatment with the PS/2 F(ab')₂ fragments

To determine the extent of inflammatory cell infiltrates in the spinal cord parenchyma after treatment with the α-CD49d (PS/2) F(ab')₂ fragments or the isotype control F(ab')₂ fragments, cross sections of the spinal cord were stained with the respective immunohistochemical markers. The quantification showed similar numbers of T cells (PS/2 F(ab')₂ median: 692 cells/mm², control F(ab')₂ median: 746 cells/mm²) and as well as B cells (PS/2 F(ab')₂ median: 102 cells/mm², control F(ab')₂ median: 119 cells/mm²), but significantly reduced plasma cell numbers (PS/2 F(ab')₂ median: 0 cells/mm², control F(ab')₂ median: 10 cells/mm²) as well as macrophages

(PS/2 F(ab')$_2$ median: 5469 cells/mm², control F(ab')$_2$ median: 7224 cells/mm²) after the treatment with α-CD49d (PS/2) F(ab')$_2$ fragments as compared to the control group (Fig. 3.2.26).
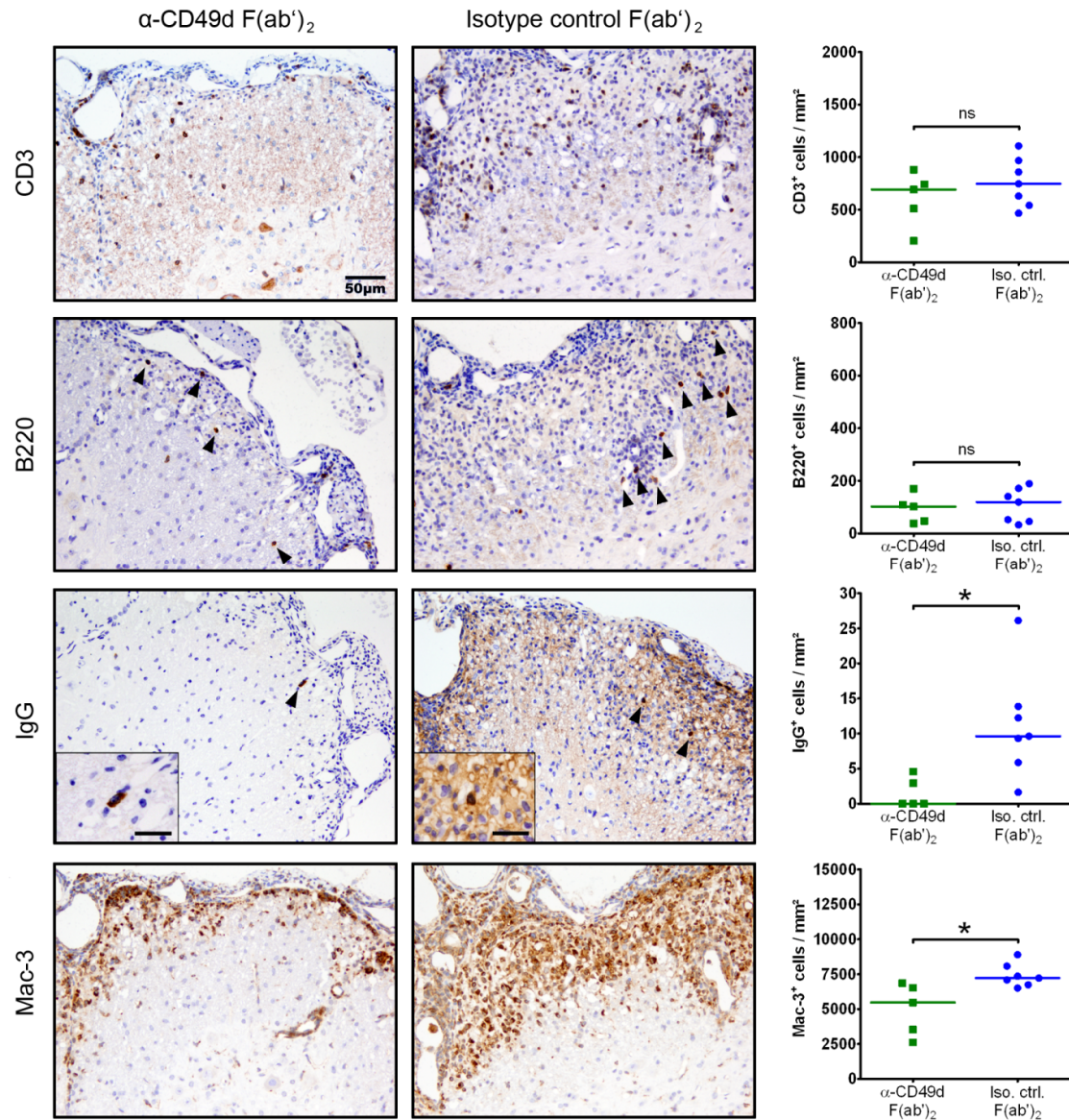
Fig. 3.2.26: Spinal cord inflammatory infiltration in OSE mice after short-term therapy with the α-CD49d (PS/2) F(ab')$_2$ fragments or isotype control F(ab')$_2$ fragments. Therapy with the α-CD49d (PS/2) F(ab')$_2$ fragments resulted in similar numbers of T cells and B cells, but significantly lower plasma cell numbers and macrophages as compared to controls. Inflammatory cell infiltrates were counted in the white matter lesion of the spinal cord after the respective immunohistochemical staining procedures. B cells and plasma cells are indicated by black arrowheads. Scale bar in inset = 20 μm.

In summary, based on the comparable decreased clinical severity, reduced white matter demyelination as well as inflammatory cell infiltration in the spinal cord after therapy with the PS/2 F(ab')$_2$ fragments and intact PS/2 antibody, it can be concluded that the therapeutic effects are independent of the Fc fragment.

3.2.4.2 Clinical outcome upon temporary blockage of CD49d receptors

A significant decrease in unblocked CD49d receptors on PBMCs that lasted over the entire treatment period was observed after natalizumab treatment in humans (Wipfler et al., 2011) In contrast, Niino et al. (2006) described a significant but temporary reduction of free CD49d receptors through the monthly dose interval. To address the question as to which effect lower PS/2 antibody dosages that show a temporary reduction of free CD49d binding sites have, long-term treatment experiments with a reduced α-CD49d (PS/2) dosage were performed.

3.2.4.2.1 Determination of an appropriate treatment dosage for temporary blockage of CD49d receptors

To determine the appropriate treatment dosage with a significant but temporary blockage of the CD49d receptors until the next infusion, different dosages of the α-CD49d (PS/2) antibody were injected once intraperitoneally (Fig. 3.2.27). At defined time points blood was collected and free CD49d receptor binding sites were investigated by flow cytometry analysis with a fluorophore-conjugated α-CD49d (PS/2) antibody. The dosage of 5 μg revealed a strong reduction of free CD49d binding sites by more than 80% for at least nine hours (Fig. 3.2.27, black curve). 24 hours after the injection the number of free CD49d receptors was still diminished by about 20%. A similar level of free CD49d binding sites as compared to before the administration was observed 48 hours after a single injection. Thus an intraperitoneal medication of 5 μg every other day turned out to be adequate for studying the treatment effects after a temporary blockage of CD49d receptors. The obtained results were compared to the PBS-treated control group as well as to the treatment group that received 75 μg every other day and showed a persistent saturation of CD49d receptors during the therapy.
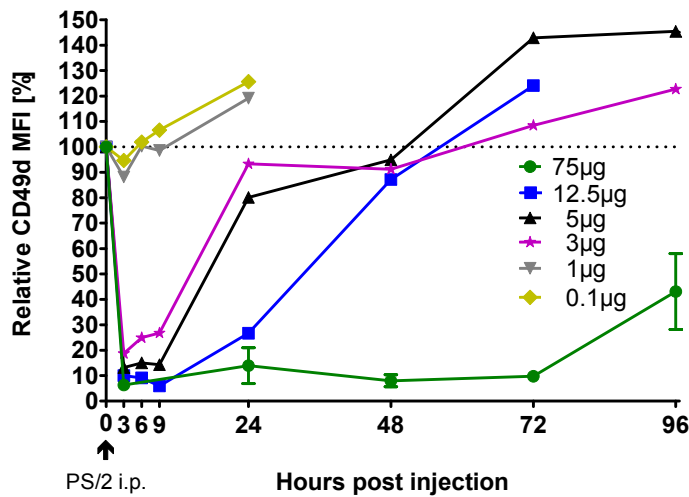
Fig. 3.2.27: Free CD49d binding sites after a single intraperitoneal injection of different α-CD49d (PS/2) antibody dosages. The 5 µg PS/2 injection every other day turned out to be suitable to study therapeutic effects after a temporary blockage of CD49d receptors. Before and at definite time points after a single intraperitoneal injection of different α-CD49d (PS/2) antibody dosages in adult mice, blood was collected and flow cytometry analysis performed. The detection of free CD49d binding sites occurred with a fluorophore-conjugated α-CD49d (PS/2) antibody. Relative MFI is given for all WBCs and was calculated by the median fluorescence intensity of interest minus the median fluorescence intensity of the isotype control. Data are mean values ± SEM. 75 µg injection: n = 3-10, all other dosages: n = 1.

3.2.4.2.2 No impact on the clinical disease course with temporary blockage of CD49d receptors

Randomization of mice showed a similar average age (5 µg PS/2: 41.9 ± 4.5d, 75 µg PS/2: 42.1 ± 2.8d, PBS: 42.3 ± 3.2d) (Tab. 3.2.6) and a similar mean clinical score at therapy onset in the group treated with 5 µg α-CD49d (PS/2) antibody as compared to the both control groups (5 µg PS/2: 1.7 ± 0.1, 75 µg PS/2: 1.5 ± 0.1, PBS: 1.5 ± 0.1). The group treated with 5 µg α-CD49d (PS/2) antibody showed a shift of the sex ratio towards male mice.

Mice treated with 5 µg PS/2 antibody every other day showed a severe disease progression comparable to the PBS-treated group. No treatment effect was evident. The peak of disease severity was reached on day 6 in the group treated with 5 µg α-CD49d (PS/2) antibody and on day 7 in the PBS-treated group showing similar maximal clinical scores (day 6: 5 µg PS/2 3.1 ± 0.1, day 7: PBS 3.0 ± 0.1) (Fig. 3.2.28). At the end of the experiment both groups had high clinical scores (day 31: 5 µg PS/2 2.3 ± 0.2, day 7: PBS 2.2 ± 0.3). By contrast the treatment dosage of 75 µg α-CD49d (PS/2) antibody

resulted in a significant reduction of the clinical severity as compared to the group treated with 5 µg α-CD49d (PS/2) antibody.

Tab. 3.2.6: Randomization of mice for the long-term therapy with a reduced α-CD49d PS/2 dosage. Data are shown as mean ± SEM.

	5 µg α-CD49d (PS/2)	75 µg α-CD49d (PS/2)	PBS
Mean age at therapy onset in days	41.9 ± 4.5	42.1 ± 2.8	42.3 ± 3.2
Sex ratio ♀ / ♂	2 / 5	6 / 6	6 / 6
Mean clinical score at therapy onset in days	1.7 ± 0.1	1.5 ± 0.1	1.5 ± 0.1
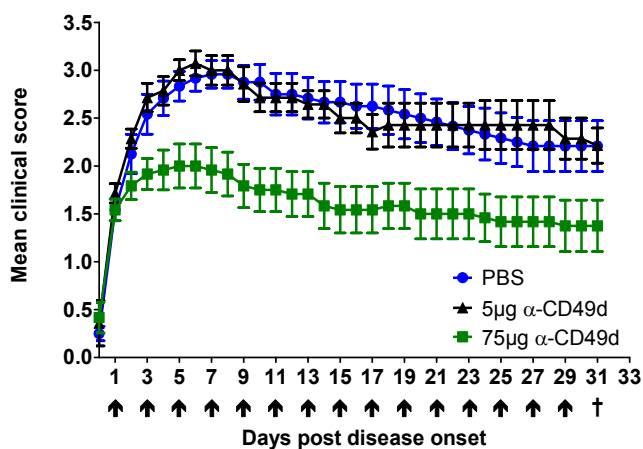
Fig. 3.2.28: Disease course in OSE mice during long-term therapy with 5 µg- and 75 µg α-CD49d (PS/2) antibody or PBS. Therapy with 5 µg of α-CD49d (PS/2) antibody had no impact on clinical severity. Clinical scores were comparable with the PBS-treated control group. Treatment was started when mice showed a clinical score ≥ 1.0 either with 5 µg α-CD49d (PS/2) antibody, 75 µg α-CD49d (PS/2) antibody or PBS intraperitoneally. Medication time points are indicated by black arrows. Clinical scores were monitored every day. Two days after the last injection CNS pathology was investigated, as indicated by a dagger. Data are mean values ± SEM. 5 µg α-CD49d (PS/2): n = 7. 75 µg α-CD49d (PS/2) and PBS: n = 12.

3.2.4.2.3 No significant influence on white matter demyelination in the spinal cord upon temporary blockage of CD49d receptors

The percentage of white matter demyelination in the spinal cord was minimally, non-significantly reduced after therapy with the 5 µg α-CD49d (PS/2) antibody (median: 8.1%) as compared to the PBS control group (median: 8.7%) (Fig. 3.2.29). By contrast treatment with the dosage of 75 µg α-CD49d (PS/2) antibody resulted in a reduction of white matter demyelination as compared to the therapy with 5 µg α-CD49d (PS/2) antibody, but this difference did not reach significance (median: 75 µg PS/2 3.4%).
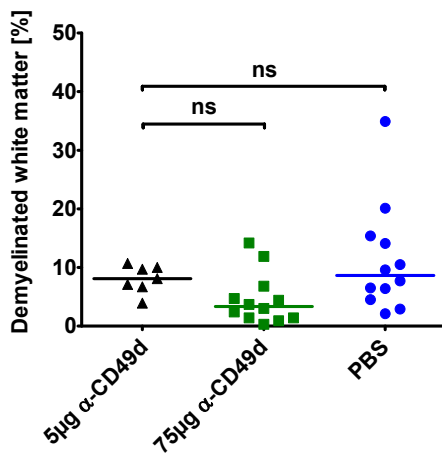
Fig. 3.2.29: White matter demyelination in OSE mice after long-term therapy with 5 µg and 75 µg α-CD49d (PS/2) antibody or PBS. A similar extent of white matter demyelination after therapy with 5 µg α-CD49d (PS/2) antibody as compared to the PBS-treated controls was evident. Thus, no therapy effect of the 5 µg antibody dosage was observed. Myelinated as well as demyelinated white matter was determined in the spinal cord after LFB/PAS staining. The percentage of demyelinated white matter was calculated relative to the whole white matter area.

3.2.4.2.4 Diminished inflammatory cell infiltration in the spinal cord after temporary blockage of CD49d receptors

To investigate whether a temporary blockage of CD49d receptors has as influence on the inflammatory cell infiltrates in the spinal cord parenchyma, the number of T cells (CD3), B cells (B220), plasma cells (IgG) and macrophages (Mac-3) was quantified and compared to the group with a persistent saturation of CD49d receptors during medication as well as to the PBS treated group.

Inflammatory cell infiltrates showed a significant reduction in T cells (5 µg PS/2 median: 102 cells/mm², PBS median: 445 cells/mm²) as well as macrophages (5 µg PS/2 median: 162 cells/mm², PBS median: 493 cells/mm²) after the therapy with 5 µg α-CD49d (PS/2) antibody as compared to the PBS group (Fig. 3.2.30). Furthermore, the number of B cells (5 µg PS/2 median: 15 cells/mm², PBS median: 74 cells/mm²) and plasma cells (5 µg PS/2 median: 8 cells/mm², PBS median: 37 cells/mm²) were also decreased, but not significantly. The comparison with the results obtained from the group with a persistent CD49d receptor blockage showed similar T cell numbers (5 µg PS/2 median: 102 cells/mm², 75 µg PS/2 median: 115 cells/mm²), increased numbers of macrophages (5 µg PS/2 median: 162 cells/mm², 75 µg PS/2 median: 110 cells/mm²) as well as of B cells (5 µg PS/2 median: 15 cells/mm², 75 µg PS/2 median: 2 cells/mm²). Significantly higher numbers of plasma cells were present (5 µg PS/2 median: 8 cells/mm², 75 µg PS/2 median: 0 cells/mm²).
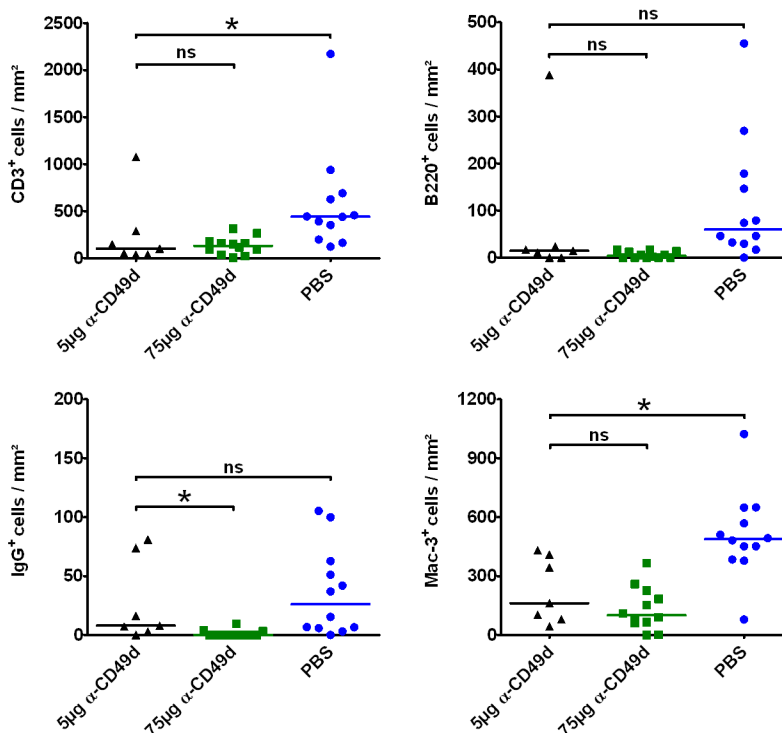
Fig. 3.2.30: Spinal cord inflammatory infiltration in OSE mice after long-term therapy with 5 µg and 75 µg α-CD49d (PS/2) antibody or PBS. Therapy with 5 µg α-CD49d (PS/2) antibody resulted in reduced T cell and macrophage numbers within the spinal cord parenchyma as compared to the PBS control group. Significantly higher numbers of plasma cells were present in the 5 µg α-CD49d (PS/2) antibody treatment group compared to the group treated with 75 µg. Inflammatory cell infiltrates were counted in the white matter lesions of the spinal cord after the respective immunohistochemical staining procedures.

In summary, the temporary blockage of CD49d receptors resulted in decreased T cell and macrophage numbers, but the degree of white matter demyelination as well as the clinical severity were comparable to the PBS control group.

3.2.4.3 Internalization of receptor-antibody complexes during PS/2 antibody therapy

The following experiments aimed at analyzing whether treatment with α-CD49d (PS/2) antibodies results in an internalization of receptor-antibody complexes. A single injection of 75 µg of the α-CD49d (PS/2) antibody resulted in a strong reduction of free CD49d receptor binding sites for at least 72 hours as observed during the determination of a suitable dosage for the mouse therapy experiments (Fig. 3.2.1). Afterwards the number of free CD49d receptor binding sites increased steadily. On the other hand, bound α-CD49d (PS/2) antibody showed a decrease within the first 72 hours while a persistent strong reduction of free CD49d binding sites was shown. I therefore hypothesized an internalization of the receptor-antibody complexes.

To examine this, 75 µg of the α-CD49d (PS/2) antibody was injected intraperitoneally in adult mice. Afterwards blood was collected at definite time points. First the percentage number of free CD49d binding sites on WBCs was examined by flow cytometry staining with the same antibody clone as administered therapeutically. As shown beforehand (Fig. 3.2.1), free CD49d receptor binding sites were reduced > 90 percent already 0.5 hours after the therapeutic antibody injection (Fig. 3.2.31 A, green curve). The receptor saturation lasted until 72 hours after the injection. 96 hours after injection about 60 percent of free CD49d receptor binding sites were measured. About 120 hours after the injection similar free CD49d receptor binding site levels as compared to before the injection were reached.

To determine whether the number of CD49d receptors on the cell surface is altered after the injection of the α-CD49d (PS/2) antibody, it was necessary to detect the CD49d receptors at another domain as by the injected antibody. The α-CD49d antibody clone 9C10 was found to be suitable due to only a minor epitope overlap between this antibody and the α-CD49d antibody clone PS/2. Staining of naïve cells in vitro with both clones in the same sample showed a decrease of the median

fluorescence intensity by about 10 percent as compared to single stainings of the respective antibody clones (Fig. 3.2.31 B). Therefore, the detection of the CD49d receptor quantity on the cell surface was done with the α-CD49d (clone: 9C10) antibody and showed a reduction of about 35 percent 0.5 hours after the injection of the therapeutic α-CD49d (clone: PS/2) antibody (Fig. 3.2.31 A, black curve). 24 hours after the therapeutic antibody injection the number of CD49d receptors dropped further to 30 percent and did not begin to rise again until 72 hours after the α-CD49d (clone: PS/2) antibody injection. The decrease in cell surface CD49d receptors by more than 50 percent supported the hypothesis that receptor-antibody complexes are internalized.

In a next step bound α-CD49d (clone: PS/2) antibody after therapeutic injection was analyzed on the cell surface as well as in the intracellular compartment to further corroborate the hypothesis. A quantification of bound PS/2 antibody to the receptors on the cell surface showed a reduction of about 35 percent 72 hours after the injection as compared to the levels 0.5 hours after the injection (Fig. 3.2.31 A, dark blue curve). Afterwards, bound PS/2 antibody decreased further until almost no bound antibody was detectable 144 hours after the therapeutic injection. Furthermore, the flow cytometry detection of intracellularly located PS/2 antibody showed high numbers already 0.5 hours after the injection, followed by a continuous decrease (Fig. 3.2.31 A, light blue curve).

The same effects were observed when analyzing CD4$^+$ T cells (Fig. 3.2.31 C) as well as B220$^+$ B cells separately (Fig. 3.2.31 D).
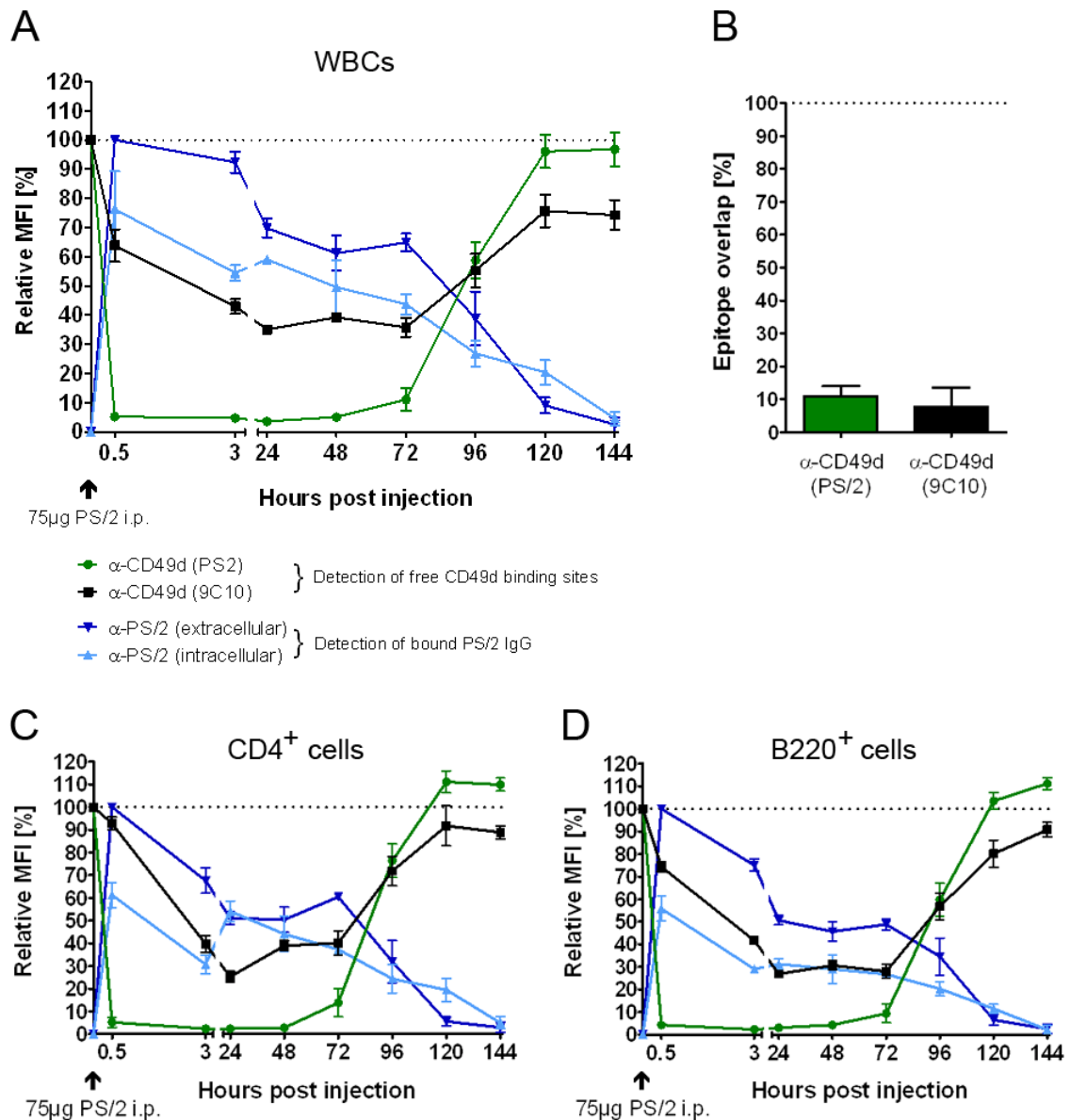
Fig. 3.2.31: Determination of antibody internalization of WBCs during therapy with the α-CD49d (clone: PS/2) antibody. A partial internalization of receptor-antibody complexes during the therapy with α-CD49d (clone: PS/2) antibody was found (A). Before and at definite time points after a single intraperitoneal injection of 75 µg of the α-CD49d (clone: PS/2) antibody in adult mice, blood was collected and flow cytometry analysis performed. Detection of free CD49d binding sites occurred with a fluorophore-conjugated α-CD49d (clone: PS/2) antibody (green curve). The number of CD49d receptors was investigated by a fluorophore-conjugated α-CD49d (clone: 9C10) antibody (black curve). To measure the proportion of bound PS/2 antibody to CD49d receptors on the cell surface (dark blue curve) as well as the amount of intracellular located PS/2 antibody (light blue curve) upon the injection, a fluorophore-conjugated α-PS/2 antibody was used.

To investigate the extent of epitope overlap between α-CD49d antibody clone: 9C10 and clone: PS/2, naïve cells were simultaneously stained with both clones and the obtained median fluorescence intensities compared to single stainings of the respective clones (B). The flow cytometry analysis revealed nearly no epitope overlap between the α-CD49d antibodies clone: 9C10 and clone: PS/2.

Partial antibody internalization could be shown when investigating all WBCs (A), CD4^{+} T cells (C) as well as B220^{+} B cells (D). Relative MFI was calculated by the median fluorescence intensity of interest minus the median fluorescence intensity of the isotype control. Data are mean values ± SEM. (A), (C), (D) n = 3-6; (B) n = 3.

Thus, the reduction in free CD49d binding sites for at least 72 hours after the injection (Fig. 3.2.31 A, green curve) with a simultaneous reduction in CD49d receptors on the cell surface (Fig. 3.2.31 A, black curve), a decrease in bound PS/2 antibody to the receptors on the cell surface (Fig. 3.2.31 A, dark blue curve) and, finally, the intracellular detection of PS/2 antibody (Fig. 3.2.31 A, light blue curve) all indicate a partial internalization of CD49d receptor-antibody complexes.

4 Discussion

Natalizumab, a humanized monoclonal antibody directed against α-4 integrin has been approved for the treatment of MS. Although natalizumab is a highly beneficial drug which effectively reduces clinical relapses, some patients do not respond to the therapy. The histopathological effects after natalizumab therapy are still unknown.

In the present study the histopathology in a cohort of natalizumab-treated MS patients was investigated and compared to MS patients with no prior natalizumab therapy. Furthermore, the inflammatory infiltrates after natalizumab therapy were correlated with clinical and therapy-related data. In the second part of the thesis, the results of natalizumab therapy in humans were reviewed in a B cell-dependent EAE model of MS (OSE).

4.1 Histopathological changes after natalizumab therapy

MS patients treated with natalizumab showed typical MS pathology with inflammatory demyelinated lesions in the CNS. The immunohistochemical characterization revealed that inflammatory infiltrates were mainly composed of T cells and macrophages as well as some B cells and plasma cells. In the following section, the main findings regarding CNS inflammation are discussed: a) increased plasma cell numbers compared to controls and b) T cell infiltration despite natalizumab therapy.

4.1.1 Increased plasma cell numbers in the CNS due to natalizumab therapy

Plasma cell numbers were significantly increased in active demyelinating lesions as well as in inactive demyelinated lesions as compared to MS patients with no prior natalizumab therapy (Fig. 3.1.1, Fig. 3.1.2). Controls with no prior natalizumab treatment were matched for disease duration, as increased plasma cell numbers are described in MS patients with longer disease duration (Ozawa et al., 1994; Kuhlmann et al., 2002; Frischer et al., 2009). In addition, in the group of natalizumab-treated

patients a statistical correlation of plasma cell numbers with disease duration showed no effect of the disease duration on plasma cell numbers (Fig. 3.1.4, Suppl. Tab. 1). This may indicate that higher plasma cell numbers are truly related to the natalizumab treatment itself. However, plasma cell numbers were also not dependent on therapy duration (Fig. 3.1.5, Suppl. Tab. 2) or the time interval between last natalizumab injection and biopsy (Fig. 3.1.6, Suppl. Tab. 3). Most patients received other immunosuppressive and / or immunomodulatory therapies prior to natalizumab and natalizumab was chosen due to persistent disease activity. This raises the question as to whether the plasma cell accumulation occurred due to therapy failure even before natalizumab was started. In this situation, lower plasma cell numbers with a longer treatment interval would be expected. However, also no negative correlation of plasma cell numbers with longer ongoing natalizumab therapy was found (Fig. 3.1.5, Suppl. Tab. 2). Furthermore, the observation of the tendency of higher plasma cell numbers within the first 3½ months after cessation of the therapy, when natalizumab is still pharmacologically active (Wipfler et al., 2011), as compared to the patients who underwent biopsy later than 3½ months after the last natalizumab infusion, speaks against the assumption that plasma cells accumulated before the natalizumab treatment, and supports the hypothesis of a natalizumab-related effect (Fig. 3.1.9). In general, in my study results comparing subgroups have to be interpreted with caution due to low patient numbers. Immunosuppressive and immunomodulatory agents such as mitoxantrone and IFN-ß have effects on several cytokines, adhesion molecules, integrins and MMPs and result in inhibition of immune cell migration into the CNS (Vollmer et al., 2010; Dhib-Jalbut and Marks, 2010). Therefore, it could also be that significantly lower plasma cell numbers in the controls with no prior natalizumab therapy are due to a better response to immunosuppressive and / or immunomodulatory agents as compared to natalizumab-treated patients. However, a significant reduction in plasma cell numbers was observed both in biopsy (Fig. 3.1.1) and autopsy controls (Fig. 3.1.2). In the latter group autopsy was performed between the years 1971 and 1994 when drugs for MS treatment in Europe had not yet been approved, so that patients were treatment naïve (Pozzilli et al., 2002). Thus, I concluded that plasma cell accumulation in natalizumab-treated patients is most likely due to the medication itself.

α-4 integrin, the alpha component of VLA-4, is the target molecule of natalizumab and is involved in the transmigration process of immune cells through the BBB (Engelhardt and Ransohoff, 2012). In natalizumab treatment naïve patients, immune cells differ in the VLA-4 expression (Niino et al., 2006). For instance, VLA-4 levels on B cells are increased by about 1.7-fold and on memory B cells by about 2.4-fold as compared to T cells and memory T cells, respectively. In an *in vitro* model of the BBB, it was shown that B cells migrate more efficiently than T cells from the same individual across human brain-derived endothelial cells (HBEC) (Alter et al., 2003). Compared to B cells significantly higher levels of VLA-4 are observed in healthy humans on plasmablasts (2.9-fold) and plasma cells (3.5-fold) (Caraux et al., 2010), possibly resulting in a more efficient transmigration across the BBB. Natalizumab binds to VLA-4 and this can be shown by a reduction in free VLA-4 binding sites. Yet, it does not reduce free VLA-4 binding sites to the same extent on the different immune cell subsets. It was shown that after natalizumab therapy, free VLA-4 binding sites as determined by the percent reduction in MFI were more efficiently decreased on T cells (by 49%) as compared to B cells (by 29%) (Niino et al., 2006). Furthermore, a correlation was observed between VLA-4 expression and migratory capacity of PBMCs across HBECs *in vitro* (Niino et al., 2006). Thus, it seems possible that after natalizumab treatment B cells as compared to T cells transmigrate more efficiently into the CNS. The significant but not complete blockage of VLA-4 receptors on T cells after natalizumab therapy is in line with the T cell numbers observed in the CNS after natalizumab therapy: Although T cells are found within lesions (indicating that the transmigration is not completely blocked), T cells are lower in the first 3½ months after treatment was stopped (a certain percentage of VLA-4 binding sites are occupied by the medication) as compared to T cells numbers found longer than 3½ months after the last natalizumab infusion, when VLA-4 is not bound by the antibody anymore (Fig. 3.1.9). However, plasma cells in natalizumab-treated patients were even increased compared to controls and tended to be higher when natalizumab was pharmacologically active (< 3½ mos.) as compared to a longer time interval when no more treatment effect is expected (> 3½ mos.) (Fig. 3.1.9). Natalizumab, on the one hand, interferes with the interaction between VLA-4 and VCAM-1 and thus hinders immune cells to enter the CNS, but on the other hand, it also increases the influx of immune cells out of the bone marrow into the peripheral

blood circulation. This was shown in α-4 integrin-deficient mice (Scott et al., 2003). In humans natalizumab therapy leads to 1.5-fold increased lymphocyte numbers in the peripheral blood (Krumbholz et al., 2008). Among the lymphocyte population the highest increase in absolute cell numbers after natalizumab therapy was shown for pre B cells (7.4-fold) followed by B cells (2.8-fold), CD8$^+$ T cells (1.8-fold), plasmablasts (1.5 fold) and CD4$^+$ T cells (1.5-fold) (Krumbholz et al., 2008). Therefore, one possible explanation for the observed plasma cell accumulation in the CNS after natalizumab therapy could be the insufficient blockage of VLA-4 receptors allowing transmigration into the CNS and an increased number of plasma cell precursors in the peripheral blood due to release from the bone marrow. B cells / plasma cells might also enter the CNS independent of VLA-4 using the LFA-1/ICAM-1 as an alternative pathway as it was shown for Th17 cells in EAE (Rothhammer et al., 2011).

The development into long-lived plasma cells is a multistep process with several plasma cell precursors (Meinl et al., 2006). This raises the question as to which cell stage is migrating into the CNS. Pre B cells originate from stem cells in the bone marrow and migrate to secondary lymphatic organs, where they become mature (Meinl et al., 2006). Once they come in contact with an antigen they differentiate in an antigen-driven germinal center reaction to memory B cells and plasmablasts and then enter the peripheral circulation. Plasmablasts can migrate into the bone marrow and differentiate into non-dividing plasma cells. Due to anti-apoptotic stimuli from their microenvironment they can survive for a long time in the bone marrow (Winter et al., 2012). It is assumed that long-lived plasma cells stay within these survival niches and do not migrate (Radbruch et al., 2006). Therefore, it is very unlikely that the plasma cell accumulation in the natalizumab-treated patients results from migration of long-lived plasma cells out of the bone marrow into the CNS. Meinl et al. (2006) suggested four possible pathways for the appearance of long-lived plasma cells in the CNS of MS patients. First, circulating peripheral plasmablasts transmigrate into the CNS where they differentiate into plasma cells. Second, memory B cells enter the CNS and undergo local antigen-driven differentiation into plasmablasts and plasma cells. Third, memory B cells migrate into germinal-center-like structures in meninges where they undergo differentiation into plasmablasts and plasma cells. Alternatively, a differentiation to plasma cells from naïve B cells in germinal-center-like structures is

also discussed. Fourth, memory B cells enter the CNS and differentiate locally into plasmablasts and plasma cells in an antigen independent bystander reaction. Plasma cells arising from pathway number four may constitute only a minor number because in infectious CNS disease, it has been shown that most produced immunoglobulins are directed against the causative agent (Meinl et al., 2006). Furthermore germinal-center-like structures as necessary in pathway number three are described predominantly in secondary-progressive MS patients (Serafini et al., 2004; Magliozzi et al., 2007). Therefore pathway number three would only be plausible for one third of the natalizumab-treated patients investigated in my study as the other patients had a relapsing-remitting disease course (Tab. 2.1). In addition, no difference in plasma cell numbers could be observed between patients with a relapsing-remitting and secondary-progressive disease course. Plasma cell accumulation in the CNS of relapsing-remitting natalizumab treated patients could thus be 1) either due to plasmablast transmigration into the CNS and following differentiation into plasma cells or 2) transmigration of memory B cell that differentiate into plasma cells in response to antigen outside of follicles.

In addition, natalizumab could have further effects promoting plasma cell accumulation. For instance, an up-regulation of the genes MS4A1, PAX5, POU2AF1 and SPIB were identified in WBCs after natalizumab therapy which suggests an increased B cell differentiation to plasma cells (Lindberg et al., 2008). Moreover, a B cell-friendly environment in the CNS after natalizumab therapy could possibly also promote differentiation of local B cells to plasma cells.

Although natalizumab is an effective MS drug, the findings of increased plasma cell numbers in the CNS after natalizumab therapy could have implications for the treatment strategy of MS patients. Neuromyelitis optica (NMO) is an antibody-mediated inflammatory demyelinating disease characterized by the occurrence of pathogenic antibodies directed against the aquaporin-4 (AQP-4) water channel, which is expressed in astrocytic foot processes at the BBB (Lennon et al., 2005). Several lines of evidence show that NMO patients do not respond to natalizumab therapy and treatment may even result in worsening of the disease (Barnett et al., 2012; Kleiter et al., 2012; Jacob et al., 2012). In a subgroup of MS patients with early active

demyelinating lesions, immunoglobulin and complement are present (so-called immunopattern II), suggesting a key role for B cells and plasma cells in mediating disease pathology (Lucchinetti et al., 2000). Therefore, treatment of these patients with natalizumab could have negative effects due to increased plasma cell recruitment into the CNS, resulting in disease exacerbation. However, this is highly speculative since if pathogenic antibodies indeed play a role in mediating pathology, these could also be produced in the periphery, as is also suggested for NMO (Jarius et al., 2010; Chihara et al., 2011; Jarius et al., 2011).

4.1.2 T cell numbers in the CNS are affected after natalizumab therapy

T cell numbers were not significantly reduced in active demyelinating lesions as well as in inactive demyelinated lesions as compared to MS patients with no prior natalizumab therapy (Fig. 3.1.1, Fig. 3.1.2). Yet T cell numbers tended to be decreased when intervals between the last natalizumab infusion and biopsy were shorter and natalizumab still active (interval < 3½ mos.) as compared to longer intervals (> 3½ mos.) (Fig. 3.1.9). In addition, a positive correlation of perivascular $CD4^+$ T cells and the interval between last natalizumab infusion and biopsy was found (Suppl. Fig. 3). These results indicate that despite the natalizumab therapy T cells enter the CNS; however, they seem to be present in lower numbers, when the medication is pharmacologically active. Again, it must be stressed that definite conclusions cannot be drawn due to low patient numbers in subgroups. Although an effective prevention of T cell migration into the CNS after blockage of VLA-4 receptors was shown in an animal model of EAE (Bartholomäus et al., 2009), these results show that natalizumab therapy can hinder only a certain proportion of T cells to enter the CNS. This is also supported by the positive correlation of T cells with longer therapy duration (Suppl. Fig. 2). An explanation for these results could be the fact that natalizumab indeed leads to a significant but not complete reduction of the VLA-4 receptors on blood cells (Niino et al., 2006). Furthermore, a subset of the quantified T cells could be comprised of Th17 cells. This T cell subset has also been implicated in the pathogenesis of MS (Brucklacher-Waldert et al., 2009; Fletcher et al., 2010). In EAE it was shown that Th17 cells are able to enter the CNS independently of VLA-4, suggesting migration via the

choroid plexus into the brain parenchyma in a LFA-1/ICAM-1 dependent manner (Rothhammer et al., 2011).

4.1.3 No indication for "rebound" of inflammatory cells within lesions after discontinuation of natalizumab therapy

Single reports described increased lesion activity after discontinuation of natalizumab and considered it as rebound (Vellinga et al., 2008; Killestein et al., 2010). The pathological correlate of a possible rebound effect is unclear and could either consist of 1) a disproportionally high number of lesions after cessation of therapy with pathology of the single lesion indistinguishable from typical MS lesions, or 2) lesions with increased numbers of inflammatory cells due to an increased influx from the periphery. To investigate the second hypothesis, inflammatory infiltrates were correlated with the interval between last natalizumab infusion and biopsy. Except for a correlation of perivascular CD4$^+$ T cells no correlation of other immune cell subsets with this time interval was found. The fact that T cells in the natalizumab-treated group tended to be decreased as compared to MS patients with no prior natalizumab therapy suggests that the correlation of the CD4$^+$ T cell numbers is rather due to a disease return than to a rebound activity. Importantly, no cases with unusual high numbers of inflammatory cells were observed. These results support other recent studies which showed unchanged WBC numbers in the CSF as well as no significant increase in lesion activity after cessation of natalizumab (Stüve et al., 2006 a; Stüve et al., 2009 b; O'Connor et al., 2011; Melis et al., 2013).

In conclusion, although natalizumab is known to be an effective drug for MS treatment, it could be shown that natalizumab does not completely prevent immune cells from entering the CNS. Plasma cell numbers were even increased after natalizumab therapy as compared to controls with no prior natalizumab therapy. Due to the important role also for B cells / plasma cells in MS pathogenesis, these findings could be of therapeutic relevance.

4.2 Effects after natalizumab analogon therapy in a B cell-dependent mouse model of MS

In the following section peripheral and central effects after therapy with a natalizumab analogon (PS/2 antibody) in a B cell-dependent mouse model (OSE) are discussed.

4.2.1 Comparable peripheral effects on blood cells after PS/2 antibody therapy in a B cell-dependent EAE model of MS as compared to natalizumab therapy in humans

Before PS/2 antibody therapy flow cytometry analysis of WBCs revealed the highest expression of VLA-4 on monocytes followed by NK cells, B cells / plasma cells, T cells and granulocytes (Fig. 3.2.2 A, C). This expression pattern is very similar to the VLA-4 expression observed on human blood cells (Niino et al., 2006; Wipfler et al., 2011; Harrer et al., 2011; Harrer et al., 2012). Treatment with PS/2 antibody significantly decreased VLA-4 expression on all investigated immune cell subsets (Fig. 3.2.2 A, C), as it was also shown in humans after natalizumab therapy (Niino et al., 2006; Wipfler et al., 2011; Harrer et al., 2011; Harrer et al., 2012). Furthermore, an increase in WBC numbers was observed after PS/2 antibody therapy (Fig. 3.2.4 A) with a pronounced effect on B cells (Fig. 3.2.4 B), which was demonstrated in humans after natalizumab therapy as well (Krumbholz et al., 2008). Thus, before and after blockage of VLA-4 comparable effects on WBCs in the B cell-dependent mouse model of demyelination as in humans are found.

4.2.2 PS/2 antibody therapy is effective when given early in the disease course

After disease onset untreated OSE mice showed a progressive disease course with steady worsening of symptoms until day 7 followed by a slight recovery (Fig. 3.2.5, Fig. 3.2.11 A). Treatment with 75 µg PS/2 antibody after the first clinical symptoms showed beneficial effects on the clinical outcome already few days after the first injection (Fig. 3.2.5, Fig. 3.2.11 A). This is in line with another study demonstrating reduced clinical severity after PS/2 antibody therapy in a T cell-mediated mouse model of EAE when given immediately after the onset of the disease (Theien et al., 2001).

Histological analysis of the CNS revealed significantly reduced white matter demyelination after short-term as well as long-term treatment as compared to controls (Fig. 3.2.6, Fig. 3.2.12). The marked decrease in demyelinated white matter area after the long-term treatment as compared to the short-term treatment suggests mainly a reduction of oedema. In EAE the occurrence of oedema was especially observed in the spinal cord during the acute disease phase and appeared to be due to the BBB disruption (Stohl et al., 1979; Floris et al., 2004). Although no electron microscopy was performed, immunohistochemical staining of several myelin proteins revealed no evidence of remyelination (data not shown). The quantification of inflammatory cell infiltrates after PS/2 antibody therapy showed a significant reduction in all investigated immune cell subsets after the long-term treatment as compared to controls (Fig. 3.2.7, Fig 3.2.13). No differential effect on a particular immune cell subset was observed with the chosen dosage of 75 µg PS/2 antibody.

The beneficial effect on the clinical outcome is in accordance with human findings: Short-term treatment studies showed that already a single natalizumab dosage significantly decreased Gd-enhancing lesion volume a few weeks after the medication (O'Connor et al., 2004). Two natalizumab infusions revealed the same results (Tubridy et al., 1999) and six infusions showed in addition lower relapse rates (Miller et al., 2003; O'Connor et al., 2005). Data after long-term monotherapy with natalizumab were mainly obtained in the AFFIRM study (Polman et al., 2006; Calabresi et al., 2007; Rudick et al., 2007; Havrdova et al., 2009; Hutchinson et al., 2009). Natalizumab treatment over the course of two years reduced the risk of sustained progression of disability by 42 percent and the relapse rate by 68 percent (Polman et al., 2006). In addition, higher patient numbers were observed to be free of disease after natalizumab therapy (Havrdova et al., 2009). However, natalizumab is also associated with the risk of PML (Langer-Gould et al., 2005; Kleinschmidt-DeMasters et al., 2005; Lindå et al., 2009). The incidence of PML in natalizumab treated patients is less than 1 percent and is further declining in patients who are serum negative for anti-JCV virus antibody titers, with no prior or current immunosuppressive therapy and with a natalizumab therapy duration shorter than 2 years (Bloomgren et al., 2012; Kawamoto et al., 2012).

In humans a significant decrease in free VLA-4 receptors on PBMCs was described after natalizumab therapy. However, controversial data have been published on how long receptors remain blocked. Wipfler et al., (2011) described a persistent reduction in the free VLA-4 receptors throughout the entire treatment period. In contrast, Niino et al. (2006) showed that free VLA-4 receptors rose again before the next natalizumab infusion. Therefore, therapy effects were also investigated in the OSE mouse model with a lower antibody dosage that showed an initial, but not persistent, reduction of VLA-4 receptors, mimicking the situation described by Nino et al. (2006). Therapy with the lower PS/2 antibody dosage resulted in significantly reduced numbers of T cells and macrophages (Fig. 3.2.30) in the spinal cord lesions. However, B cells and plasma cells were not significantly decreased, possibly indicating a more efficient transmigration into the CNS compared to T cells and macrophages. No effect on clinical severity (Fig. 3.2.28) and white matter demyelination (Fig. 3.2.29) was observed. These results indicate that a temporary blockage of VLA-4 receptors in the OSE mouse model has some effects on the immune cells within CNS lesions, but is not beneficial with regard to demyelination and clinical outcome.

PS/2 antibody therapy after the peak of disease had no effect on the clinical course, white matter demyelination and spinal cord infiltration (Fig. 3.2.14, Fig. 3.2.15, Fig. 3.2.16). Other studies applying the PS/S antibody in a T cell-mediated relapsing-EAE model in later disease stages also showed no therapeutic effect (Tsunoda et al., 2007) or even a worsening of symptoms (Theien et al., 2001). In humans only minor studies have been published for natalizumab therapy in progressive MS patients, and no clear therapeutic efficacy has been demonstrated (Cadavid et al., 2013).

Discontinuation of PS/2 therapy showed no return of the disease activity (Fig. 3.2.17). The extent of white matter demyelination and spinal cord infiltration was similar 15 days as well as two days after the last PS/2 injection and was decreased as compared to controls (Fig. 3.2.18, Fig. 3.2.12, Fig. 3.2.19, Fig. 3.2.13). The OSE mouse model might be unsuitable to study rebound effects due to the monophasic disease course. However, the results are in line with the human findings in this study that showed no evidence of rebound activity after stopping natalizumab therapy (see chapter 4.1.3).

4.2.3 Mode of action of PS/2 antibody

Natalizumab was designed on an IgG4 framework to increase the biological pharmacological half-life, but also to reduce effector functions as compared to other human immunoglobulin G classes (Léger et al., 1997; Mountain and Adair, 1992). Therefore, natalizumab does not activate complement and can only bind to FcRI on human monocytes (Jefferis and Kumararatne, 1990). By contrast, PS/2 was generated in rats and belongs to the IgG class 2b. This isotype is able to bind complement component C1q (Hugh-Jones et al., 1983) as well as to interact with FcRI and FcRII (Woof et al., 1986; Haagen et al., 1995), raising the question as to whether the therapeutic effects of the PS/2 antibody are not only caused by blocking the VLA-4 receptors but also by effector functions related to the Fc region. However, short-term treatment with PS/2 F(ab')$_2$ fragments showed significantly decreased clinical severity and white matter demyelination as compared to the therapy with the isotype control F(ab')$_2$ fragments (Fig. 3.2.24, Fig. 3.2.25). The beneficial clinical effect after treatment with the PS/2 F(ab')$_2$ fragments was the same as shown for the intact PS/2 antibody (Fig. 3.2.24). Moreover, therapy with the PS/2 F(ab')$_2$ fragments also revealed a comparable white matter demyelination (Fig. 3.2.25) and the same peripheral effects as compared to the intact PS/2 antibody (Fig. 3.2.23). These results indicate that the therapeutic effect of the PS/2 antibody therapy is mostly due to the specific binding to its target α-4 integrin and is not related to Fc functions. This mode of action is also assumed for the natalizumab treatment in humans.

After PS/2 antibody treatment, antibody-receptor complexes may be internalized. Recent studies suggested that binding of natalizumab to α-4 integrin resulted in an internalization of the antibody-receptor complex (Benkert et al., 2012). My studies could confirm these findings in the OSE mouse model, indicating a partial internalization of CD49d receptor-antibody complexes. The internalization effect is not only described for natalizumab and the PS/2 antibody, but also for another rodent α-4 integrin antibody (Leone et al., 2003; Fleming et al., 2010), indicating a common effect for antibodies directed against α-4 integrin.

In conclusion, the present results show that the natalizumab analogon therapy is also effective in a B cell-dependent mouse model of MS. Natalizumab analogon therapy was beneficial when given early in the disease course, but not when administered in late disease stages, correlating to the observations in MS treated with natalizumab. In contrast to the human studies in which an increase in plasma cells after natalizumab therapy was observed, all investigated inflammatory cell subsets including T and B cells, plasma cells and macrophages were decreased after natalizumab analogon therapy. My studies confirm that the therapeutic effect is mediated by antibody binding and not Fc mediated, leading to partial antibody-receptor internalization.

References

A

Alter A, Duddy M, Hebert S, Biernacki K, Prat A, Antel JP, Yong VW, Nuttall RK, Pennington CJ, Edwards DR, Bar-Or A. (2003). Determinants of human B cell migration across brain endothelial cells. J Immunol; 170(9):4497-505.

B

Bakker DA, Ludwin SK. Blood-brain barrier permeability during Cuprizone-induced demyelination. (1987). Implications for the pathogenesis of immune-mediated demyelinating diseases. J Neurol Sci; 78(2):125-37.

Blakemore WF, Franklin RJ. (2008). Remyelination in experimental models of toxin-induced demyelination. Curr Top Microbiol Immunol; 318:193-212.

Baranzini SE, Jeong MC, Butunoi C, Murray RS, Bernard CC, Oksenberg JR. (1999). B cell repertoire diversity and clonal expansion in multiple sclerosis brain lesions. J Immunol; 163(9):5133-44.

Barcellos LF, Oksenberg JR, Begovich AB, Martin ER, Schmidt S, Vittinghoff E, Goodin DS, Pelletier D, Lincoln RR, Bucher P, Swerdlin A, Pericak-Vance MA, Haines JL, Hauser SL; Multiple Sclerosis Genetics Group. (2003). HLA-DR2 dose effect on susceptibility to multiple sclerosis and influence on disease course. Am J Hum Genet; 72(3):710-6.

Barnett MH, Prineas JW, Buckland ME, Parratt JD, Pollard JD. (2012). Massive astrocyte destruction in neuromyelitis optica despite natalizumab therapy. Mult Scler; 18(1):108-12.

Baron JL, Madri JA, Ruddle NH, Hashim G, Janeway CA Jr. (1993). Surface expression of alpha 4 integrin by CD4 T cells is required for their entry into brain parenchyma. J Exp Med; 177(1):57-68.

Bartholomäus I, Kawakami N, Odoardi F, Schläger C, Miljkovic D, Ellwart JW, Klinkert WE, Flügel-Koch C, Issekutz TB, Wekerle H, Flügel A. (2009). Effector T cell interactions with meningeal vascular structures in nascent autoimmune CNS lesions. Nature; 462(7269):94-8.

Bauer M, Brakebusch C, Coisne C, Sixt M, Wekerle H, Engelhardt B, Fässler R. (2009). Beta1 integrins differentially control extravasation of inflammatory cell subsets into the CNS during autoimmunity. Proc Natl Acad Sci U S A; 106(6):1920-5.

Benkert TF, Dietz L, Hartmann EM, Leich E, Rosenwald A, Serfling E, Buttmann M, Berberich-Siebelt F. (2012). Natalizumab exerts direct signaling capacity and supports a pro-inflammatory phenotype in some patients with multiple sclerosis. PLoS One; 7(12):e52208.

Bettelli E, Pagany M, Weiner HL, Linington C, Sobel RA, Kuchroo VK. (2003). Myelin oligodendrocyte glycoprotein-specific T cell receptor transgenic mice develop spontaneous autoimmune optic neuritis. J Exp Med; 197(9):1073-81.

Bettelli E, Baeten D, Jäger A, Sobel RA, Kuchroo VK. (2006). Myelin oligodendrocyte glycoprotein-specific T and B cells cooperate to induce a Devic-like disease in mice. J Clin Invest; 116(9):2393-402.

Bloomgren G, Richman S, Hotermans C, Subramanyam M, Goelz S, Natarajan A, Lee S, Plavina T, Scanlon JV, Sandrock A, Bozic C. (2012). Risk of natalizumab-associated progressive multifocal leukoencephalopathy. N Engl J Med; 366(20):1870-80.

Brocke S, Piercy C, Steinman L, Weissman IL, Veromaa T. (1999). Antibodies to CD44 and integrin alpha4, but not L-selectin, prevent central nervous system inflammation and experimental encephalomyelitis by blocking secondary leukocyte recruitment. Proc Natl Acad Sci U S A; 96(12):6896-901.

Brucklacher-Waldert V, Stuerner K, Kolster M, Wolthausen J, Tolosa E. (2009). Phenotypical and functional characterization of T helper 17 cells in multiple sclerosis. Brain; 132(Pt 12):3329-41.

Brück W, Porada P, Poser S, Rieckmann P, Hanefeld F, Kretzschmar HA, Lassmann H. (1995). Monocyte/macrophage differentiation in early multiple sclerosis lesions. Ann Neurol; 38(5):788-96.

Brück W. (2005). Clinical implications of neuropathological findings in multiple sclerosis. J Neurol; 252 Suppl 3:iii10-iii14.

C

Cadavid D, Jurgensen S, Lee S. (2013). Impact of natalizumab on ambulatory improvement in secondary progressive and disabled relapsing-remitting multiple sclerosis. PLoS One; 8(1):e53297.

Calabresi PA, Giovannoni G, Confavreux C, Galetta SL, Havrdova E, Hutchinson M, Kappos L, Miller DH, O'Connor PW, Phillips JT, Polman CH, Radue EW, Rudick RA, Stuart WH, Lublin FD, Wajgt A, Weinstock-Guttman B, Wynn DR, Lynn F, Panzara MA; AFFIRM and SENTINEL Investigators. (2007). The incidence and significance of anti-natalizumab antibodies: results from AFFIRM and SENTINEL. Neurology; 69(14):1391-403.

Caraux A, Klein B, Paiva B, Bret C, Schmitz A, Fuhler GM, Bos NA, Johnsen HE, Orfao A, Perez-Andres M; Myeloma Stem Cell Network. (2010). Circulating human B and plasma cells. Age-associated changes in counts and detailed characterization of circulating normal CD138- and CD138+ plasma cells. Haematologica; 95(6):1016-20.

Chan A, Lee DH, Linker R, Mohr A, Toyka KV, Gold R. (2007). Rescue therapy with anti-CD20 treatment in neuroimmunologic breakthrough disease. J Neurol; 254(11):1604-6.

Chihara N, Aranami T, Sato W, Miyazaki Y, Miyake S, Okamoto T, Ogawa M, Toda T, Yamamura T. (2011). Interleukin 6 signaling promotes anti-aquaporin 4 autoantibody production from plasmablasts in neuromyelitis optica. Proc Natl Acad Sci U S A; 108(9):3701-6.

Chitnis T. (2007). The role of CD4 T cells in the pathogenesis of multiple sclerosis. Int Rev Neurobiol; 79:43-72.

Coisne C, Mao W, Engelhardt B. (2009). Cutting edge: Natalizumab blocks adhesion but not initial contact of human T cells to the blood-brain barrier in vivo in an animal model of multiple sclerosis. J Immunol; 182(10):5909-13.

Colombo M, Dono M, Gazzola P, Roncella S, Valetto A, Chiorazzi N, Mancardi GL, Ferrarini M. (2000). Accumulation of clonally related B lymphocytes in the cerebrospinal fluid of multiple sclerosis patients. J Immunol; 164(5):2782-9.

Constantinescu CS, Farooqi N, O'Brien K, Gran B. (2011). Experimental autoimmune encephalomyelitis (EAE) as a model for multiple sclerosis (MS). Br J Pharmacol; 164(4):1079-106.

Cross AH, Stark JL, Lauber J, Ramsbottom MJ, Lyons JA. (2006). Rituximab reduces B cells and T cells in cerebrospinal fluid of multiple sclerosis patients. J Neuroimmunol; 180(1-2):63-70.

D

del Pilar Martin M, Cravens PD, Winger R, Frohman EM, Racke MK, Eagar TN, Zamvil SS, Weber MS, Hemmer B, Karandikar NJ, Kleinschmidt-DeMasters BK, Stüve O. (2008). Decrease in the numbers of dendritic cells and CD4+ T cells in cerebral perivascular spaces due to natalizumab. Arch Neurol; 65(12):1596-603.

del Pilar Martin M, Cravens PD, Winger R, Kieseier BC, Cepok S, Eagar TN, Zamvil SS, Weber MS, Frohman EM, Kleinschmidt-Demasters BK, Montine TJ, Hemmer B, Marra CM, Stüve O. (2009). Depletion of B lymphocytes from cerebral perivascular spaces by rituximab. Arch Neurol; 66(8):1016-20.

Dhib-Jalbut S, Marks S. (2010). Interferon-beta mechanisms of action in multiple sclerosis. Neurology; 74 Suppl 1:S17-24.

E

Engelhardt B, Laschinger M, Schulz M, Samulowitz U, Vestweber D, Hoch G. (1998). The development of experimental autoimmune encephalomyelitis in the mouse requires alpha4-integrin but not alpha4beta7-integrin. J Clin Invest; 102(12):2096-105.

Engelhardt B, Ransohoff RM. (2012). Capture, crawl, cross: the T cell code to breach the blood-brain barriers. Trends Immunol; 33(12):579-89.

F

Fleming JC, Bao F, Cepinskas G, Weaver LC. (2010). Anti-alpha4beta1 integrin antibody induces receptor internalization and does not impair the function of circulating neutrophilic leukocytes. Inflamm Res; 59(8):647-57.

Fletcher JM, Lalor SJ, Sweeney CM, Tubridy N, Mills KH. (2010). T cells in multiple sclerosis and experimental autoimmune encephalomyelitis. Clin Exp Immunol; 162(1):1-11.

Floris S, Blezer EL, Schreibelt G, Döpp E, van der Pol SM, Schadee-Eestermans IL, Nicolay K, Dijkstra CD, de Vries HE. (2004). Blood-brain barrier permeability and monocyte infiltration in experimental allergic encephalomyelitis: a quantitative MRI study. Brain; 127(Pt 3):616-27.

Frischer JM, Bramow S, Dal-Bianco A, Lucchinetti CF, Rauschka H, Schmidbauer M, Laursen H, Sorensen PS, Lassmann H. (2009). The relation between inflammation and neurodegeneration in multiple sclerosis brains. Brain; 132(Pt 5):1175-89.

G

Gold R, Linington C, Lassmann H. (2006). Understanding pathogenesis and therapy of multiple sclerosis via animal models: 70 years of merits and culprits in experimental autoimmune encephalomyelitis research. Brain; 129(Pt 8):1953-71.

Golde WT, Gollobin P, Rodriguez LL. (2005). A rapid, simple, and humane method for submandibular bleeding of mice using a lancet. Lab Anim (NY); 34(9):39-43.

H

Haagen IA, Geerars AJ, Clark MR, van de Winkel JG. (1995). Interaction of human monocyte Fc gamma receptors with rat IgG2b. A new indicator for the Fc gamma RIIa (R-H131) polymorphism. J Immunol; 154(4):1852-60.

Haanstra KG, Hofman SO, Lopes Estêvão DM, Blezer EL, Bauer J, Yang LL, Wyant T, Csizmadia V, 't Hart BA, Fedyk ER. (2013). Antagonizing the α4β1 integrin, but not α4β7, inhibits leukocytic infiltration of the central nervous system in rhesus monkey experimental autoimmune encephalomyelitis. J Immunol; 190(5):1961-73.

Hamann A, Andrew DP, Jablonski-Westrich D, Holzmann B, Butcher EC. (1994). Role of alpha 4-integrins in lymphocyte homing to mucosal tissues in vivo. J Immunol; 152(7):3282-93.

Handel AE, Giovannoni G, Ebers GC, Ramagopalan SV. (2010). Environmental factors and their timing in adult-onset multiple sclerosis. Nat Rev Neurol; 6(3):156-66.

Harrer A, Wipfler P, Einhaeupl M, Pilz G, Oppermann K, Hitzl W, Afazel S, Haschke-Becher E, Strasser P, Trinka E, Kraus J. (2011). Natalizumab therapy decreases surface expression of both VLA-heterodimer subunits on peripheral blood mononuclear cells. J Neuroimmunol; 234(1-2):148-54.

Harrer A, Pilz G, Einhaeupl M, Oppermann K, Hitzl W, Wipfler P, Sellner J, Golaszewski S, Afazel S, Haschke-Becher E, Trinka E, Kraus J. (2012). Lymphocyte subsets show different response patterns to in vivo bound natalizumab--a flow cytometric study on patients with multiple sclerosis. PLoS One; 7(2):e31784.

Hauser SL, Waubant E, Arnold DL, Vollmer T, Antel J, Fox RJ, Bar-Or A, Panzara M, Sarkar N, Agarwal S, Langer-Gould A, Smith CH; HERMES Trial Group. (2008). B-cell depletion with rituximab in relapsing-remitting multiple sclerosis. N Engl J Med; 358(7):676-88.

Havrdova E, Galetta S, Hutchinson M, Stefoski D, Bates D, Polman CH, O'Connor PW, Giovannoni G, Phillips JT, Lublin FD, Pace A, Kim R, Hyde R. (2009). Effect of natalizumab on clinical and radiological disease activity in multiple sclerosis: a retrospective analysis of the Natalizumab Safety and Efficacy in Relapsing-Remitting Multiple Sclerosis (AFFIRM) study. Lancet Neurol; 8(3):254-60.

Hellwig K, Schimrigk S, Fischer M, Haghikia A, Müller T, Chan A, Gold R. (2008). Allergic and nonallergic delayed infusion reactions during natalizumab therapy. Arch Neurol; 65(5):656-8.

Herndon RM. (2003). In: Herndon RM (ed). Multiple Sclerosis: Immunology, Pathology, and Pathophysiology. New York, NY: Demos Medical Publishing LLC.

Holzmann B, McIntyre BW, Weissman IL. (1989). Identification of a murine Peyer's patch--specific lymphocyte homing receptor as an integrin molecule with an alpha chain homologous to human VLA-4 alpha. Cell; 56(1):37-46.

Howell OW, Reeves CA, Nicholas R, Carassiti D, Radotra B, Gentleman SM, Serafini B, Aloisi F, Roncaroli F, Magliozzi R, Reynolds R. (2011). Meningeal inflammation is widespread and linked to cortical pathology in multiple sclerosis. Brain; 134(Pt 9):2755-71.

Hughes-Jones NC, Gorick BD, Howard JC. (1983). The mechanism of synergistic complement-mediated lysis of rat red cells by monoclonal IgG antibodies. Eur J Immunol; 13(8):635-41.

Hutchinson M, Kappos L, Calabresi PA, Confavreux C, Giovannoni G, Galetta SL, Havrdova E, Lublin FD, Miller DH, O'Connor PW, Phillips JT, Polman CH, Radue EW, Rudick RA, Stuart WH, Wajgt A, Weinstock-Guttman B, Wynn DR, Lynn F, Panzara MA; AFFIRM and SENTINEL Investigators. (2009). The efficacy of natalizumab in patients with relapsing multiple sclerosis: subgroup analyses of AFFIRM and SENTINEL. J Neurol; 256(3):405-15.

J

Jacob A, Hutchinson M, Elsone L, Kelly S, Ali R, Saukans I, Tubridy N, Boggild M. (2012). Does natalizumab therapy worsen neuromyelitis optica? Neurology; 79(10):1065-6.

Jain P, Coisne C, Enzmann G, Rottapel R, Engelhardt B. (2010). Alpha4beta1 integrin mediates the recruitment of immature dendritic cells across the blood-brain barrier during experimental autoimmune encephalomyelitis. J Immunol; 184(12):7196-206.

Jarius S, Franciotta D, Paul F, Ruprecht K, Bergamaschi R, Rommer PS, Reuss R, Probst C, Kristoferitsch W, Wandinger KP, Wildemann B. (2010). Cerebrospinal fluid antibodies to aquaporin-4 in neuromyelitis optica and related disorders: frequency, origin, and diagnostic relevance. J Neuroinflammation; 7:52.

Jarius S, Paul F, Franciotta D, Ruprecht K, Ringelstein M, Bergamaschi R, Rommer P, Kleiter I, Stich O, Reuss R, Rauer S, Zettl UK, Wandinger KP, Melms A, Aktas O, Kristoferitsch W, Wildemann B. (2011). Cerebrospinal fluid findings in aquaporin-4 antibody positive neuromyelitis optica: results from 211 lumbar punctures. J Neurol Sci; 306(1-2):82-90.

Jefferis R, Kumararatne DS. (1990). Selective IgG subclass deficiency: quantification and clinical relevance. Clin Exp Immunol; 81(3):357-67.

K

Kanwar JR, Harrison JE, Wang D, Leung E, Mueller W, Wagner N, Krissansen GW. (2000). Beta7 integrins contribute to demyelinating disease of the central nervous system. J Neuroimmunol; 103(2):146-52.

Kawamoto E, Nakahashi S, Okamoto T, Imai H, Shimaoka M. (2012). Anti-integrin therapy for multiple sclerosis. Autoimmune Dis; 2012:357101.

Keegan M, König F, McClelland R, Brück W, Morales Y, Bitsch A, Panitch H, Lassmann H, Weinshenker B, Rodriguez M, Parisi J, Lucchinetti CF. (2005). Relation between humoral pathological changes in multiple sclerosis and response to therapeutic plasma exchange. Lancet; 366(9485):579-82.

Killestein J, Jasperse B, Liedorp M, Seewann A, Polman Ch. (2009). Very late delayed-allergic reaction to natalizumab not associated with neutralizing antibodies. Mult Scler; 15(4):525-6.

Killestein J, Vennegoor A, Strijbis EM, Seewann A, van Oosten BW, Uitdehaag BM, Polman CH. (2010). Natalizumab drug holiday in multiple sclerosis: poorly tolerated. Ann Neurol; 68(3):392-5.

Kipp M, Clarner T, Dang J, Copray S, Beyer C. (2009). The cuprizone animal model: new insights into an old story. Acta Neuropathol; 118(6):723-36.

Kleinschmidt-DeMasters BK, Tyler KL. (2005). Progressive multifocal leukoencephalopathy complicating treatment with natalizumab and interferon beta-1a for multiple sclerosis. N Engl J Med; 353(4):369-74.

Kleiter I, Hellwig K, Berthele A, Kümpfel T, Linker RA, Hartung HP, Paul F, Aktas O; Neuromyelitis Optica Study Group. (2012). Failure of natalizumab to prevent relapses in neuromyelitis optica. Arch Neurol; 69(2):239-45.

Kondo A, Nakano T, Suzuki K. (1987). Blood-brain barrier permeability to horseradish peroxidase in twitcher and cuprizone-intoxicated mice. Brain Res; 425(1):186-90.

Korn T. (2008). Pathophysiology of multiple sclerosis. J Neurol; 255 Suppl 6:2-6.

Kornek B, Lassmann H. (2003). Neuropathology of multiple sclerosis-new concepts. Brain Res Bull; 61(3):321-6.

Krishnamoorthy G, Lassmann H, Wekerle H, Holz A. (2006). Spontaneous opticospinal encephalomyelitis in a double-transgenic mouse model of autoimmune T cell/B cell cooperation. J Clin Invest; 116(9):2385-92.

Krumbholz M, Pellkofer H, Gold R, Hoffmann LA, Hohlfeld R, Kümpfel T. (2007). Delayed allergic reaction to natalizumab associated with early formation of neutralizing antibodies. Arch Neurol; 64(9):1331-3.

Krumbholz M, Meinl I, Kümpfel T, Hohlfeld R, Meinl E. (2008). Natalizumab disproportionately increases circulating pre-B and B cells in multiple sclerosis. Neurology; 71(17):1350-4.

Kuhlmann T, Lingfeld G, Bitsch A, Schuchardt J, Brück W. (2002). Acute axonal damage in multiple sclerosis is most extensive in early disease stages and decreases over time. Brain; 125(Pt 10):2202-12.

Kuhlmann T, Lassmann H, Brück W. (2008). Diagnosis of inflammatory demyelination in biopsy specimens: a practical approach. Acta Neuropathol; 115(3):275-87.

Kumar DR, Aslinia F, Yale SH, Mazza JJ. (2011). Jean-Martin Charcot: the father of neurology. Clin Med Res; 9(1):46-9.

Kutzelnigg A, Lucchinetti CF, Stadelmann C, Brück W, Rauschka H, Bergmann M, Schmidbauer M, Parisi JE, Lassmann H. (2005). Cortical demyelination and diffuse white matter injury in multiple sclerosis. Brain; 128(Pt 11):2705-12.

L

Langer-Gould A, Atlas SW, Green AJ, Bollen AW, Pelletier D. (2005). Progressive multifocal leukoencephalopathy in a patient treated with natalizumab. N Engl J Med; 353(4):375-81.

Léger OJ, Yednock TA, Tanner L, Horner HC, Hines DK, Keen S, Saldanha J, Jones ST, Fritz LC, Bendig MM. (1997). Humanization of a mouse antibody against human alpha-4 integrin: a potential therapeutic for the treatment of multiple sclerosis. Hum Antibodies; 8(1):3-16.

Lennon VA, Kryzer TJ, Pittock SJ, Verkman AS, Hinson SR. (2005). IgG marker of optic-spinal multiple sclerosis binds to the aquaporin-4 water channel. J Exp Med; 202(4):473-7.

Leone DR, Giza K, Gill A, Dolinski BM, Yang W, Perper S, Scott DM, Lee WC, Cornebise M, Wortham K, Nickerson-Nutter C, Chen LL, LePage D, Spell JC, Whalley ET, Petter RC, Adams SP, Lobb RR, Pepinsky RB. (2003). An assessment of the mechanistic differences between two integrin alpha 4 beta 1 inhibitors, the monoclonal antibody TA-2 and the small molecule BIO5192, in rat experimental autoimmune encephalomyelitis. J Pharmacol Exp Ther; 305(3):1150-62.

Leussink VI, Lehmann HC, Hartung HP, Gold R, Kieseier BC. (2008). Type III systemic allergic reaction to natalizumab. Arch Neurol; 65(6):851-2; author reply 852.

Lindå H, von Heijne A, Major EO, Ryschkewitsch C, Berg J, Olsson T, Martin C. (2009). Progressive multifocal leukoencephalopathy after natalizumab monotherapy. N Engl J Med; 361(11):1081-7.

Lindberg RL, Achtnichts L, Hoffmann F, Kuhle J, Kappos L. (2008). Natalizumab alters transcriptional expression profiles of blood cell subpopulations of multiple sclerosis patients. J Neuroimmunol; 194(1-2):153-64.

Litzenburger T, Fässler R, Bauer J, Lassmann H, Linington C, Wekerle H, Iglesias A. (1998). B lymphocytes producing demyelinating autoantibodies: development and function in gene-targeted transgenic mice. J Exp Med; 188(1):169-80.

Lublin FD, Reingold SC. (1996). Defining the clinical course of multiple sclerosis: results of an international survey. National Multiple Sclerosis Society (USA) Advisory Committee on Clinical Trials of New Agents in Multiple Sclerosis. Neurology; 46(4):907-11.

Lucchinetti C, Brück W, Parisi J, Scheithauer B, Rodriguez M, Lassmann H. (2000). Heterogeneity of multiple sclerosis lesions: implications for the pathogenesis of demyelination. Ann Neurol; 47(6):707-17.

M

McMahon EJ, Cook DN, Suzuki K, Matsushima GK. (2001). Absence of macrophage-inflammatory protein-1alpha delays central nervous system demyelination in the presence of an intact blood-brain barrier. J Immunol; 167(5):2964-71.

Magliozzi R, Howell O, Vora A, Serafini B, Nicholas R, Puopolo M, Reynolds R, Aloisi F. (2007). Meningeal B-cell follicles in secondary progressive multiple sclerosis associate with early onset of disease and severe cortical pathology. Brain; 130(Pt 4):1089-104.

Marrie RA. (2004). Environmental risk factors in multiple sclerosis aetiology. Lancet Neurol; 3(12):709-18.

Meinl E, Krumbholz M, Hohlfeld R. (2006). B lineage cells in the inflammatory central nervous system environment: migration, maintenance, local antibody production, and therapeutic modulation. Ann Neurol; 59(6):880-92.

Melis M, Cocco E, Frau J, Lorefice L, Fenu G, Coghe G, Mura M, Marrosu MG. (2013). Post-natalizumab clinical and radiological findings in a cohort of multiple sclerosis patients: 12-month follow-up. Neurol Sci. 2013 Aug 30.

Mendel I, Kerlero de Rosbo N, Ben-Nun A. (1995). A myelin oligodendrocyte glycoprotein peptide induces typical chronic experimental autoimmune encephalomyelitis in H-2b mice: fine specificity and T cell receptor V beta expression of encephalitogenic T cells. Eur J Immunol; 25(7):1951-9.

Messori L, Casini A, Gabbiani C, Sorace L, Muniz-Miranda M, Zatta P. (2007). Unravelling the chemical nature of copper cuprizone. Dalton Trans; (21):2112-4.

Miller DH, Khan OA, Sheremata WA, Blumhardt LD, Rice GP, Libonati MA, Willmer-Hulme AJ, Dalton CM, Miszkiel KA, O'Connor PW; International Natalizumab Multiple Sclerosis Trial Group. (2003). A controlled trial of natalizumab for relapsing multiple sclerosis. N Engl J Med; 348(1):15-23.

Monson NL, Brezinschek HP, Brezinschek RI, Mobley A, Vaughan GK, Frohman EM, Racke MK, Lipsky PE. (2005). Receptor revision and atypical mutational characteristics in clonally expanded B cells from the cerebrospinal fluid of recently diagnosed multiple sclerosis patients. J Neuroimmunol; 158(1-2):170-81.

Mountain A, Adair JR. (1992). Engineering antibodies for therapy. Biotechnol Genet Eng Rev; 10:1-142.

Murray TJ. (2009). Robert Carswell: the first illustrator of MS. Int MS J; 16(3):98-101.

N

Niino M, Bodner C, Simard ML, Alatab S, Gano D, Kim HJ, Trigueiro M, Racicot D, Guérette C, Antel JP, Fournier A, Grand'Maison F, Bar-Or A. (2006). Natalizumab effects on immune cell responses in multiple sclerosis. Ann Neurol; 59(5):748-54.

O

Obermeier B, Mentele R, Malotka J, Kellermann J, Kümpfel T, Wekerle H, Lottspeich F, Hohlfeld R, Dornmair K. (2008). Matching of oligoclonal immunoglobulin transcriptomes and proteomes of cerebrospinal fluid in multiple sclerosis. Nat Med; 14(6):688-93.

O'Connor PW, Goodman A, Willmer-Hulme AJ, Libonati MA, Metz L, Murray RS, Sheremata WA, Vollmer TL, Stone LA; Natalizumab Multiple Sclerosis Trial Group. (2004). Randomized multicenter trial of natalizumab in acute MS relapses: clinical and MRI effects. Neurology; 62(11):2038-43.

O'Connor P, Miller D, Riester K, Yang M, Panzara M, Dalton C, Miszkiel K, Khan O, Rice G, Sheremata W; International Natalizumab Trial Group. (2005). Relapse rates and enhancing lesions in a phase II trial of natalizumab in multiple sclerosis. Mult Scler; 11(5):568-72.

O'Connor PW, Goodman A, Kappos L, Lublin FD, Miller DH, Polman C, Rudick RA, Aschenbach W, Lucas N. (2011). Disease activity return during natalizumab treatment interruption in patients with multiple sclerosis. Neurology; 76(22):1858-65.

Owens GP, Kraus H, Burgoon MP, Smith-Jensen T, Devlin ME, Gilden DH. (1998). Restricted use of VH4 germline segments in an acute multiple sclerosis brain. Ann Neurol; 43(2):236-43.

Owens GP, Bennett JL, Lassmann H, O'Connor KC, Ritchie AM, Shearer A, Lam C, Yu X, Birlea M, DuPree C, Williamson RA, Hafler DA, Burgoon MP, Gilden D. (2009). Antibodies produced by clonally expanded plasma cells in multiple sclerosis cerebrospinal fluid. Ann Neurol; 65(6):639-49.

Ozawa K, Suchanek G, Breitschopf H, Brück W, Budka H, Jellinger K, Lassmann H. (1994). Patterns of oligodendroglia pathology in multiple sclerosis. Brain; 117 (Pt 6):1311-22.

P

Petereit HF, Moeller-Hartmann W, Reske D, Rubbert A. (2008). Rituximab in a patient with multiple sclerosis--effect on B cells, plasma cells and intrathecal IgG synthesis. Acta Neurol Scand; 117(6):399-403.

Phillips JT, O'Connor PW, Havrdova E, Hutchinson M, Kappos L, Miller DH, Polman CH, Lublin FD, Giovannoni G, Wajgt A, Lynn F, Panzara MA, Sandrock AW; AFFIRM Investigators. (2006). Infusion-related hypersensitivity reactions during natalizumab treatment. Neurology; 67(9):1717-8.

Polman CH, O'Connor PW, Havrdova E, Hutchinson M, Kappos L, Miller DH, Phillips JT, Lublin FD, Giovannoni G, Wajgt A, Toal M, Lynn F, Panzara MA, Sandrock AW; AFFIRM Investigators. (2006). A randomized, placebo-controlled trial of natalizumab for relapsing multiple sclerosis. N Engl J Med; 354(9):899-910.

Pozzilli C, Romano S, Cannoni S. (2002). Epidemiology and current treatment of multiple sclerosis in Europe today. J Rehabil Res Dev; 39(2):175-85.

Prineas JW. (1979). Multiple sclerosis: presence of lymphatic capillaries and lymphoid tissue in the brain and spinal cord. Science; 203(4385):1123-5.

Q

Qin Y, Duquette P, Zhang Y, Talbot P, Poole R, Antel J. (1998). Clonal expansion and somatic hypermutation of V(H) genes of B cells from cerebrospinal fluid in multiple sclerosis. J Clin Invest; 102(5):1045-50.

R

Radbruch A, Muehlinghaus G, Luger EO, Inamine A, Smith KG, Dörner T, Hiepe F. (2006). Competence and competition: the challenge of becoming a long-lived plasma cell. Nat Rev Immunol; 6(10):741-50.

Ransohoff RM. (2006). A mighty mouse: building a better model of multiple sclerosis. J Clin Invest; 116(9):2313-6.

Rothhammer V, Heink S, Petermann F, Srivastava R, Claussen MC, Hemmer B, Korn T. (2011). Th17 lymphocytes traffic to the central nervous system independently of α4 integrin expression during EAE. J Exp Med; 208(12):2465-76.

Rivers TM, Sprunt DH, Berry GP. (1933). Observations on attempts to produce acute disseminated encephalomyelitis in monkeys. J Exp Med; 58(1):39-53.

Rudick RA, Stuart WH, Calabresi PA, Confavreux C, Galetta SL, Radue EW, Lublin FD, Weinstock-Guttman B, Wynn DR, Lynn F, Panzara MA, Sandrock AW; SENTINEL Investigators. (2006). Natalizumab plus interferon beta-1a for relapsing multiple sclerosis. N Engl J Med; 354(9):911-23.

Rudick RA, Miller D, Hass S, Hutchinson M, Calabresi PA, Confavreux C, Galetta SL, Giovannoni G, Havrdova E, Kappos L, Lublin FD, Miller DH, O'Connor PW, Phillips JT, Polman CH, Radue EW, Stuart WH, Wajgt A, Weinstock-Guttman B, Wynn DR, Lynn F, Panzara MA; AFFIRM and SENTINEL Investigators. (2007). Health-related quality of life in multiple sclerosis: effects of natalizumab. Ann Neurol; 62(4):335-46.

S

Saxena A, Martin-Blondel G, Mars LT, Liblau RS. (2011). Role of CD8 T cell subsets in the pathogenesis of multiple sclerosis. FEBS Lett; 585(23):3758-63.

Scalfari A, Neuhaus A, Daumer M, Muraro PA, Ebers GC. (2013). Onset of secondary progressive phase and long-term evolution of multiple sclerosis. J Neurol Neurosurg Psychiatry; 00:1-9.

Schreiner B, Heppner FL, Becher B. (2009). Modeling multiple sclerosis in laboratory animals. Semin Immunopathol; 31(4):479-95.

Schrempf W, Ziemssen T. (2007). Glatiramer acetate: mechanisms of action in multiple sclerosis. Autoimmun Rev; 6(7):469-75.

Scott LM, Priestley GV, Papayannopoulou T. (2003). Deletion of alpha4 integrins from adult hematopoietic cells reveals roles in homeostasis, regeneration, and homing. Mol Cell Biol; 23(24):9349-60.

Serafini B, Rosicarelli B, Magliozzi R, Stigliano E, Aloisi F. (2004). Detection of ectopic B-cell follicles with germinal centers in the meninges of patients with secondary progressive multiple sclerosis. Brain Pathol; 14(2):164-74.

Serafini B, Rosicarelli B, Franciotta D, Magliozzi R, Reynolds R, Cinque P, Andreoni L, Trivedi P, Salvetti M, Faggioni A, Aloisi F. (2007). Dysregulated Epstein-Barr virus infection in the multiple sclerosis brain. J Exp Med; 204(12):2899-912.

Sospedra M, Martin R. (2005). Immunology of multiple sclerosis. Annu Rev Immunol; 23:683-747.

Steiner O, Coisne C, Cecchelli R, Boscacci R, Deutsch U, Engelhardt B, Lyck R. (2010). Differential roles for endothelial ICAM-1, ICAM-2, and VCAM-1 in shear-resistant T cell arrest, polarization, and directed crawling on blood-brain barrier endothelium. J Immunol; 185(8):4846-55.

Stohl W, Kaplan MS, Gonatas NK. (1979). A quantitative assay for experimental allergic encephalomyelitis in the rat based on permeability of spinal cords to 125I-human gamma-globulin. J Immunol; 122(3):920-5.

Stromnes IM, Goverman JM. (2006 a). Active induction of experimental allergic encephalomyelitis. Nat Protoc; 1(4):1810-9.

Stromnes IM, Goverman JM. (2006 b). Passive induction of experimental allergic encephalomyelitis. Nat Protoc; 1(4):1952-60.

Stüve O, Cepok S, Elias B, Saleh A, Hartung HP, Hemmer B, Kieseier BC. (2005). Clinical stabilization and effective B-lymphocyte depletion in the cerebrospinal fluid and peripheral blood of a patient with fulminant relapsing-remitting multiple sclerosis. Arch Neurol; 62(10):1620-3.

Stüve O, Marra CM, Jerome KR, Cook L, Cravens PD, Cepok S, Frohman EM, Phillips JT, Arendt G, Hemmer B, Monson NL, Racke MK. (2006 a). Immune surveillance in multiple sclerosis patients treated with natalizumab. Ann Neurol; 59(5):743-7

Stüve O, Marra CM, Bar-Or A, Niino M, Cravens PD, Cepok S, Frohman EM, Phillips JT, Arendt G, Jerome KR, Cook L, Grand'Maison F, Hemmer B, Monson NL, Racke MK. (2006 b). Altered CD4+/CD8+ T-cell ratios in cerebrospinal fluid of natalizumab-treated patients with multiple sclerosis. Arch Neurol; 63(10):1383-7.

Stüve O. (2009 a). Knowns and unknowns in the future of multiple sclerosis treatment. J Neurol Sci; 287 Suppl 1:S30-6.

Stüve O, Cravens PD, Frohman EM, Phillips JT, Remington GM, von Geldern G, Cepok S, Singh MP, Tervaert JW, De Baets M, MacManus D, Miller DH, Radü EW, Cameron EM, Monson NL, Zhang S, Kim R, Hemmer B, Racke MK. (2009 b). Immunologic, clinical, and radiologic status 14 months after cessation of natalizumab therapy. Neurology; 72(5):396-401.

T

Takeshita Y, Ransohoff RM. (2012). Inflammatory cell trafficking across the blood-brain barrier: chemokine regulation and in vitro models. Immunol Rev; 248(1):228-39.

Theien BE, Vanderlugt CL, Eagar TN, Nickerson-Nutter C, Nazareno R, Kuchroo VK, Miller SD. (2001). Discordant effects of anti-VLA-4 treatment before and after onset of relapsing experimental autoimmune encephalomyelitis. J Clin Invest; 107(8):995-1006.

Tsunoda I, Terry EJ, Marble BJ, Lazarides E, Woods C, Fujinami RS. (2007). Modulation of experimental autoimmune encephalomyelitis by VLA-2 blockade. Brain Pathol; 17(1):45-55.

Tubridy N, Behan PO, Capildeo R, Chaudhuri A, Forbes R, Hawkins CP, Hughes RA, Palace J, Sharrack B, Swingler R, Young C, Moseley IF, MacManus DG, Donoghue S, Miller DH. (1999). The effect of anti-alpha4 integrin antibody on brain lesion activity in MS. The UK Antegren Study Group. Neurology; 53(3):466-72.

V

Vellinga MM, Castelijns JA, Barkhof F, Uitdehaag BM, Polman CH. (2008). Postwithdrawal rebound increase in T2 lesional activity in natalizumab-treated MS patients. Neurology; 70(13 Pt 2):11501.

Vercellino M, Masera S, Lorenzatti M, Condello C, Merola A, Mattioda A, Tribolo A, Capello E, Mancardi GL, Mutani R, Giordana MT, Cavalla P. (2009). Demyelination, inflammation, and neurodegeneration in multiple sclerosis deep gray matter. J Neuropathol Exp Neurol; 68(5):489-502.

Vollmer T, Stewart T, Baxter N. (2010). Mitoxantrone and cytotoxic drugs' mechanisms of action. Neurology; 74 Suppl 1:S41-6.

W

Weber MS, Prod'homme T, Youssef S, Dunn SE, Rundle CD, Lee L, Patarroyo JC, Stüve O, Sobel RA, Steinman L, Zamvil SS. (2007). Type II monocytes modulate T cell-mediated central nervous system autoimmune disease. Nat Med; 13(8):935-43.

Willer CJ, Dyment DA, Risch NJ, Sadovnick AD, Ebers GC; Canadian Collaborative Study Group. (2003). Twin concordance and sibling recurrence rates in multiple sclerosis. Proc Natl Acad Sci U S A; 100(22):12877-82.

Winter O, Dame C, Jundt F, Hiepe F. (2012). Pathogenic long-lived plasma cells and their survival niches in autoimmunity, malignancy, and allergy. J Immunol; 189(11):5105-11.

Wipfler P, Oppermann K, Pilz G, Afazel S, Haschke-Becher E, Harrer A, Huemer M, Kunz A, Golaszewski S, Staffen W, Ladurner G, Kraus J. (2011). Adhesion molecules are promising candidates to establish surrogate markers for natalizumab treatment. Mult Scler; 17(1):16-23.

Woof JM, Partridge LJ, Jefferis R, Burton DR. (1986). Localisation of the monocyte-binding region on human immunoglobulin G. Mol Immunol; 23(3):319-30.

Y

Yednock TA, Cannon C, Fritz LC, Sanchez-Madrid F, Steinman L, Karin N. (1992). Prevention of experimental autoimmune encephalomyelitis by antibodies against alpha 4 beta 1 integrin. Nature; 356(6364):63-6.

A1. Supplementary Tables

Suppl. Tab. 1: Number of inflammatory cells in *active demyelinating biopsy lesions* of natalizumab treated patients depending on disease duration.

Cell number / mm²		Disease duration in years									Spearman r	P value
		2	8	10	10	12	15	16	18	19		
CD3	pv	2.9	14.3	27.5	4.4	26.5	211.4	24.5	15.1	113.1	0.611	0.086
	pa	16.7	9.4	47.5	32.6	22	316.2	33.1	127.3	71.6	0.753	0.026
	Σ	19.6	23.7	75	37	48.5	527.5	57.6	142.4	184.7	0.812	0.011
CD4	pv	1.3	5.9	12.8	2.8	16.8	109	17.7	1.2	59.8	0.435	0.250
	pa	11.9	2	19.7	25.7	14	93.6	26.8	45.7	35	0.812	0.011
	Σ	13.2	7.9	32.5	28.5	30.8	202.6	44.5	46.9	94.8	0.854	0.006
CD8	pv	1.6	8.3	14.7	1.6	9.7	102.4	6.7	13.9	53.2	0.576	0.108
	pa	4.8	7.3	27.8	7	8	222.6	6.3	81.6	36.6	0.594	0.097
	Σ	6.4	15.6	42.5	8.6	17.7	325	13	95.5	89.8	0.653	0.067
CD20	pv	0	n/a	0	0	2	7.4	0	0	0.1	0.302	0.462
	pa	0.3	n/a	0	0	0	0.4	0	0	0	-0.314	0.462
	Σ	0.3	n/a	0	0	2	7.8	0	0	0.1	-0.077	0.882
CD138	pv	0	16.6	2.5	0	1.8	43.2	0.7	18.1	8.5	0.441	0.230
	pa	0	7.7	0	4.4	3.3	90.5	1.1	8.2	2.2	0.282	0.463
	Σ	0	24.3	2.5	4.4	5.1	133.7	1.8	26.3	10.7	0.427	0.250
KiM1P	Mic.	34	n/a	0	52	46	52	26	46	19	-0.048	0.935
	Mac.	1026	n/a	390	1154	1947	1689	1376	2741	1419	0.671	0.083

pv = perivascular, pa = parenchymal, Mic. = microglia, Mac. = macrophages, n/a = data are not available

Suppl. Tab. 2: Number of inflammatory cells in *active demyelinating biopsy lesions* of natalizumab treated patients depending on therapy duration.

Cell number / mm²		Therapy duration in months										Spearman r	P value
		1	2	5.5	9	14	24	33	42	43	78		
CD3	pv	2.9	14.3	4.4	7.5	211.4	27.5	24.5	113.1	26.5	15.1	0.600	0.073
	pa	16.7	9.4	32.6	28.9	316.2	47.5	33.1	71.6	22	127.3	0.576	0.088
	Σ	19.6	23.7	37	36.4	527.6	75	57.6	184.7	48.5	142.4	0.697	0.031
CD4	pv	1.3	5.9	2.8	0	109	12.8	17.7	59.8	16.8	1.2	0.285	0.427
	pa	11.9	2	25.7	20.7	93.6	19.7	26.8	35	14	45.7	0.527	0.123
	Σ	13.2	7.9	28.5	20.7	202.6	32.5	44.5	94.8	30.8	46.9	0.697	0.031
CD8	pv	1.6	8.3	1.6	8.2	102.4	14.7	6.7	53.2	9.7	13.9	0.541	0.114
	pa	4.8	7.3	7	8.2	222.6	27.8	6.3	36.6	8	81.6	0.539	0.114
	Σ	6.4	15.6	8.6	16.4	325	42.5	13	89.8	17.7	95.5	0.649	0.049
CD20	pv	0	n/a	0	0	7.4	0	0	0.1	2	0	0.297	0.437
	pa	0.3	n/a	0	0	0.4	0	0	0	0	0	-0.479	0.194
	Σ	0.3	n/a	0	0	7.8	0	0	0.1	2	0	-0.018	0.982
CD138	pv	0	16.6	0	3.8	43.2	2.5	0.7	8.5	1.8	18.1	0.322	0.368
	Pa	0	7.7	4.4	3.8	90.5	0	1.1	2.2	3.3	8.2	0.085	0.811
	Σ	0	24.3	4.4	7.6	133.7	2.5	1.8	10.7	5.1	26.3	0.285	0.427
KiM1P	Mic.	34	n/a	52	13	52	0	26	19	46	46	-0.017	0.982
	Mac.	1026	n/a	1154	650	1689	390	1376	1419	1947	2741	0.700	0.043

pv = perivascular, pa = parenchymal, Mic. = microglia, Mac. = macrophages, n/a = data are not available

Suppl. Tab. 3: Number of inflammatory cells in *active demyelinating biopsy lesions* of natalizumab treated patients depending on interval between last infusion and biopsy / death.

Cell number / mm²

		Days after last injection									Spearman r	P value
		41	47	101	128	165	185	336	436	617		
CD3	pv	14.3	2.9	15.1	27.5	4.4	211.4	113.1	26.5	24.5	0.550	0.133
CD3	pa	9.4	16.7	127.3	47.5	32.6	316.2	71.6	22	33.1	0.333	0.385
CD3	Σ	23.7	19.6	142.4	75	37	527.6	184.7	48.5	57.6	0.433	0.250
CD4	pv	5.9	1.3	1.2	12.8	2.8	109	59.8	16.8	17.7	0.700	0.043
CD4	pa	2	11.9	45.7	19.7	25.7	93.6	35	14	26.8	0.433	0.250
CD4	Σ	7.9	13.2	46.9	32.5	28.5	202.6	94.8	30.8	44.5	0.533	0.148
CD8	pv	8.3	1.6	13.9	14.7	1.6	102.4	53.2	9.7	6.7	0.209	0.581
CD8	pa	7.3	4.8	81.6	27.8	7	222.6	36.6	8	6.3	0.083	0.843
CD8	Σ	15.6	6.4	95.5	42.5	8.6	325	89.8	17.7	13	0.150	0.708
CD20	pv	n/a	0	0	0	0	7.4	0.1	2	0	0.464	0.243
CD20	pa	n/a	0.3	0	0	0	0.4	0	0	0	-0.312	0.462
CD20	Σ	n/a	0.3	0	0	0	7.8	0.1	2	0	0.140	0.752
CD138	pv	16.6	0	18.1	2.5	0	43.2	8.5	1.8	0.7	-0.142	0.708
CD138	pa	7.7	0	8.2	0	4.4	90.5	2.2	3.3	1.1	-0.100	0.810
CD138	Σ	24.3	0	26.3	2.5	4.4	133.7	10.7	5.1	1.8	-0.100	0.810
KiM1P	Mic.	n/a	34	46	0	52	52	19	46	26	-0.095	0.840
KiM1P	Mac.	n/a	1026	2741	390	1154	1689	1419	1947	1376	0.286	0.501

pv = perivascular, pa = parenchymal, Mic. = microglia, Mac. = macrophages, n/a = data are not available

Suppl. Tab. 4: Percentage of CD49d^{+} cells and relative CD49d MFI before and after short-term treatment with α-CD49d (PS/2) antibody or PBS.

	Treatment with PS/2							
	CD49d+ cells [%]							
	CD3+	CD4+	CD8+	B220+	Syn-1+	NK1.1+	CD11b+	Gr-1+
Before treatment (mean ± SEM)	86.9 ± 2.3	84.8 ± 2.6	80.0 ± 3.9	99.8 ± 0.1	98.4 ± 0.5	97.6 ± 0.5	99.8 ± 0.2	61.4 ± 5.2
After treatment (mean ± SEM)	2.1 ± 0.8	1.3 ± 0.3	7.6 ± 1.1	13.5 ± 2.6	14.5 ± 3.5	24.1 ± 5.9	42.6 ± 9.1	2.9 ± 0.6

	Treatment with PBS							
	CD49d+ cells [%]							
	CD3+	CD4+	CD8+	B220+	Syn-1+	NK1.1+	CD11b+	Gr-1+
Before treatment (mean ± SEM)	93.1 ± 1.7	88.1 ± 2.6	85.4 ± 3.8	99.6 ± 0.2	96.0 ± 2.6	95.8 ± 1.3	99.5 ± 0.3	48.0 ± 6.1
After treatment (mean ± SEM)	90.7 ± 3.6	87.2 ± 3.6	85.9 ± 3.9	99.5 ± 0.2	95.7 ± 1.8	93.0 ± 2.0	99.3 ± 0.4	46.1 ± 6.0

	Treatment with PS/2							
	Relative CD49d MFI							
	CD3+	CD4+	CD8+	B220+	Syn-1+	NK1.1+	CD11b+	Gr-1+
Before treatment (mean ± SEM)	10.3 ± 0.4	10.2 ± 0.4	15.5 ± 2.9	30.3 ± 0.7	25.9 ± 1.0	48.7 ± 2.2	62.6 ± 1.3	4.4 ± 0.2
After treatment (mean ± SEM)	0.5 ± 0.1	0.5 ± 0.1	0.8 ± 0.2	2.1 ± 0.3	2.1 ± 0.4	1.0 ± 0.3	3.8 ± 0.5	0.3 ± 0.0

	Treatment with PBS							
	Relative CD49d MFI							
	CD3+	CD4+	CD8+	B220+	Syn-1+	NK1.1+	CD11b+	Gr-1+
Before treatment (mean ± SEM)	10.8 ± 0.3	10.5 ± 0.4	17.0 ± 1.4	28.1 ± 1.5	23.9 ± 1.3	48.4 ± 2.3	61.1 ± 2.3	4.1 ± 0.1
After treatment (mean ± SEM)	10.2 ± 0.6	10.1 ± 0.6	18.2 ± 3.2	26.9 ± 1.5	22.2 ± 1.4	43.6 ± 4.7	57.9 ± 5.6	4.4 ± 0.1

Suppl. Tab. 5: Absolute cell numbers of WBCs before and after short-term treatment with α-CD49d (PS/2) antibody or PBS.

	Treatment with PS/2								
	Absolute cell number / µl blood								
	WBC	CD3+	CD4+	CD8+	B220+	Syn-1+	NK1.1+	CD11b+	Gr-1+
Before treatment (mean ± SEM)	4061 ± 404	1051 ± 112	1092 ± 111	34 ± 15	556 ± 88	41 ± 8	160 ± 33	121 ± 28	1797 ± 263
After treatment (mean ± SEM)	13329 ±1969	2592 ± 434	2608 ± 413	83 ± 22	3033 ± 313	188 ± 33	307 ± 39	596 ± 123	3699 ± 699

	Treatment with PBS								
	Absolute cell number / µl blood								
	WBC	CD3+	CD4+	CD8+	B220+	Syn-1+	NK1.1+	CD11b+	Gr-1+
Before treatment (mean ± SEM)	3564 ± 420	1120 ± 247	1140 ± 257	10 ± 3	573 ± 81	32 ± 5	225 ± 57	105 ± 34	1157 ± 269
After treatment (mean ± SEM)	2589 ± 462	729 ± 246	741 ± 238	9 ± 4	530 ± 162	33 ± 12	153 ± 49	99 ± 24	777 ± 143

A2. Buffers and reagents

<u>Tail lysis buffer</u>
100mM Tris
5mM EDTA
200mM NaCl
0.2% SDS
pH 8.5

<u>TBE</u>
10.8g Tris
5.5g boric acid
4ml 0.5M EDTA
add 1000 ml H_2O

<u>1x PBS</u>
9.55g PBS (10x)
add 1000ml H_2O

<u>4% PFA</u>
40g PFA
add 1000ml PBS
heating up to 60°C while constantly
stirring to solve the PFA
some drops of 1M NaOH
until the PFA is solved
pH 7.6

<u>1% Eosin solution</u>
2g Eosin-G CertiStain
198ml 70% isopropanol
filtered
few drops glacial acetic acid before use

<u>LFB solution</u>
1g LFB
1000ml 96% EtOH
5ml 10% acetic acid

<u>Bielschowsky developer solution</u>
20ml 37% formalin
0.5g citric acid
2 drops 65% nitric acid
100ml dest. H_2O
add 50ml PBS

<u>Citric acid buffer</u>
2.1g citric acid
add 1000ml H_2O
pH 6

<u>Tris-ethylenediaminetetraacetic acid
(Tris-EDTA) buffer</u>
1.21g trizma base
1ml 0.1M EDTA
Add 1000ml dest. H_2O
pH 9.0

<u>Protease-solution</u>
25mg protease
add 60ml H_2O

<u>3,3'-diaminobenzidine tetrachloride
(DAB) solution</u>
25mg DAB
20µl 30% H_2O_2

<u>AEC stock solution</u>
12.5g 3-amino-9 ethylcarbazol
250ml dimethylformamid

Acetate stock solution
1.73ml glacial acetic acid
4.03g sodium acetate trihydrate
add 1000ml ddH$_2$O
pH 5.2

AEC developer solution
4ml AEC stock solution
56ml acetate stock solution
20µl H$_2$O$_2$ (30%)

Buffer for blood collection
1mM EDTA in PBS
pH 7.5

FACS buffer
0.1% BSA
0.1% sodium azide
add 1000ml PBS

1x BD RBC lysis buffer
dilute BD FACS lysing solution
(10x concentrated)
1:10 with dH$_2$O

1x BD perm/wash buffer
Dilute BD perm/wash solution
(10x concentrated)
1:10 with dH$_2$O

Digestion buffer
(20mM sodium acetate trihydrate solution)
0.68g sodium acetate trihydrate
add 250ml ultrapure water
pH 4.5

Washing buffer
(10mM Tris/HCl)
0.39g Tris (hydroxymethyl) aminomethane
Add 250ml ultrapure water
pH 7.5

4x sample buffer
50mM Tris
10% Glycerol
2% SDS
0.025% bromophenol blue
pH 6.8

Coomassie solution
30mg coomassie G-250
add 500ml ddH$_2$O
stirred until coomassie is solved
add 0.75ml HCl (33%)

A3. Chemicals, reagents and manufacturers

3-amino-9 ethylcarbazol	Merck KgaA, Darmstadt, Germany
acetic acid	Merck KgaA, Darmstadt, Germany
acrylamid/bisacrylamid (30%) (mixing ratio 37.5:1)	Roth, Karlsruhe, Germany
agarose	StarPure, StarLab GmbH, Ahrensberg, Germany
ammonium hydroxide	Merck KgaA, Darmstadt, Germany
APS	Fluka Chemie GmbH, Buchs, Switzerland
β-mercaptoethanol	Sigma-Aldrich Chemie GmbH, Steinheim, Germany
BD cytofix/cetoperm	BD Biosciences, Heidelberg, Germany
BD FACS lysing solution (10x)	BD Biosciences, Heidelberg, Germany
BD perm/wash solution (10x)	BD Biosciences, Heidelberg, Germany
boric acid	Roth, Karlsruhe, Germany
bromophenol blue	Roth, Karlsruhe, Germany
BSA	SERVA Electrophoresis GmbH, Heidelberg, Germany
citric acid	Merck KgaA, Darmstadt, Germany
coomassie G-250	Biorad, Munich, Germany
copper sulphate	Merck KgaA, Darmstadt, Germany
DAB	Sigma-Aldrich Chemie GmbH, Steinheim, Germany
DePeX	VWR international, Darmstadt, Germany
Dimethylformamid	Sigma-Aldrich Chemie GmbH, Steinheim, Germany
dNTPs	Invitrogen GmbH, Karlsruhe, Germany
EDTA	Roth, Karlsruhe, Germany
Eosin-G CertiStain	Merck KgaA, Darmstadt, Germany
ethidium bromide	Sigma-Aldrich Chemie GmbH, Steinheim, Germany
EtOH absolute	Merck KgaA, Darmstadt, Germany
FACS antibodies	BD Biosciences, Heidelberg, Germany
	Biolegend, Fell, Germany
	eBioscience, NatuTec GmbH, Frakfurt, Germany
FCS	Biochrom AG, Berlin, Germany
formalin	Merck KgaA, Darmstadt, Germany
glacial acetic acid	Sigma-Aldrich Chemie GmbH, Steinheim, Germany
glycerol	Sigma-Aldrich Chemie GmbH, Steinheim, Germany
H_2O_2	Merck KgaA, Darmstadt, Germany
Histology antibodies	AbD Serotec, Oxford, UK

	Amersham Amersham/GE Healthcare Europe GmbH Freiburg, Germany
	Covance, Princeton, USA
	Dako DakoCytomation Glostrup, Denmark
	Dianova GmbH, Hamburg, Germany
isopropanol	Merck KgaA, Darmstadt, Germany
Immobilized pepsin agarose	Perbio science, Bonn, Germany
Ketamine	Inresa, Freiburg, Germany
LFB	BDH Laboratory supplies, VWR Int. Ltd., Poole, UK
lithium carbonate	Merck KgaA, Darmstadt, Germany
Mayer's hemalum	Merck KgaA, Darmstadt, Germany
methanol	Merck KgaA, Darmstadt, Germany
NaCl	Merck KgaA, Darmstadt, Germany
NaOH	Merck KgaA, Darmstadt, Germany
nitric acid	Merck KgaA, Darmstadt, Germany
Paraffine	Paraplast Plus, Tyco Healthcare GmbH, Neustadt an der Donau, Germany
PBS (10x)	Dulbecco, Biochrom AG, Berlin, Germany
PBS (sterile)	Dulbecco, w/o Mg2+, Ca2+, Biochrom AG, Berlin, Germany
PCR kit (genotyping)	GoTaq, Promega GmbH, Mannheim, Germany
periodic acid	Merck KgaA, Darmstadt, Germany
PFA	Merck KgaA, Darmstadt, Germany
POX	Extravidin, Sigma-Aldrich Chemie GmbH, Steinheim, Germany
Precision Plus Protein^{TM} standard marker	Biorad, Munich, Germany
Primer for genotyping	Microsynth, Wolfurt-Bahnhof, Austria
proteinase (type XXIV)	Sigma-Aldrich Chemie GmbH, Steinheim, Germany
proteinase K	Roche, Mannheim, Germany
Schiff's solution	Merck KgaA, Darmstadt, Germany
SDS	Sigma-Aldrich Chemie GmbH, Steinheim, Germany
silver nitrate	Roth, Karlsruhe, Germany
sodium acetate trihydrate	Sigma-Aldrich Chemie GmbH, Steinheim, Germany
sodium azide	Sigma-Aldrich Chemie GmbH, Steinheim, Germany
sodium chloride	Sigma-Aldrich Chemie GmbH, Steinheim, Germany
sodium thiosulfate	Merck KgaA, Darmstadt, Germany
TEMED	Roth, Karlsruhe, Germany
tris	Roth, Karlsruhe, Germany

tris (hydroxymethyl) aminomethane	Sigma-Aldrich Chemie GmbH, Steinheim, Germany
trypan blue solution (0.4%)	Sigma-Aldrich Chemie GmbH, Steinheim, Germany
xylazine	Inresa, Freiburg, Germany
xylol	Merck KgaA, Darmstadt, Germany

A4. Equipment and manufacturers

Brain-slice-matrix	Braintree Scientific Inc. Braintree, MA, USA
cell^A software	Olympus Europa GmbH, Hamburg, Germany
centrifuge 5810 R	Eppendorf AG, Hamburg, Germany
centrifuge 5415 R	Eppendorf AG, Hamburg, Germany
FACS instrument FACSCalibur	BD Bioscience, Heidelberg, Germany
FACS instrument FACSCanto II	BD Bioscience, Heidelberg, Germany
FACS tubes	BD Bioscience, Heidelberg, Germany
FlowJo Software	Tree Star Inc. Ashland, OR, USA
gel-documentation device	BioSciTec GmbH, Frankfurt/Main, Germany
gel rack & power supply SubCell GT & PowerPack 300	Biorad, Munich, Germany
glass slides (superfrost plus)	Menzel, Braunschweig, Germany
GraphPad Prism software	GraphPad Software, Inc. La Jolla , CA, USA
incubator Cellstar	Nunc GmbH, Wiesbaden, Germany
microscope BX41	Olympus, Europa GmbH, Hamburg, Germany
microtome	Leica, Wetzlar, Germany
microwave	Bosch, Gerlingen-Schillerhöhe, Germany
Mini PROTEAN® 3 Electrophoresis Cell System	BioRad Laboratories Inc. Hercules, CA, USA
NanoDrop ND-1000	Thermo Fisher scientific GmbH, Schwerte, Germany
Neubauer counting chamber	Brand GmbH & Co KG, Wertheim, Germany
ocular morphometric grid	Olympus Europa GmbH, Hamburg, Germany
Shandon Histocentre 2	Thermo Fisher scientific GmbH, Schwerte, Germany
T3 Biocycler	Biometra GmbH, Göttingen, Germany
tissue processor TP 1020	Leica, Wetzlar, Germany
Vivaspin column 50kDa MWCO	Sartotius Stedim Biotech GmbH, Göttingen, Germany
Vivaspin column 30kDa MWCO	Sartotius Stedim Biotech GmbH, Göttingen, Germany

Acknowledgements

I would like to thank my supervisor Dr. Imke Metz for her excellent support and guidance.

I am grateful to Prof. Dr. Wolfgang Brück for giving me the opportunity to work and write my thesis in the department of neuropathology.

Furthermore, I would like to thank Dr. Stefan Nessler and Dr. Niels Kruse for their theoretical support. I thank Dr. Fred Lühder and Martina Ott for the assistance on the flow cytometry device as well as Dr. Wiebke Wemheuer for the help on the SDS-PAGE.

I would also like to thank my thesis committee Prof. Dr. Wolfgang Brück, Prof. Dr. Alexander Flügel and Prof. Dr. Jürgen Wienands for their critical and supporting comments during the progress report meetings.

I wish to thank Jasmin Reichl, Mareike Gloth, Doris Bode, Brigitte Maruschak, Uta Scheidt as well as Astrid Wohltmann for their technical assistance.

In addition I would like to thank Christine Crozier, Julia Gellersen and foremost Cynthia Bunker for the administrative support, Sven Müller for the help with the biopsy archive as well as my colleagues in the department of neuropathology.

Personal thanks go out to my parents Maria and Werner as well as my brother Martin. Finally, I thank Eileen for the helpful creative distractions and Svenja for her patience and love.

Curriculum vitae

Personal data

Name	Darius Häusler
Date / place of birth	October 19, 1981 in Schweidnitz, Poland
Nationality	german

Current professional affiliation

Institute of Neuropathology, University Medical Center Göttingen, Germany

Phone: +49 551 39 8468

E-mail: darius.haeusler@med.uni-goettingen.de

Education

Since 10/2009	Institute of Neuropathology, University Medical Center Göttingen, Germany Since 04/2010 Ph.D. student (Molecular Medicine)
10/2003 – 09/2008	Georg-August University Göttingen, Germany Biological studies Degree: Diplom
2002	Wirtschaftsgymnasium (BBS I), Northeim, Germany Abitur

Professional experience

Since 10/2009	Institute of Neuropathology, University Medical Center Göttingen, Germany Research project: "Impact of natalizumab therapy on human pathology and an animal model of multiple sclerosis (EAE) with special focus on B cell / plasma cell inflammation" Supervisor: Dr. Imke Metz

10/2008 – 09/2009	Sartorius Stedim Biotech GmbH, Göttingen, Germany
	Department: Microbiological analysis
	Internship

04/2008 – 07/2008	Johann-Friedrich-Blumenbach-Institute for Zoology and Anthropology
	Prof. Dr. R. Willmann
	Scientific assistance and coaching of students in the department of zoology

08/2007 – 05/2008	Johann-Friedrich-Blumenbach-Institute for Zoology and Anthropology
	Diploma thesis: "Ontogenetic evolution of thorax musculature in mayflies (Insecta: Ephemeroptera)
	Supervisor: Dr. Thomas Hörnschemeyer

Publications

2012	Metz I, Radue EW, Oterino A, Kümpfel T, Wiendl H, Schippling S, Kuhle J, Sahraian MA, Gray F, Jakl V, **Häusler D**, Brück W. (2012). Pathology of immune reconstitution inflammatory syndrome in multiple sclerosis with natalizumab-associated progressive multifocal leukoencephalopathy. Acta Neuropathol; 123(2):235-45.

2011	Pflanz K, Jallerat E, **Häusler D**, Hollas M, Andag U. Patent zur Flüssigkeitstransport- und analytischer Testvorrichtung. DE202011005455.